GLOBAL RADIATIVE HEATING WITH APPLICATION TO THE DYNAMICS OF THE LOWER STRATOSPHERE

by

THOMAS GILBERT DOPPLICK

B.S., St. Louis University (1964)
B.S. in Meteorology, University of Utah (1965)

SUBMITTED IN PARTIAL FULFILLMENT
OF THE REQUIREMENT FOR THE
DEGREE OF DOCTOR OF
PHILOSOPHY

at the

MASSACHUSETTS INSTITUTE OF TECHNOLOGY
April, 1970

Signature of Author . . . . . .
Department of Meteorology, April 15, 1970

Certified by . . . . . .
Thesis Supervisor

Accepted by . . . . . .
Chairman, Departmental Committee on Graduate Students

GLOBAL RADIATIVE HEATING WITH APPLICATION TO THE DYNAMICS OF THE LOWER STRATOSPHERE

by

THOMAS GILBERT DOPPLICK

Submitted to the Department of Meteorology on April 15, 1970 in partial fulfillment of the requirements for the degree of Doctor of Philosophy.

ABSTRACT

Monthly zonal mean global radiative heating rates have been obtained from the surface to 10 mb for all twelve months. Seasonal profiles of the contribution by each constituent are presented in addition to the seasonal profiles of net thermal cooling and total radiative heating. Radiation cools the troposphere almost everywhere with maximum cooling in the tropics. The tropical stratosphere is heated by radiation but radiation cools the stratosphere in high latitudes with the warmer hemisphere showing more cooling. Approximate solutions of radiative heating are developed using the monthly mean radiative parameters and are combined with the geopotential and temperature fields to study the energetics of the Northern Hemisphere lower stratosphere on a daily basis for 1964. Significant leakage of energy from the troposphere occurs throughout the year and absorption of this energy in the lower stratosphere maintains the eddies for all months except January. In winter there is significant transmission of tropospheric energy into the upper stratosphere which suggests a close coupling of the upper and lower atmospheres. The seasonal circulations are examined and it is found that the spring warming of 1964 was due to a period of enhanced convergence of tropospheric energy flux. In the fall absorption of tropospheric energy intensifies the flow. The role of radiation is to destroy available potential energy for all months of the year.

Thesis Supervisor: Reginald E. Newell

Title: Professor of Meteorology

Acknowledgements

The opportunity for graduate education at M.I.T. was provided by the U.S. Air Force Institute of Technology and the author is very grateful for their support. Professor Newell has been a constant source of intellectual stimulation and an excellent thesis advisor. During the course of this study Professor Austin aided the author on several occasions in his capacity as graduate advisor. Original data were provided by Drs. Eugene Rasmusson and Thomas Vonder Haar and Mr. Wayne Hering. The Environmental Technical Applications Center, USAF, Washington, D.C. made available monthly mean cloud maps for 1964 and the National Center for Atmospheric Research, Boulder, Colorado kindly provided geopotential and temperature data for the troposphere for 1964. Lt. Colonel John Perry was instrumental in steering the author to numerous data sources. Mr. Robert Crosby provided timely programming assistance and Miss Isabelle Kole and Mr. Steven Ricci drafted the figures. This study was supported by the U.S. Atomic Energy Commission under Contract No. AT (30-1) 2241.

TABLE OF CONTENTS

LIST OF FIGURES

I. Introduction

Meteorologists have long been aware that the primary energy source for the earth-atmosphere system is solar radiation and that thermal radiation is the energy sink. In the mean there is a net gain of energy in low latitudes by the earth-atmosphere system and a loss of energy in high latitudes. This led early meteorologists to postulate that the driving force for atmospheric motions was differential heating of the atmosphere by radiation. However, for the bulk of the mass of the atmosphere, the troposphere, there is actually maximum radiative cooling in low latitudes and smaller radiative cooling in middle and high latitudes. Recent observational studies (Newell et al. 1970a,b) show the importance of sensible heat and the release of latent heat in addition to radiative heating in providing the energy source for driving the tropospheric motions. Nevertheless, radiative heating by atmospheric gases is an important component of the net diabatic heating of the atmosphere and is the only component above the regions of release of latent heat. Knowledge of radiative heating is indispensable in studies of energetics of the atmosphere and in constructing numerical models of the atmosphere.

Sections II, III and IV of this study are concerned with the problem of obtaining numerical solutions of the radiative transfer equations using known radiative parameters, i.e. temperature, absorber distributions, etc. For the first time monthly mean global radiative

heating rates have been obtained and show significant differences between the hemispheres, particularly in the lower stratosphere.

In Section V approximate numerical solutions of radiative heating in the Northern Hemisphere* lower stratosphere are coupled with the wind and temperature fields to study the dynamics of the lower stratosphere. A very detailed picture is obtained of the general circulation of the lower stratosphere including radiative effects.

---

*Hereafter Northern Hemisphere will be abbreviated as N.H. and Southern Hemisphere as S.H.

II. Radiative Transfer in the Earth's Atmosphere

Radiative transfer in gases is a very interesting although complex phenomenon which is of fundamental importance in understanding the physics of the earth's atmosphere. The complexity of gaseous transfer is due to the complicated molecular and atomic structure which gives rise to absorption, emission and scattering of electromagnetic radiation, the physics of which can only be explained through the quantum mechanical nature of radiation. Through the years there has evolved a sizeable literature concerning gaseous transfer as applied to the earth's atmosphere and no attempt will be made here to summarize this material in one brief chapter. An excellent summary of our current knowledge of atmospheric radiation is provided by Kondratiev (1969) who provides an abundant number of references. For the basic theory of atmospheric radiation, Goody's (1964a) book is recommended. The report by Rodgers (1967a) also contains many references and the author has drawn extensively from Rodgers' work, extending the radiative parameters and improving the frequency integrations.

A. Infrared Radiation

In principle one can formulate the complete radiative transfer equations for the radiative flux vector $\vec{F}$ but analytic and numerical solutions are very difficult to obtain. Even for the simplest case of one-dimensional, plane geometry analytic solutions are in general reducible only to integral equations and numerical solutions are required. Assuming a plane horizontally stratified atmosphere, the

net radiative flux arriving at level z from below in some frequency interval $\Delta\nu_r$ (in cm^{-1}) is given by:

$$F_r^{\uparrow}(z) = B_r(g)\,T_r(z,g) + \int_0^z B_r(z')\frac{d}{dz'}T_r(z,z')\,dz'$$

Similarly the net radiative flux arriving at level z from above is given by:

$$F_r^{\downarrow}(z) = \int_z^{\infty} B_r(z')\frac{d}{dz'}T_r(z,z')\,dz'$$

where $B_r(z')$ is the Planck function which depends only on the temperature at level z' and the spectral interval $\Delta\nu_r$, (g) represents the ground and $T_r(z,z')$ is the transmission function given by:

$$T_r(z,z') = \frac{2}{\Delta\nu_r}\int_{\Delta\nu_r} E_{i3}\left(\tau_\nu(z,z')\right)d\nu \qquad (2.1)$$

Here $\tau_\nu(z,z')$ is the monochromatic optical depth and E_{i3} is the exponential integral of third order which takes into account the integration over all zenith angles. The assumption is made here that the frequency interval $\Delta\nu_r$ is small enough so that the Planck function may be regarded as constant for the interval $\Delta\nu_r$. It is also assumed that local thermodynamic equilibrium exists and that the transmission function for overlap of absorbers 1 and 2 is given by:

$$T_r(z,z') = T_{r1}(z,z') \times T_{r2}(z,z')$$

The thermal cooling rate is obtained by differentiating the net flux at level z.

$$C_r(z) = -\frac{1}{C_p \rho} \frac{d}{dz}\left(F_r^{\uparrow} + F_r^{\downarrow}\right) \qquad (2.2)$$

where C_p is the specific heat at constant pressure and ρ is the density. Total thermal cooling is obtained by summing over the contributing spectral intervals.

B. Solar Radiation

Solar radiation passing through the atmosphere is depleted by the atmospheric gases according to the absorber amount u. For a plane horizontally stratified atmosphere (u = u(z)), the solar flux arriving at level z is:

$$S(z) = \int S_{o\nu}\, T_\nu\left(u(z)M\right) d\nu$$

Here $S_{o\nu}$ is the solar flux arriving at the top of the atmosphere, $T_\nu\left(u(z)M\right)$ is the transmissivity from the top of the atmosphere to level z and M is the magnification factor for slant paths through the atmosphere (see section III H.). The radiative heating rate

is given by:

$$H(z) = \frac{1}{\rho c_p M} \frac{\partial}{\partial z} S(z)$$

For the actual atmosphere overlap of absorbers must be taken into account as well as proper consideration of reflected and transmitted diffuse flux from clouds and the ground. Additionally an integration over sun angle is required.

III. Global Radiative Parameters – their Spectral Properties and Sources

Monthly mean radiative flux profiles from 1000 mb to 5 mb have been obtained for all months of the year from 85°N-80°S. Summarized below are the radiative parameters used in the flux computations including their spectral properties and sources.

A. Water Vapor

A.1 Thermal Spectral Properties

The Goody Random model (Goody 1964a), fitted in 19 spectral intervals (Rodgers and Walshaw 1966) combined with a continuum absorption and the Curtis-Godson approximation, has been used to represent water vapor transmission.

$$\tau(m,u) = \exp\left(-\frac{1}{\delta}\left(\frac{1}{(km)^2} + \frac{1}{k\pi\alpha_0 u}\right)^{-\frac{1}{2}} - \underline{K}u\right)$$

Where k is the mean line strength, δ is the mean spacing, α_0 is the half width at one atmosphere and $\underline{K}$ is a continuum absorption coefficient. The Curtis-Godson approximation has been extended by Godson (see Rodgers and Walshaw loc. cit. and Rodgers 1967a) to include temperature (θ) variations of line intensity and half width.

$$u = \int C(p) \frac{P_s}{g} \Psi(\theta)\, p\, dp \qquad (g\ cm^{-2})$$

$$m = \int C(p) \frac{P_s}{g} \Phi(\theta)\, dp \qquad (g\ cm^{-2}) \tag{3.1}$$

Where p is pressure in atmospheres, C(p) is the mass mixing ratio, P_s is 1013.246 mb and g is the acceleration of gravity. $\Phi(\theta)$ and $\Psi(\theta)$ are given by:

$$\Phi(\theta) = \sum_i K_i(\theta) \Big/ \sum_i K_i(\theta_0)$$

$$\Psi(\theta) = \left(\frac{\sum_i \left[K_i(\theta)\, \alpha_0(\theta) \right]^{1/2}}{\sum_i \left[K_i(\theta_0)\, \alpha_0(\theta_0) \right]^{1/2}} \right)^2$$

where the sum is over the contributing lines and θ_0 is the standard temperature. Empirically $\Phi(\theta)$ and $\Psi(\theta)$ can be expressed by:

$$\log \Phi(\theta) = a(\theta - 260) + b(\theta - 260)^2$$

$$\log \Psi(\theta) = a'(\theta - 260) + b'(\theta - 260)^2$$

(See Rodgers and Walshaw loc. cit. and Rodgers 1967a for numerical values.)

The frequency integration is obtained by summing over 20 discrete spectral intervals which span the entire frequency spectrum. Overlap of H_2O with CO_2 and O_3 is taken into account.

A.2 Solar Visible Spectral Properties

No water vapor absorption is considered in the visible portion of the solar spectrum ($< .7\,\mu$).

A.3 Solar Near Infrared Spectral Properties

Integrated absorption over entire bands has been measured by Howard et al. (1955) who give experimental fits of the following form:

$$A(m,p) = C_0 u \qquad u < v$$

$$= C_1 + C_2 \log u \qquad u > v$$

$$A \equiv \int_{\Delta\nu} A_\nu \, d\nu \qquad (A_\nu \text{ fractional absorption})$$

$$u = m^a p^b$$

The parameter v delineates between weak and strong absorption and is determined empirically. (See Rodgers 1967a for numberical values.) The following water vapor near infrared bands (in μ) have been evaluated: .8, .9, 1.1, 1.38, 1.9, 2.7, 3.3 and 6.3. For overlap with CO_2 the statistical model transmission based on fits to inte-

grated absorption by Howard et al. (loc. cit.) has the form:

$$T(m,p) = \exp\left(-\sqrt{\frac{1}{(km)^2} + \frac{1}{Lmp}}\right)$$

A.4 Water Vapor Atmospheric Distribution

Monthly zonal mean cross sections of specific humidity from 85^{o}N-16^{o}S, 1000-300 mb were provided by Dr. Eugene Rasmusson of the Geophysical Fluid Dynamics Laboratory, Princeton, New Jersey based on the M.I.T. General Circulation Data Library. To obtain the remaining S.H. profiles the corresponding month in the N.H. was reflected and adjusted for best fit near 15^{o}S (e.g. January N.H. was used for July S.H.). However, Starr et al. (1969) give annual zonal mean humidity profiles for the IGY (1958) which show there is less water vapor in the S.H. than in the N.H. From their annual zonal means, ratios for equivalent latitudes and pressures were derived (e.g. $[\bar{q}]_{20°N}/[\bar{q}]_{20°S}$ at 1000 mb). The annual S.H. reflected profiles were adjusted relative to the annual Northern Hemisphere M.I.T. profiles to agree with the ratios obtained from Starr et al. Equal adjustment was made for all reflected months. A value of .002 g/kg was used above 150 mb based on the observations by Mastenbrook (1968). Interpolation was accomplished by interpolating log (mixing ratio) in log (pressure).

B. Carbon Dioxide

B.1 Thermal Spectral Properties

Only the 15 μ band is considered and it is taken to have a width of 200 cm^{-1} centered near 667 cm^{-1}. The integrated absorption as given by Rodgers and Walshaw (loc. cit.) is:

$$A = \sum_{n=1}^{3} a_n u^{n/2} \qquad u < V$$

$$\sum_{n=0}^{3} b_n (\log u)^n \qquad u > V$$

$$u = \int c(p) \frac{p_s}{g} p \, dp$$

Here u is expressed in atm-cm and V delineates between weak and strong absorption.

B.2 Solar Visible Spectral Properties

No CO_2 absorption is considered in the visible spectrum.

B.3 Solar near Infrared Spectral Properties

Experimental fits to measured integrated absorption of entire bands (see Section III.A.3) have also been used for CO_2. The following CO_2 near infrared bands (in μ) have been evaluated: 1.4, 1.6, 2.0, 2.7, 4.3, 4.8 and 5.2.

B.4 Carbon Dioxide Atmospheric Distribution

CO_2 is considered well mixed through the whole atmosphere at 320 ppm.

C. Ozone

C.1 Thermal Spectral Properties

Below 200 mb the new random model of Malkmus (1967), fitted by Rodgers (1968) to the laboratory measurements of Walshaw (1957) for the 9.6 μ band, has been used with the Curtis-Godson approximation.

$$T(m,p) = \exp\left(-\frac{\pi\alpha_0 p}{2\delta}\left(\left(1+\frac{4Km}{\pi\alpha_0 p}\right)^{\frac{1}{2}}-1\right)\right)$$

$$u = \int c(p)\,\frac{p_s}{g}\,p\,dp \qquad (g\ cm^{-2})$$

$$m = \int c(p)\,\frac{p_s}{g}\,dp \qquad (g\ cm^{-2})$$

The Curtis-Godson approximation is quite good for H_2O and CO_2 but is known to be poor for the 9.6 μ band of O_3 (Walshaw and Rodgers 1963, Clark and Hitschfeld 1964). However, the amount of ozone below 200 mb is small and use of this approximation results in only minor errors in the thermal cooling of the troposphere.

A possible improvement of the Curtis-Godson approximation is to go to a higher parameter model. Hence above 200 mb the two path version of the random model (Rodgers 1968) has been used.

$$T(m_1,p_1,m_2,p_2) = \exp\left(\frac{2\pi\alpha_0}{\delta}\left(\beta_1+\beta_2-p_1-p_2\right)\right)$$

$$2\beta_i^2 = \rho_1^2(1+\gamma_1) + \rho_2^2(1+\gamma_2) \pm \sqrt{\left(\rho_1^2(1+\gamma_1) - \rho_2^2(1+\gamma_2)\right)^2 + 4\rho_1^2\rho_2^2\gamma_1\gamma_2}$$

$$\gamma_i = \frac{K m_i}{\pi \alpha_i}$$

To obtain a higher approximation than the Curtis-Godson approximation, the development by Goody (1964b) is followed. For a homogeneous path the optical depth is:

$$\tau_\nu = k_\nu m$$

where k_ν is the absorption coefficient and m is the amount of absorbing matter. For a single Lorentz line

$$K_\nu = \frac{S\alpha}{\pi(\nu^2+\alpha^2)}$$

where α is the Lorentz line width and S is the line intensity. Consider the cosine transform of the optical depth.

$$f(t) = \int_{-\infty}^{\infty} \tau_\nu \cos \nu t \, d\nu$$

For the Lorentz profile for a homogeneous path

$$f(t) = \bar{S}\,\bar{m}\,e^{-\bar{\alpha}t} \tag{3.2}$$

Where the bar refers to a homogeneous path. For a non-homogeneous path

$$f(t) = \int S\,e^{-\alpha t}\,dm \tag{3.3}$$

Matching the first two powers of t in the expansion of eqs. (3.2) and (3.3) we obtain the Curtis-Godson approximation.

$$\bar{S}\,\bar{m} = \int S\,dm$$

$$\bar{S}\,\bar{\alpha}\,\bar{m} = \int S\alpha\,dm$$

For two homogeneous paths in series at standard temperature ($S = \bar{S}$), the optical depth becomes:

$$\tau_\nu = \frac{\bar{S}\,\bar{\alpha}_1\,\bar{m}_1}{\pi(\nu^2+\alpha_1^2)} + \frac{\bar{S}\,\bar{\alpha}_2\,\bar{m}_2}{\pi(\nu^2+\alpha_2^2)}$$

The cosine transform is

$$f(t) = \bar{S}\,\bar{m}_1\,e^{-\bar{\alpha}_1 t} + \bar{S}\,\bar{m}_2\,e^{-\bar{\alpha}_2 t} \tag{3.4}$$

Expanding eqs. (3.3) and (3.4) in powers of t and matching terms we obtain

$$\begin{aligned}
\bar{S}\,\bar{m}_1 + \bar{S}\,\bar{m}_2 &= \int S\,dm \\
\bar{S}\,\bar{\alpha}_1\,\bar{m}_1 + \bar{S}\,\bar{\alpha}_2\,\bar{m}_2 &= \int S\alpha\,dm \\
\bar{S}\,\bar{\alpha}_1^2\,\bar{m}_1 + \bar{S}\,\bar{\alpha}_2^2\,\bar{m}_2 &= \int S\alpha^2\,dm \\
\bar{S}\,\bar{\alpha}_1^3\,\bar{m}_1 + \bar{S}\,\bar{\alpha}_2^3\,\bar{m}_2 &= \int S\alpha^3\,dm
\end{aligned} \tag{3.5}$$

If we neglect temperature variations of the line intensity, note that $\alpha/\alpha_o = \rho$ and define

$$M \equiv \int dm \qquad U \equiv \int \rho\,dm$$

$$V \equiv \int \rho^2\,dm \qquad W \equiv \int \rho^3\,dm$$

then eqs. (3.5) can be written as:

$$\begin{aligned}
\bar{m}_1 + \bar{m}_2 &= M \\
\bar{\rho}_1\,\bar{m}_1 + \bar{\rho}_2\,\bar{m}_2 &= U \\
\bar{\rho}_1^2\,\bar{m}_1 + \bar{\rho}_2^2\,\bar{m}_2 &= V \\
\bar{\rho}_1^3\,\bar{m}_1 + \bar{\rho}_2^3\,\bar{m}_2 &= W
\end{aligned}$$

This is a nonlinear system of equations which must be solved for $\bar{m}_1$, $\bar{\rho}_1$, $\bar{m}_2$, $\bar{\rho}_2$. Fortunately this system reduces to a quadratic in $\bar{\rho}$.

$$(U\bar{P}_i - V)^2 = (M\bar{P}_i - U)(V\bar{P}_i - W)$$

Goody (1964b) employed a three-parameter model for ozone and found a factor of 3 to a factor of 12 decrease in errors compared to the Curtis-Godson approximation. Although the four parameter model has not been extensively tested, it seems reasonable to anticipate significant improvement over the Curtis-Godson approximation.

C.2 Solar Visible Spectral Properties

Ozone absorption in the visible and ultraviolet is based on absorption data given by Inn and Tanaka (1953) and Vigroux (1953).

C.3 Solar Near Infrared Spectral Properties

No absorption by ozone is considered in the near infrared.

C.4 Ozone Atmospheric Distribution

Monthly mean cross sections along 75°W from 85°-9°N have been graciously provided by Mr. Wayne Hering based on observations of the North America Ozone Network for the 5 year period 1963-1967. In Table I are listed the 8 stations from which cross sectional data have been derived.

Table I

North American ozone stations which were used to construct ozone cross sections.

Canal Zone	9.0°N	79.6°W
Grand Turk	21.5°N	71.1°W
Cape Kennedy	28.5°N	80.5°W
Tallahassee	30.4°N	84.3°W
Wallops Island	37.8°N	75.3°W
Bedford	42.5°N	71.3°W
Goose Bay	53.3°N	60.4°W
Thule	76.5°N	68.8°W

In general observations were not available above 10 mb and Hering et al. (1967) point out that individual ascents are calibrated against total ozone measurements by assuming the ozone mixing ratio above 10 mb is constant. The small number of balloon measurements above 30 km generally support the constant mixing ratio assumption. It was also assumed in this study that the mixing ratio above 10 mb was constant. However, recent rocket measurements (Hilsenrath et al. 1969 and Krueger 1969) found the peak ozone mixing ratio to be centered near 34 km. In addition, Hilsenrath et al. show a decrease of the mixing ratio above 34 km with a secondary peak at 62 km. Clearly more ozone measurements are urgently needed above the balloon bursting altitudes.

There have been very few measurements made of the vertical distribution of ozone in the S.H. and to obtain S.H. profiles the corresponding N.H. values were reflected for use in the S.H. (e.g. January N.H. was used for July S.H.). However, there are significant seasonal variations between the hemispheres as is seen in the global distribution of total ozone (Fig. 1) which shows clearly the asymmetry of the hemispheres. The global distribution of total ozone was compiled from monthly mean Umkehr measurements along 75°W which were obtained from the publications of Ozone Data for the World (Meteorological Service of Canada, 1960-1968) and represent 2-9 year averages. Ratios of total ozone for equivalent latitudes of the reflected month and the S.H. month (e.g. 20°N January, 20°S July) were derived and used to adjust the reflected N.H. vertical profiles. Equal adjustment was made at all pressure levels. Global seasonal cross sections of ozone are presented in Figs. 2-5.

D. Molecular Oxygen

D.1 Solar Near Infrared Properties

Only the .76 μ band has been evaluated. The integrated absorption has the same form as in Section III A.3 based on observations by Houghton (1963).

D.2 Molecular Oxygen Atmospheric Distribution

O_2 is taken to have a constant mixing ratio at the standard value.

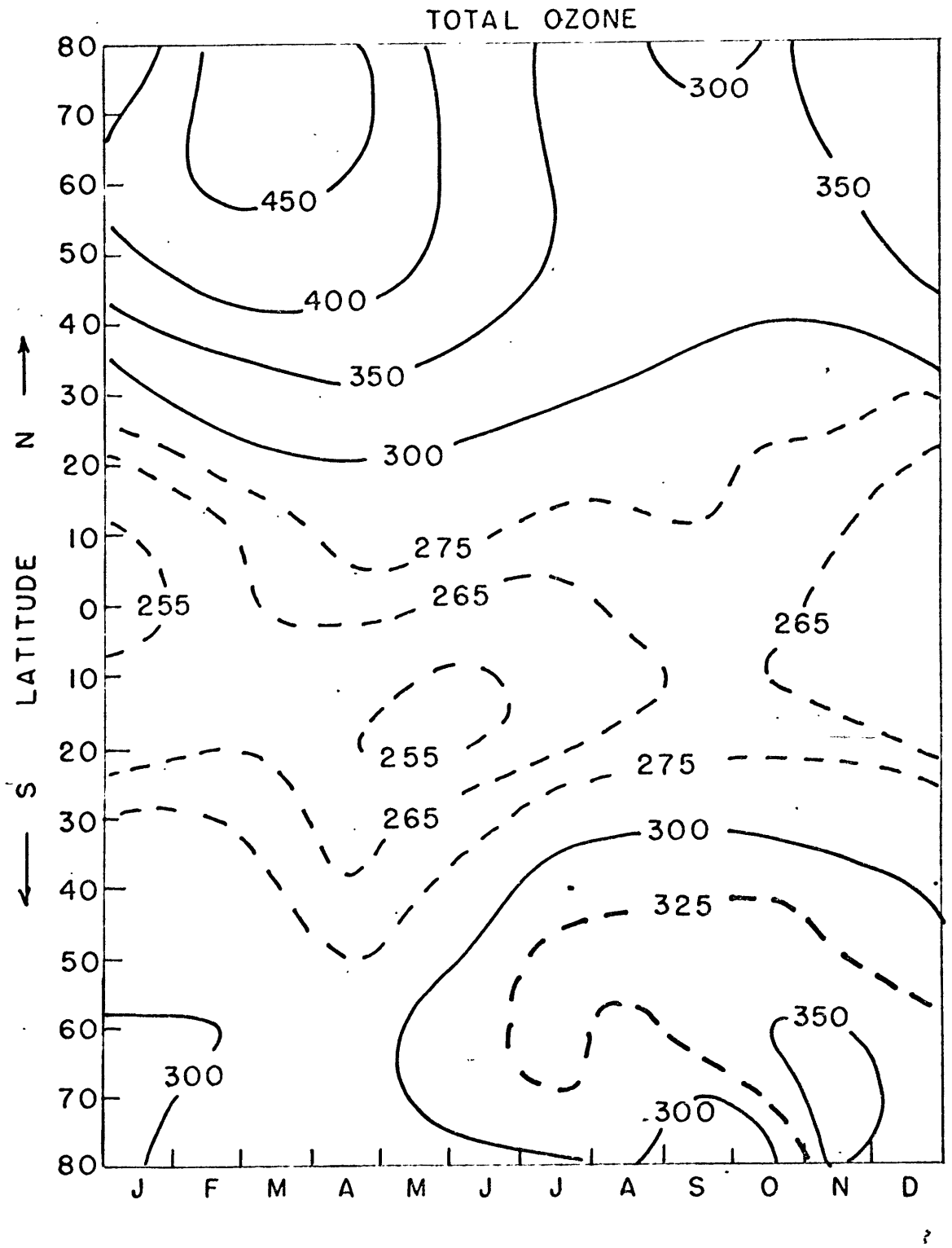
TOTAL OZONE
80
70
60
50
40
30
20
10
0
10
20
30
40
50
60
70
80
N
S
LATITUDE
300
350
450
400
350
300
275
265
255
265
255
275
265
300
325
350
300
300
J
F
M
A
M
J
J
A
S
O
N
D

Figure 1.

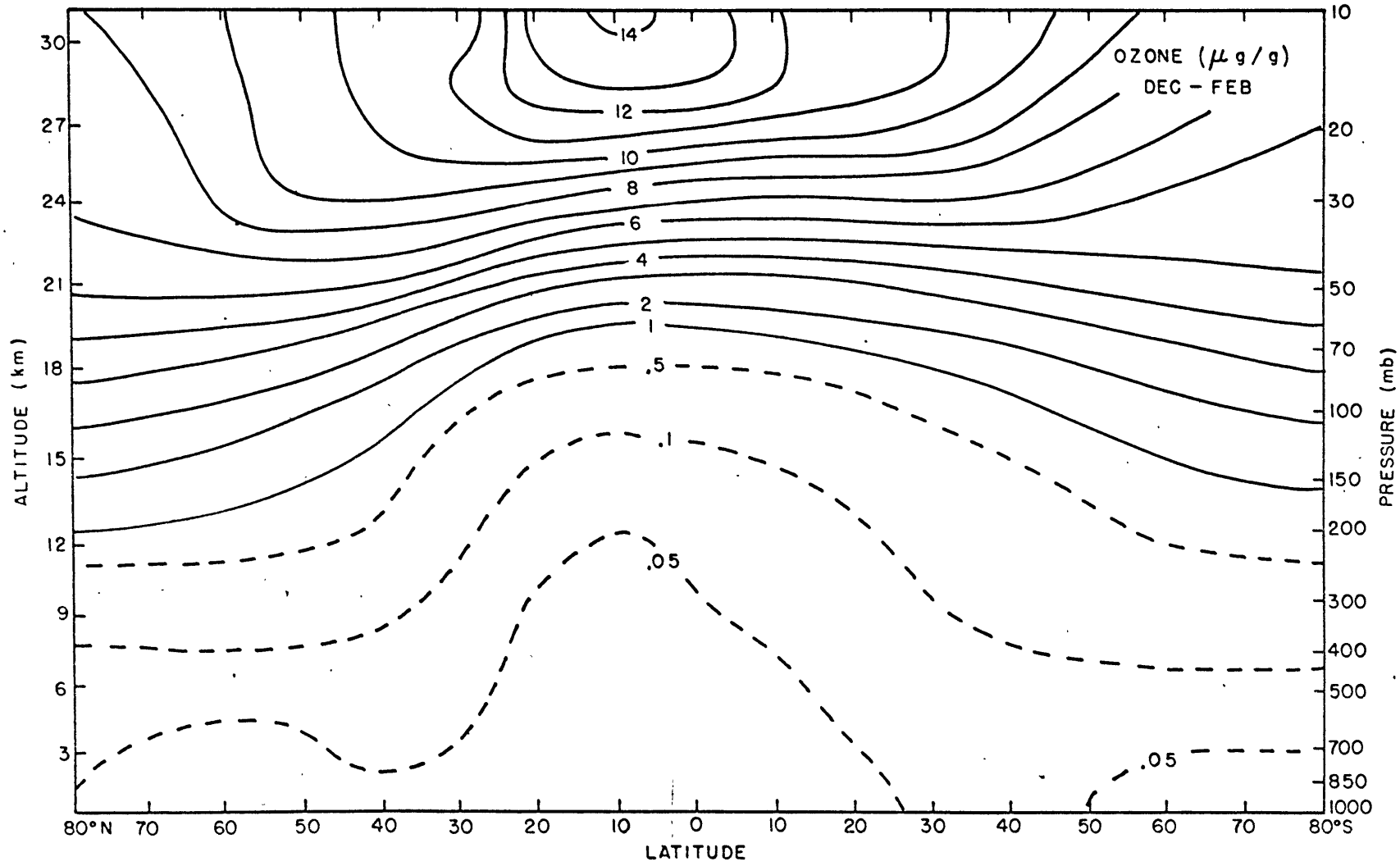
OZONE (μg/g)
DEC - FEB
14
12
10
8
6
4
2
1
.5
.1
.05
.05
ALTITUDE (km)
PRESSURE (mb)
30
27
24
21
18
15
12
9
6
3
10
20
30
50
70
100
150
200
300
400
500
700
850
1000
80°N 70 60 50 40 30 20 10 0 10 20 30 40 50 60 70 80°S
LATITUDE

Figure 2.

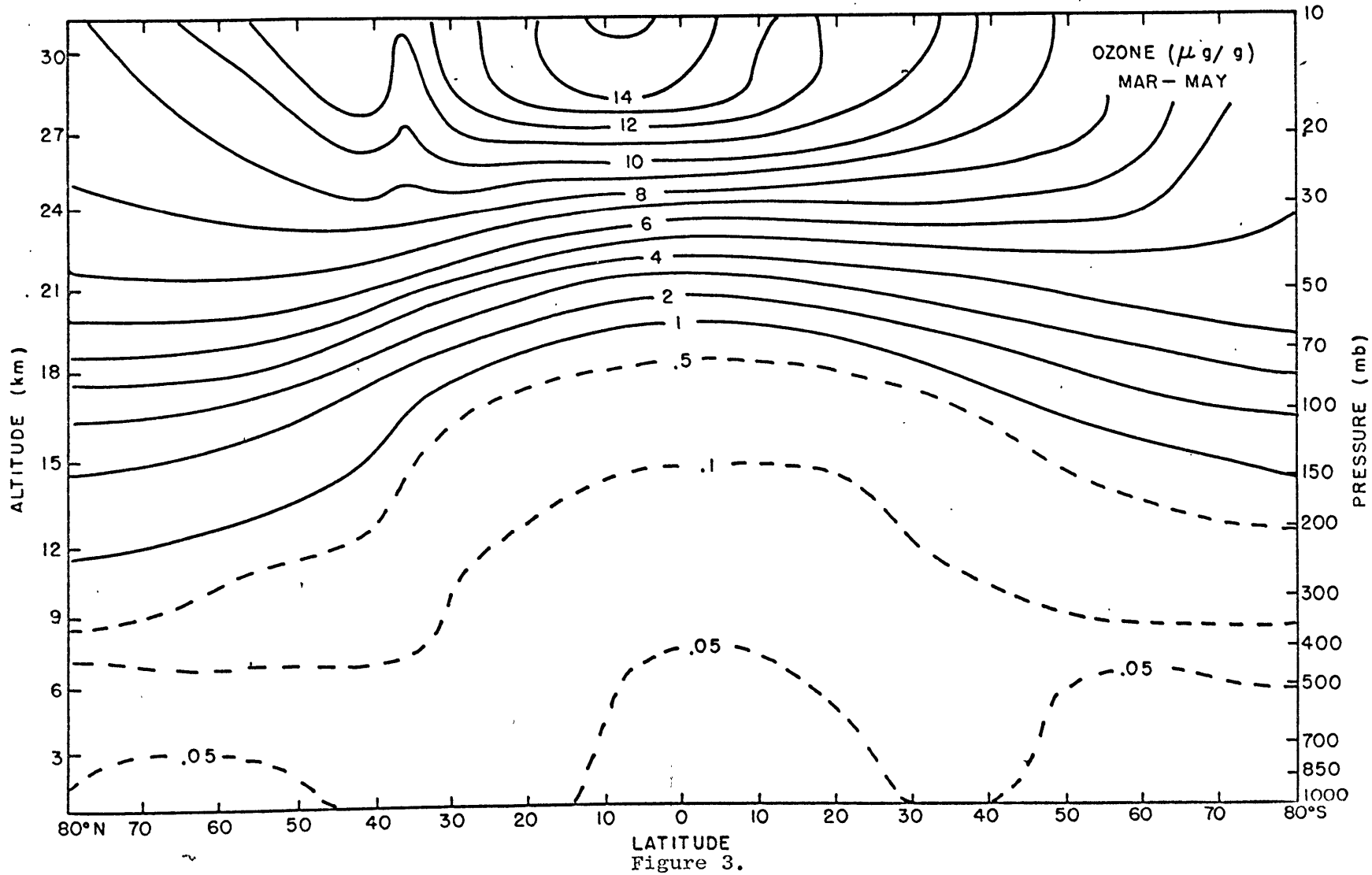
OZONE (μg/g)
MAR – MAY
14
12
10
8
6
4
2
1
.5
.1
.05
.05
.05
ALTITUDE (km)
30
27
24
21
18
15
12
9
6
3
PRESSURE (mb)
10
20
30
50
70
100
150
200
300
400
500
700
850
1000
80°N 70 60 50 40 30 20 10 0 10 20 30 40 50 60 70 80°S
LATITUDE

Figure 3.

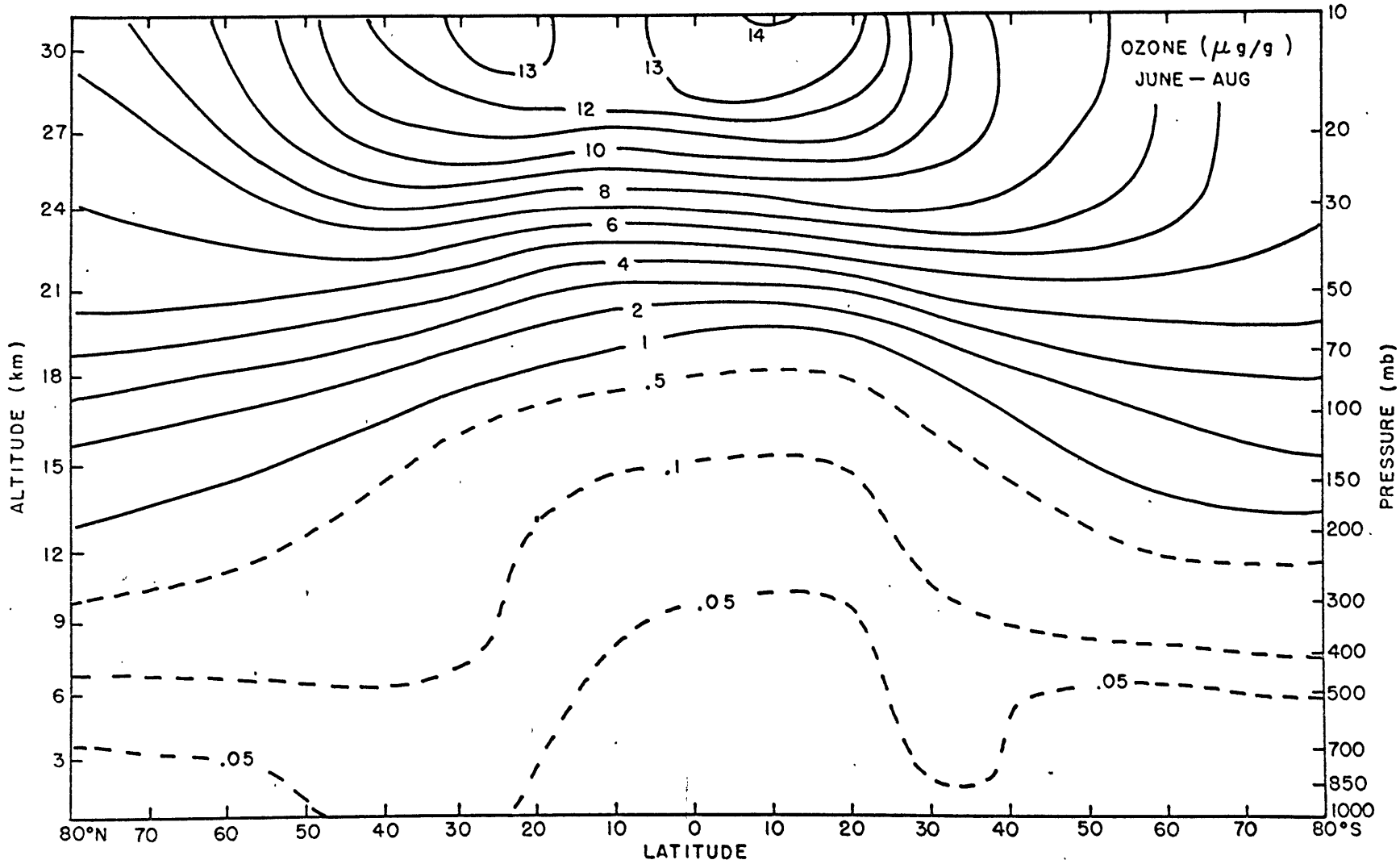
OZONE (μg/g)
JUNE — AUG
ALTITUDE (km)
PRESSURE (mb)
LATITUDE
80°N 70 60 50 40 30 20 10 0 10 20 30 40 50 60 70 80°S
30 27 24 21 18 15 12 9 6 3
10 20 30 50 70 100 150 200 300 400 500 700 850 1000
14
13
13
12
10
8
6
4
2
1
.5
.1
.05
.05
.05

Figure 4.

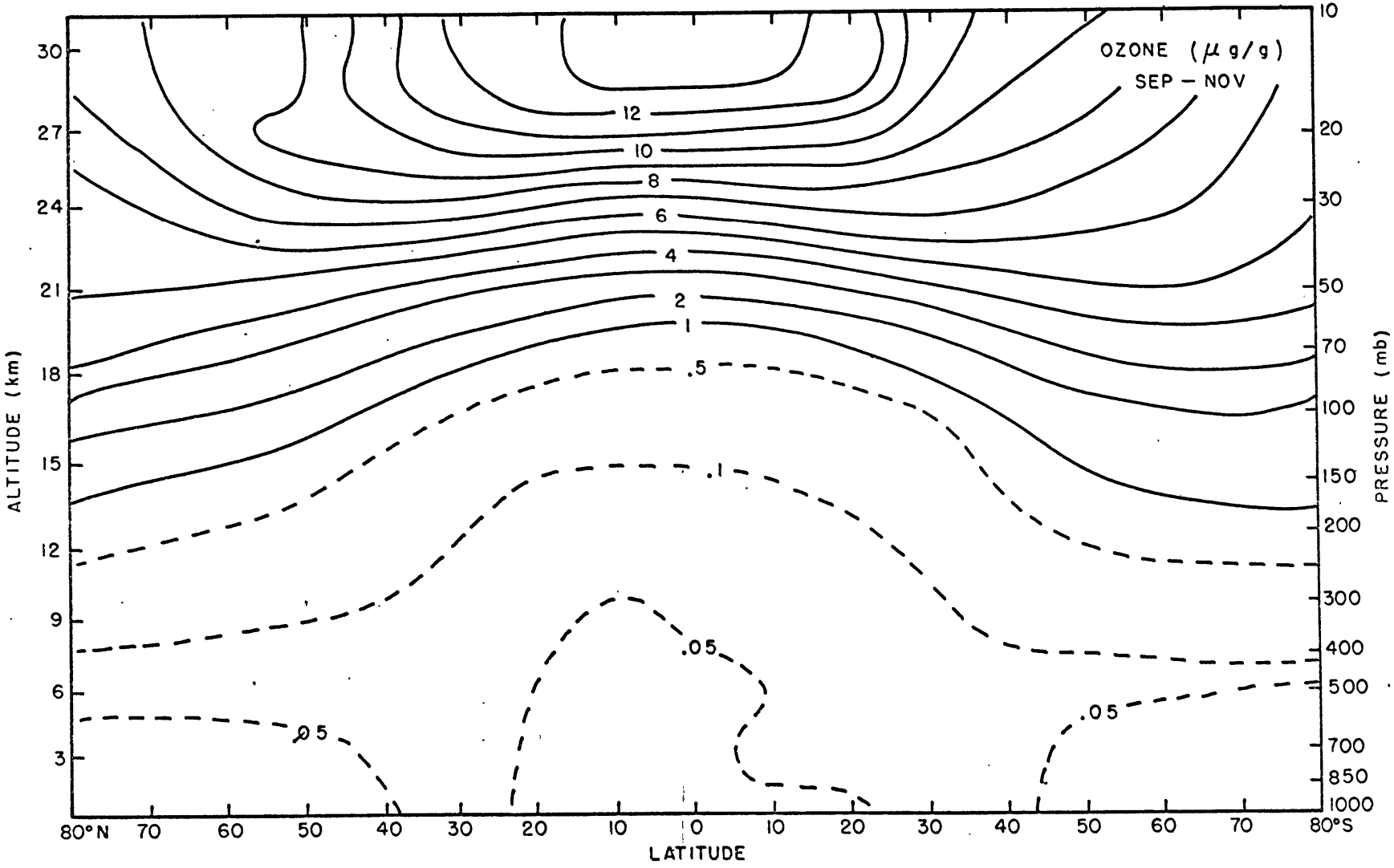
OZONE (μ g/g)
SEP – NOV
12
10
8
6
4
2
1
.5
.1
.05
.05
.05
ALTITUDE (km)
30
27
24
21
18
15
12
9
6
3
PRESSURE (mb)
10
20
30
50
70
100
150
200
300
400
500
700
850
1000
80°N 70 60 50 40 30 20 10 0 10 20 30 40 50 60 70 80°S
LATITUDE

Figure 5.

E. Temperature

E.1 Atmospheric Distribution

Monthly zonal mean temperature profiles were constructed from several sources which are listed below.

a) 85°N-35°N, 100-150 mb: 5 year zonal averages were obtained from the M.I.T. General Circulation Data Library.

b) 30°N-30°S, 1000-20 mb: 6 year zonal averages were derived from Newell et al. (1970b).

c) 40°S-80°S, 1000-20 mb: Zonal averages were derived from the U.S. Navy Marine Climatic Atlas of the World, Vol. VII, Antarctic (1965) representing $\sim$ 5-10 year averages.

d) 85°N-20°N, 100-10 mb: 2 year zonal averages were derived by combining the results of Richards (1967) with present results.

e) 85°N-30°S, 5-.1 mb: Monthly mean cross sections were derived by Mrs. D. Berry at M.I.T. based on observations of the Meteorological Rocket Network (1963-1967) and rocket grenade data (Smith et al. 1960-1966, Muller 1964, Rofe 1968).

f) 40°S-80°S, 5-.1 mb: N.H. values were reflected for corresponding S.H. month and adjusted for best continuity with 20 mb temperatures.

Six-year averages were used in the tropics to reduce any bias that might be introduced by the quasi-biennial oscillation. Global seasonal cross sections of temperature are presented in Figs. 6-9.

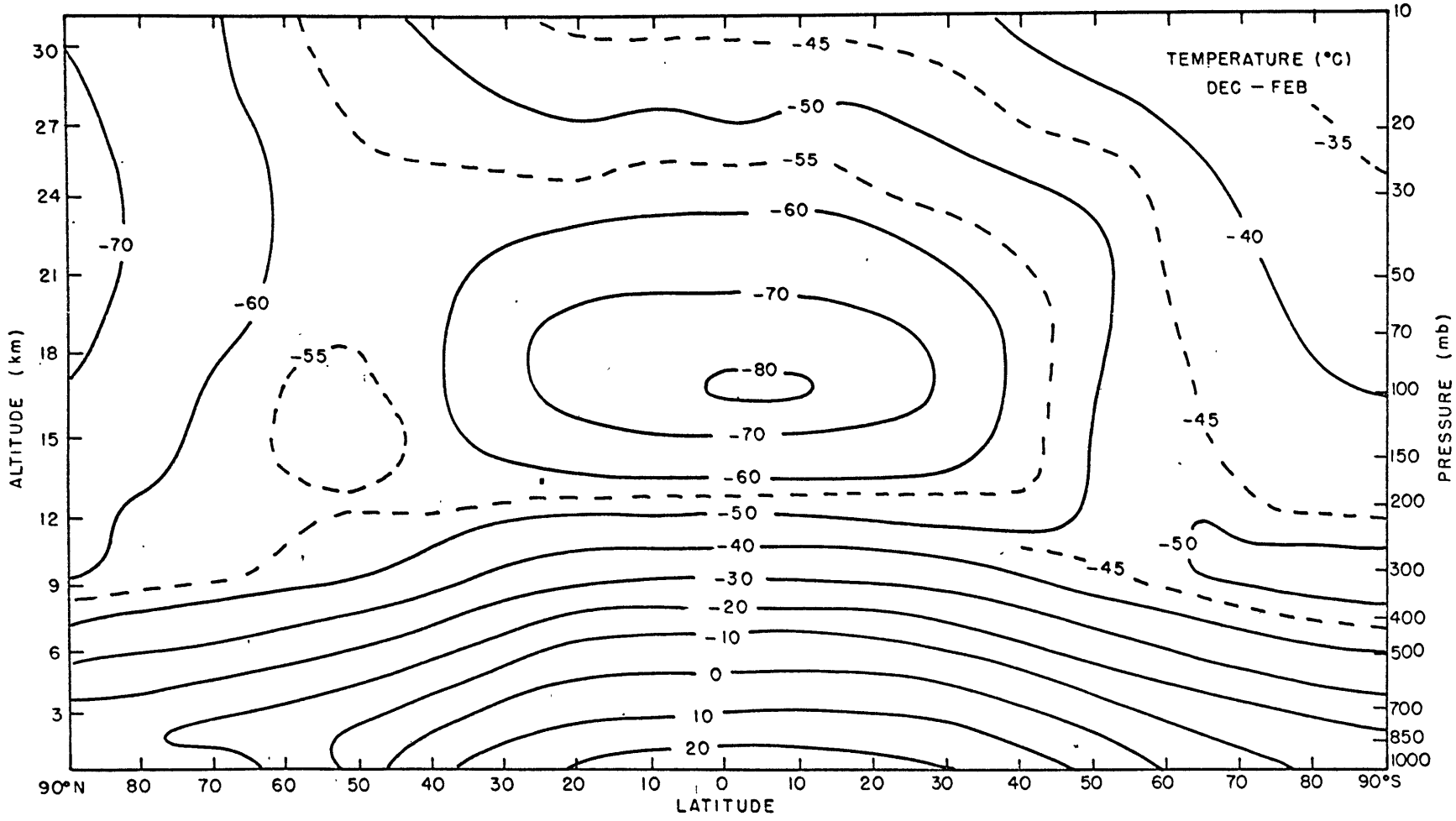
TEMPERATURE (°C)
DEC – FEB
ALTITUDE (km)
PRESSURE (mb)
LATITUDE
90°N
90°S
-45
-50
-55
-60
-70
-80
-35
-40
-30
-20
-10
0
10
20

Figure 6.

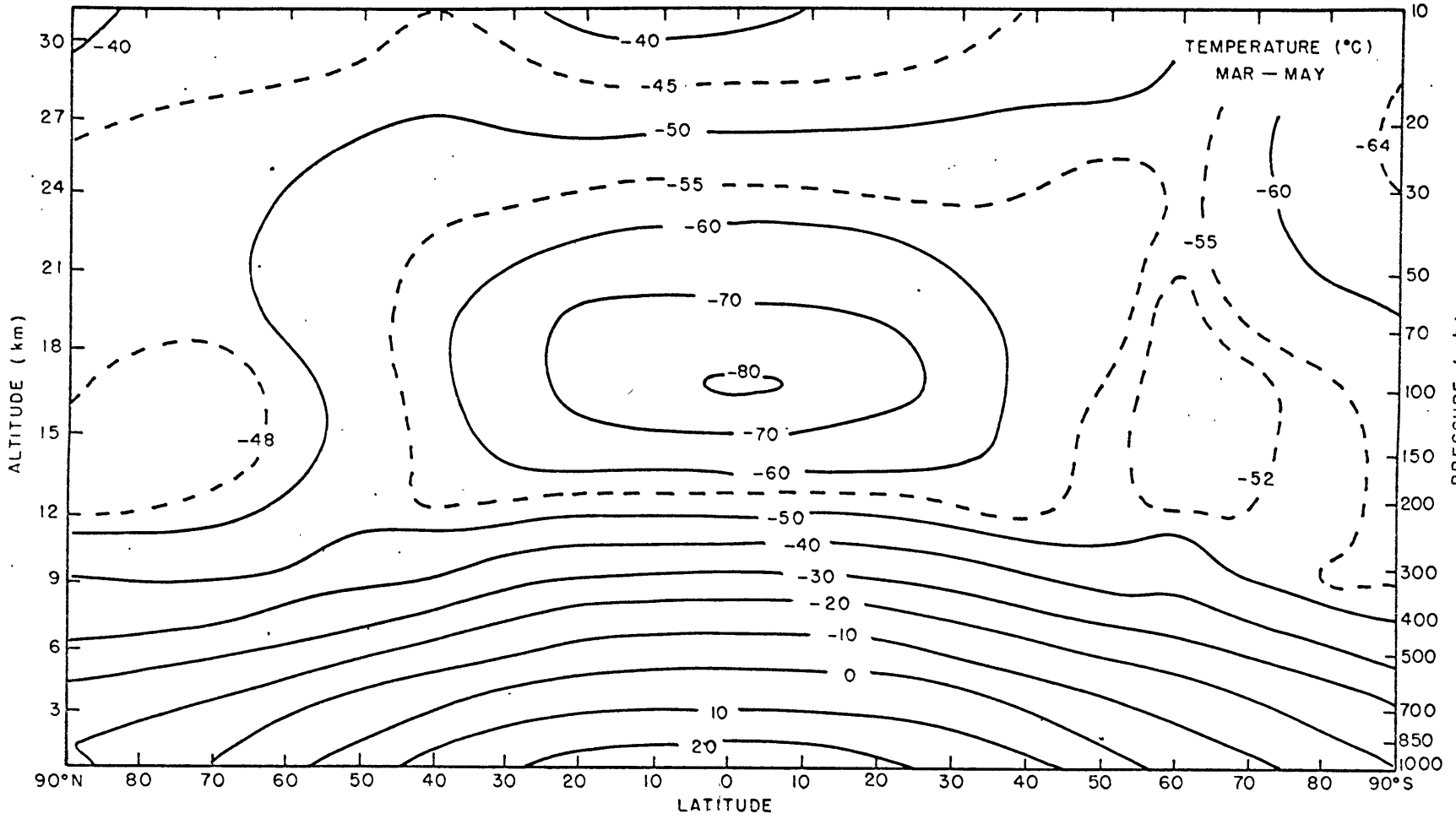
TEMPERATURE (°C)
MAR — MAY
-40
-45
-50
-55
-60
-70
-80
-48
-64
-52
ALTITUDE (km)
PRESSURE (mb)
30
27
24
21
18
15
12
9
6
3
10
20
30
50
70
100
150
200
300
400
500
700
850
1000
90°N 80 70 60 50 40 30 20 10 0 10 20 30 40 50 60 70 80 90°S
LATITUDE

Figure 7.

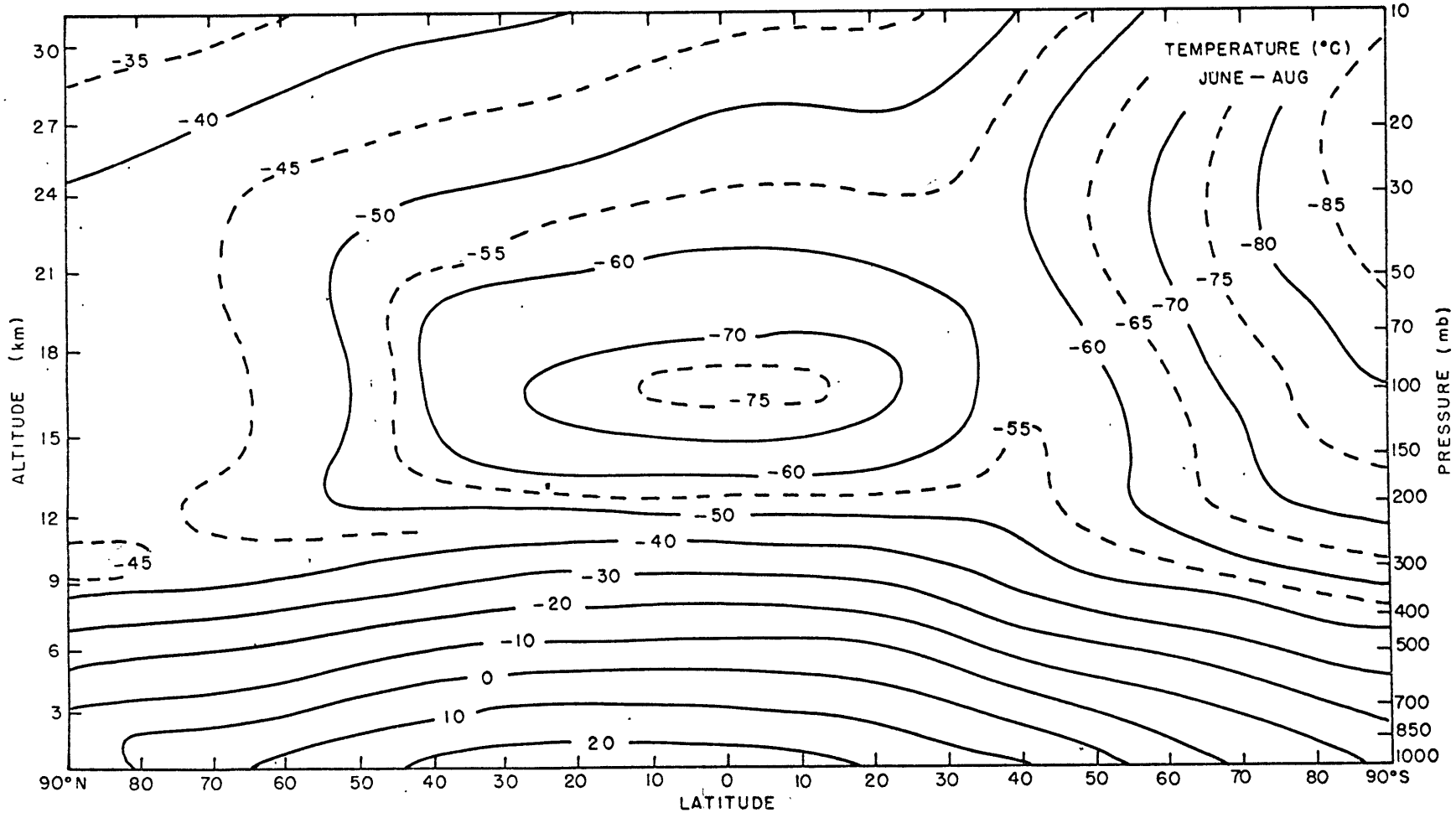
TEMPERATURE (°C)
JUNE — AUG
ALTITUDE (km)
PRESSURE (mb)
LATITUDE
90°N
90°S
-35
-40
-45
-50
-55
-60
-70
-75
-65
-80
-85
-30
-20
-10
0
10
20

Figure 8.

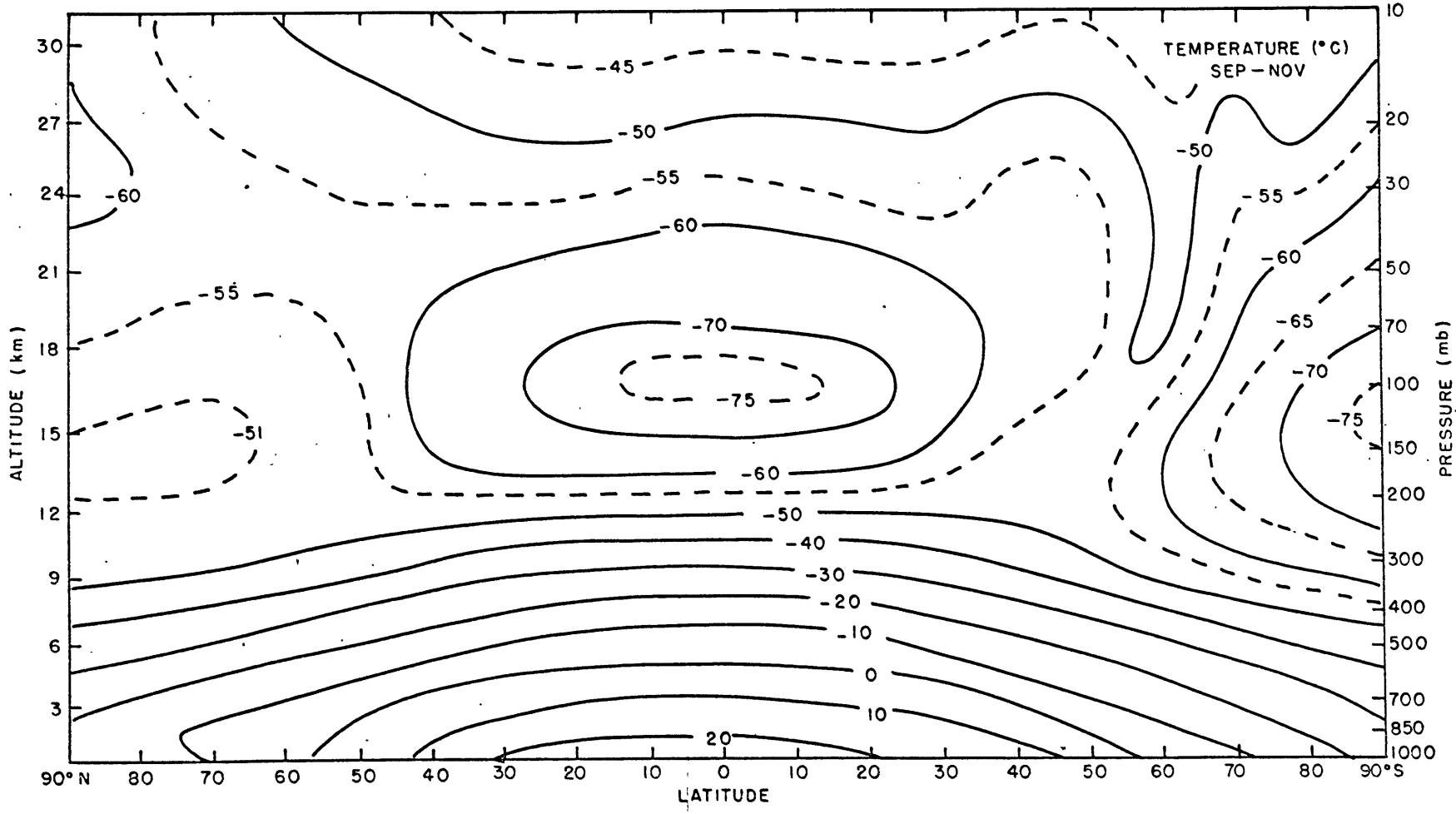
TEMPERATURE (°C)
SEP – NOV
ALTITUDE (km)
PRESSURE (mb)
LATITUDE
90° N
90° S
-45
-50
-55
-60
-70
-75
-51
-40
-30
-20
-10
0
10
20
-65

Figure 9.

F. Clouds.

F.1 Thermal Spectral Properties

All of the available cloud information has been assembled into three general classes: high, middle and low clouds. This classification is expanded upon in Section III F.4 below. Low and middle clouds are assumed to be black bodies and are allowed for by setting the temperatures beyond a cloud surface equal to the temperature at the cloud surface. High clouds are assumed to 50% black.

F.2 Solar Visible Properties

High, middle and low clouds are assumed to scatter but not absorb at wavelengths $< .7\,\mu$. The following transmissivities and reflectivities are assumed:

	Transmissivity	Reflectivity
High	.79	.21
Middle	.46	.54
Low	.34	.66

These values were rather arbitrarily chosen from the values given by Rodgers (1967a). It is known that the reflectivity is a function of wavelength, solar zenith angle and the cloud optical thickness. The values chosen here represent a gross parameterization but with so few observations and the lack of a directly applicable theoretical development, there remained little else that could be done.

F.3 Solar Near Infrared Properties

The following transmissivities, absorptivities and reflectivities are assumed.

	Transmissivity	Reflectivity	Absorptivity
High	.77	.19	.04
Middle	.34	.46	.20
Low	.20	.50	.30

F.4 Atmospheric Distribution of Clouds

Cloud information suitable for use in radiative flux computations is very scarce due partly to the problems in global observations and partly due to the many varieties of cloud distributions that occur. Prior to satellite observations studies of cloud distributions were based solely on surface observations (e.g. London 1957, Telegas and London 1954). Satellite observations are now giving global observations of sky cover but vertical resolution is in general still lacking. One attempt at inferring the vertical distribution of clouds from satellite photographs has been made by Mr. Richard Cram at the University of Wisconsin using digitized ESSA photographs from the National Environmental Satellite Center (NESC), Washington, D.C. These digitized ESSA photographs were computer grided by NESC on polar stereographic and mercator projections to give global coverage. Mr. Cram subjectively analyzed the photographs over 10^{o} squares for total sky cover for selected days during December, 1967-November, 1968. The percentage of high, middle and low clouds was also estimated

based on brightness. However, the gray range is small and the percentage of high clouds is probably underestimated. Thirty-six squares were analyzed within a latitude band and the poleward limit of analysis was determined by the amount of sunlight, being 60^{o} for the summer hemisphere and 40^{o} for the winter hemisphere. Data sampling was random within a month with about 7-11 days sampled per month, giving approximately 252-396 observations per month within a latitude circle. Dr. Thomas Vonder Haar graciously made this data available to the author and the Wisconsin data has been used extensively in the flux computations.

To obtain total cloud cover in the N.H. high latitudes, monthly hemispheric maps of total sky cover for the N.H. (70^{o}N-10^{o}N) for 1964 were used. These cloud data were derived from TIROS VII and VIII nephanalyses and were kindly provided by the Environmental Technical Applications Center, USAF. The maps were further analyzed on polar stereographic maps to obtain estimates of total cloud cover from 75^{o}N-85^{o}N. Gridpoint data were obtained at every 10^{o} longitude and zonal averages computed. For high latitudes in the S.H., the zonal mean amounts of total cloud cover given by Gabities (1960) were used. The global zonal mean cloud amounts are presented in Fig. 10.

London's (loc. cit.) study was used to distribute the total cloud cover into amounts of high, middle and low cloud wherever Wisconsin data was absent. London's results were taken to apply to January, April, July and October and interpolation was accomplished for the remaining months. The cloud bases and tops were partially

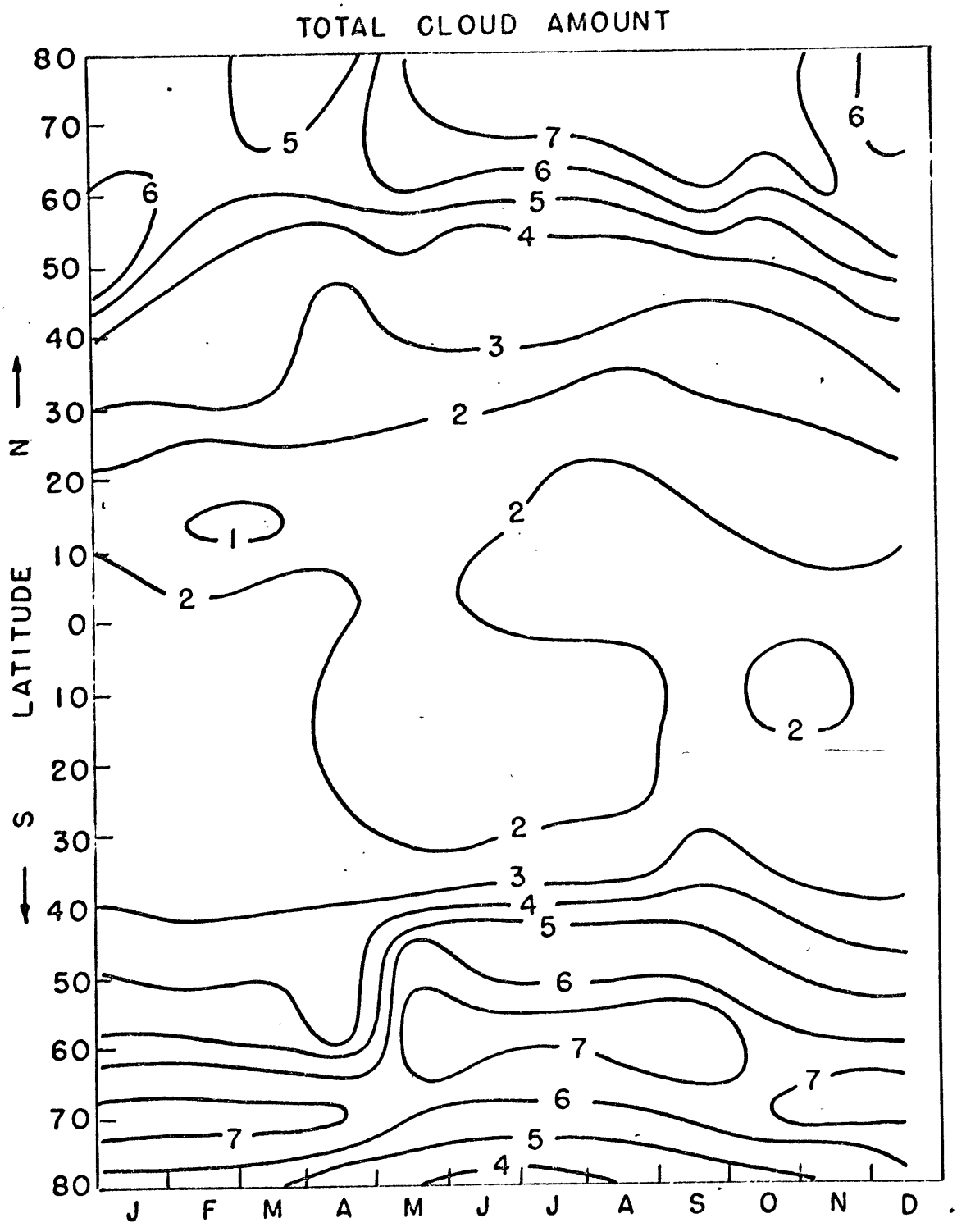
TOTAL CLOUD AMOUNT
80
70
60
50
40
30
20
10
0
10
20
30
40
50
60
70
80
N
LATITUDE
S
J F M A M J J A S O N D
1
2
3
4
5
6
7

Figure 10.

taken from London by assuming that low clouds have the same bases as 'stratus' clouds and middle clouds have the same bases as 'altostratus' clouds. Equatorwards of 50^{o} low and middle clouds are assumed to be 150 and 100 mb thick and polewards of 50^{o} low and middle clouds are assumed to be 100 and 50 mb thick. N.H. cloud bases and tops were reflected for use in the S.H. A summary of observations of cirrus clouds in the Handbook of Geophysics (1961) indicates that the height of cirrus clouds follows the height of the tropopause with the largest frequency of cirrus occurring below the tropopause. Monthly mean tropopause heights were obtained from 85^{o}N-80^{o}S using daily IGY cross sections of temperature along 75^{o}W for 1958 and cirrus tops were taken to be 50 mb below the tropopause. Cirrus clouds were assumed to have a thickness of 50 mb.

G. Diffuse Radiation

In order to evaluate the transmission function (eq. 2.1) it is necessary to integrate over all zenith angles to take account of all diffuse flux arriving at level z. Expanding E_{i3} in eq. (2.1), $T_r(z,z')$ can be written as:

$$T_r(z,z') = 2\int_0^{\pi/2} T_r(z,z',\theta)\,\sin\theta\cos\theta\,d\theta$$

$$T_r(z,z',\theta) = \frac{1}{\Delta\nu_r}\int_{\Delta\nu_r} T_\nu(z,z',\theta)\,d\nu$$

Using the Curtis-Godson approximation

$$T_r(z, z', \theta) \cong \overline{\overline{T}}_r(m \sec\theta, u)$$

where $\overline{\overline{T}}_r$ is the band model transmission and m and u are given by eq. (3.1). The Elsasser (1942) approximation is used here to carry out the integration over all zenith angles to give:

$$T_r(z, z') = \overline{\overline{T}}_r(1.66m, u)$$

Rodgers and Walshaw (loc. cit.) indicate this approximation gives a maximum relative error in the cooling rate of about 1.5%.

H. Magnification Factor

The magnification factor was taken from Rodgers (1967a)

$$M = \frac{35 \sec\psi}{\sqrt{1224 + (\sec\psi)^2}}$$

where ψ is the solar zenith angle. The limit $M \longrightarrow 35$ as $\sec\psi \longrightarrow \infty$ is approximately correct for a scale height of 8 km and no refraction. The integration over sun angle was done by integrating from noon to sunset and doubling the results.

I. Surface Albedo

The surface albedos were taken from Sellers (1965) and are listed below.

Lat.	80N	70	60	50	40	30	20	10	0
Albedo	.54	.35	.18	.13	.11	.10	.10	.09	.07

Lat.	80S	70	60	50	40	30	20	10	0
Albedo	.75	.40	.19	.12	.07	.08	.08	.08	.07

J. Earth-Sun Distance

The monthly mean earth-sun distances obtained from the Smithsonian Tables (1951) have been included in the computations.

K. Solar Scattering from Clouds and Ground

Reflected and transmitted solar flux from clouds and the ground is assumed to be diffuse and the Elsasser diffuse approximation (see Section III G.) is used to compute the diffuse transmissivity. In the solar radiation computations the solar beam is followed through the atmosphere and wherever a cloud boundary is encountered the solar beam is resolved into three components: a direct transmitted beam, diffuse transmitted radiation and diffuse reflected radiation. Clouds are allowed for by weighing the three components by the fraction of sky cover.

IV. Computations of Radiative Heating for the Global Atmosphere

It is obvious from Section III that total radiative heating is a complicated function of the radiative parameters and that in order to understand total radiative heating it is necessary to understand the contribution by each radiative constituent. For this reason seasonal profiles of radiative heating for each constituent are examined prior to examining the field of total radiative heating. The seasonal profiles were obtained by averaging the monthly results which form each season.

A. Thermal Cooling

A.1 Water Vapor

Presented in Figs. 11 and 12 is the global thermal cooling by water vapor for December-February and June-August. The 9.6 μ (970-1100 cm^{-1}) and the 15 μ (567-767 cm^{-1}) bands were substracted out of the integration over the water vapor spectrum and are presented separately in a later section of this paper.

It is readily seen that water vapor acts to cool the atmosphere everywhere which is due to an increase of thermal flux with height. The computed thermal flux was not separated into the upward and downward components but observations in the troposphere (Kondratiev loc. cit.) show that the downward flux decreases with height faster than the upward flux decreases with height. Maximum cooling occurs in the troposphere in low latitudes for both seasons associated with

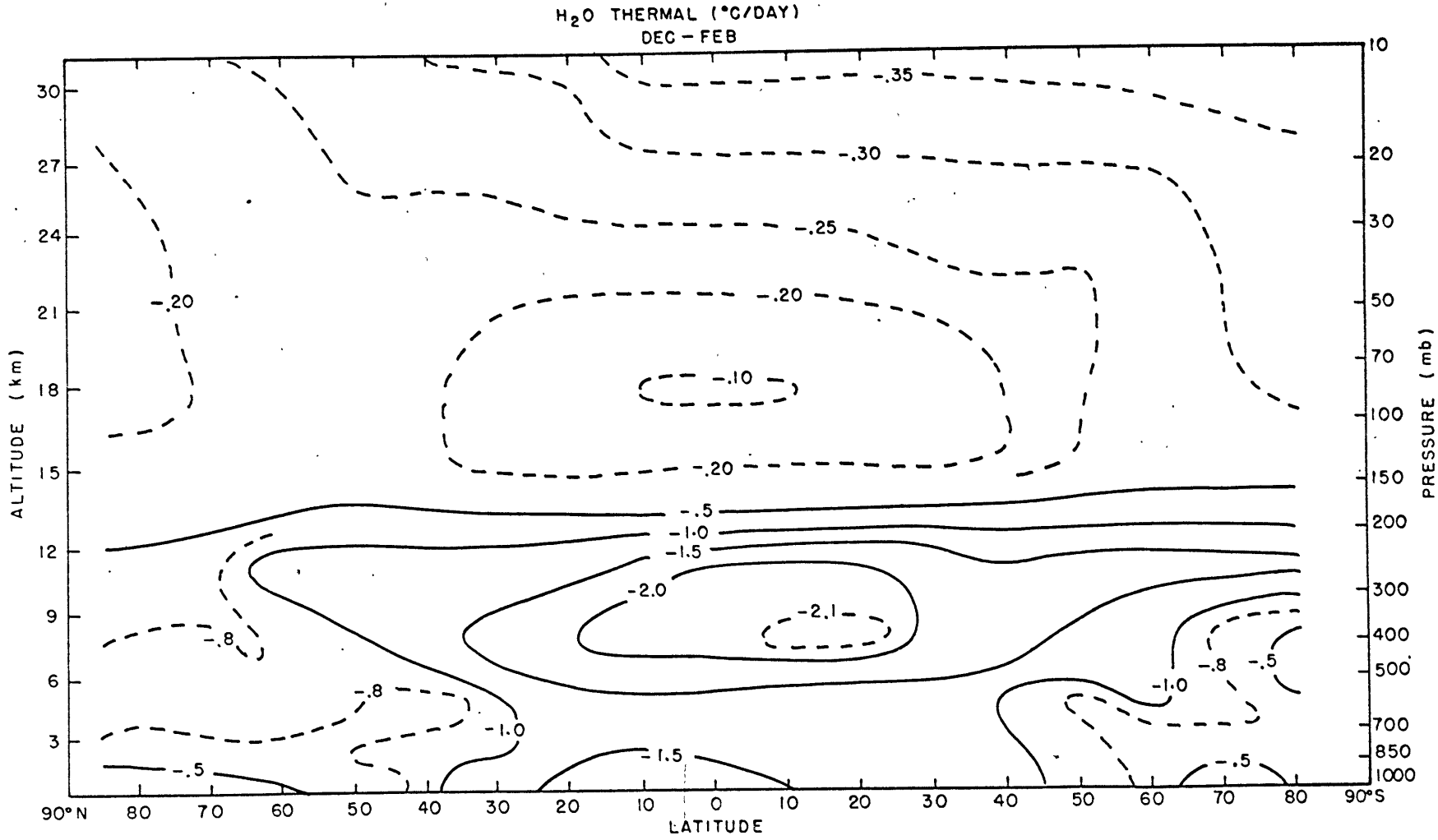
H_2O THERMAL (°C/DAY)
DEC – FEB
ALTITUDE (km)
PRESSURE (mb)
LATITUDE
90°N
90°S
-.35
-.30
-.25
-.20
-.10
-.5
-1.0
-1.5
-2.0
-2.1
-.8

Figure 11.

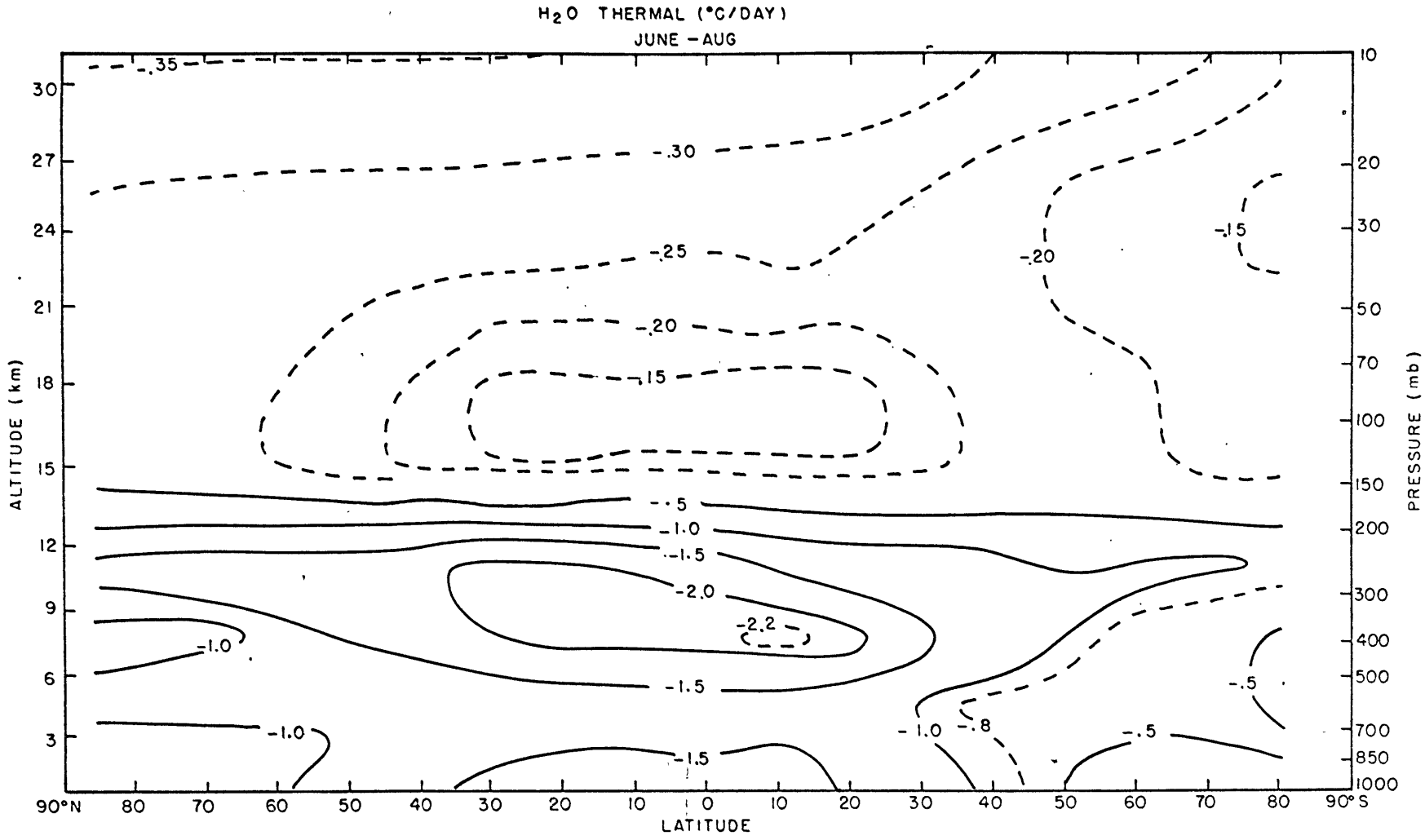
H_2O THERMAL (°C/DAY)
JUNE – AUG
ALTITUDE (km)
PRESSURE (mb)
LATITUDE
90°N
90°S
-.35
-.30
-.25
-.20
-.15
-.5
-1.0
-1.5
-2.0
-2.2
-.8

Figure 12.

the large vertical gradients of water vapor and temperature. Relative minima of cooling are also found in the troposphere because of the influence of clouds with increased cooling above a cloud and decreased cooling below a cloud. An example of enhanced cooling above clouds is the cooling in the upper troposphere (above 400 mb) in middle and high latitudes in the summer hemisphere where high latitude cloudiness radiates at temperatures much lower than the warmer lower troposphere.

Above 200 mb thermal cooling by water vapor follows closely the temperature field. Of notable interest are the minimum cooling rates in the vicinity of the tropical tropopause due to the warmer temperatures above and below the tropopause with the smallest cooling rates occurring for the colder tropopause in December-February. Above the tropical tropopause the temperature increases with height as does the cooling rate. Note also for the high latitude stratosphere ($<$ 100 mb) that the S.H. summer is warmer than the N.H. summer and this results in more cooling in the former. In the winter the situation is reversed and less cooling occurs in the S.H. winter stratosphere.

A.2 Ozone

Presented in Figs. 13 and 14 is the global thermal cooling by the 9.6μ band of ozone for December-February and June-August. Overlap with water vapor is taken into account so that the cooling in the troposphere is actually due to water vapor. The dominant characteristic for both seasons is the thermal heating above the tropical tropopause associated with the large vertical gradients of the ozone

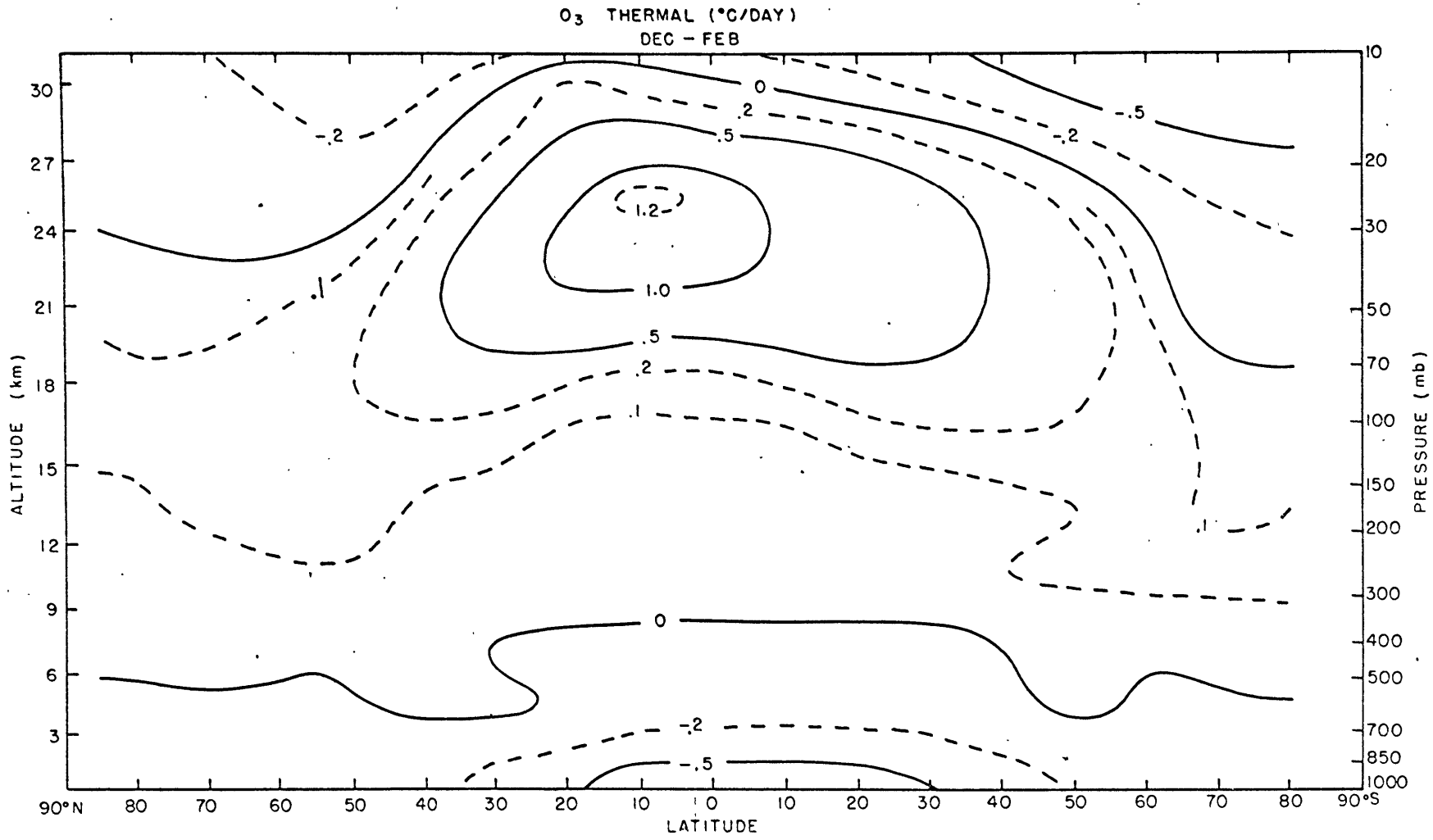
O_3 THERMAL (°C/DAY)
DEC - FEB
ALTITUDE (km)
PRESSURE (mb)
LATITUDE
90°N
90°S
0
.2
.5
-.2
-.5
1.2
1.0
.1

Figure 13.

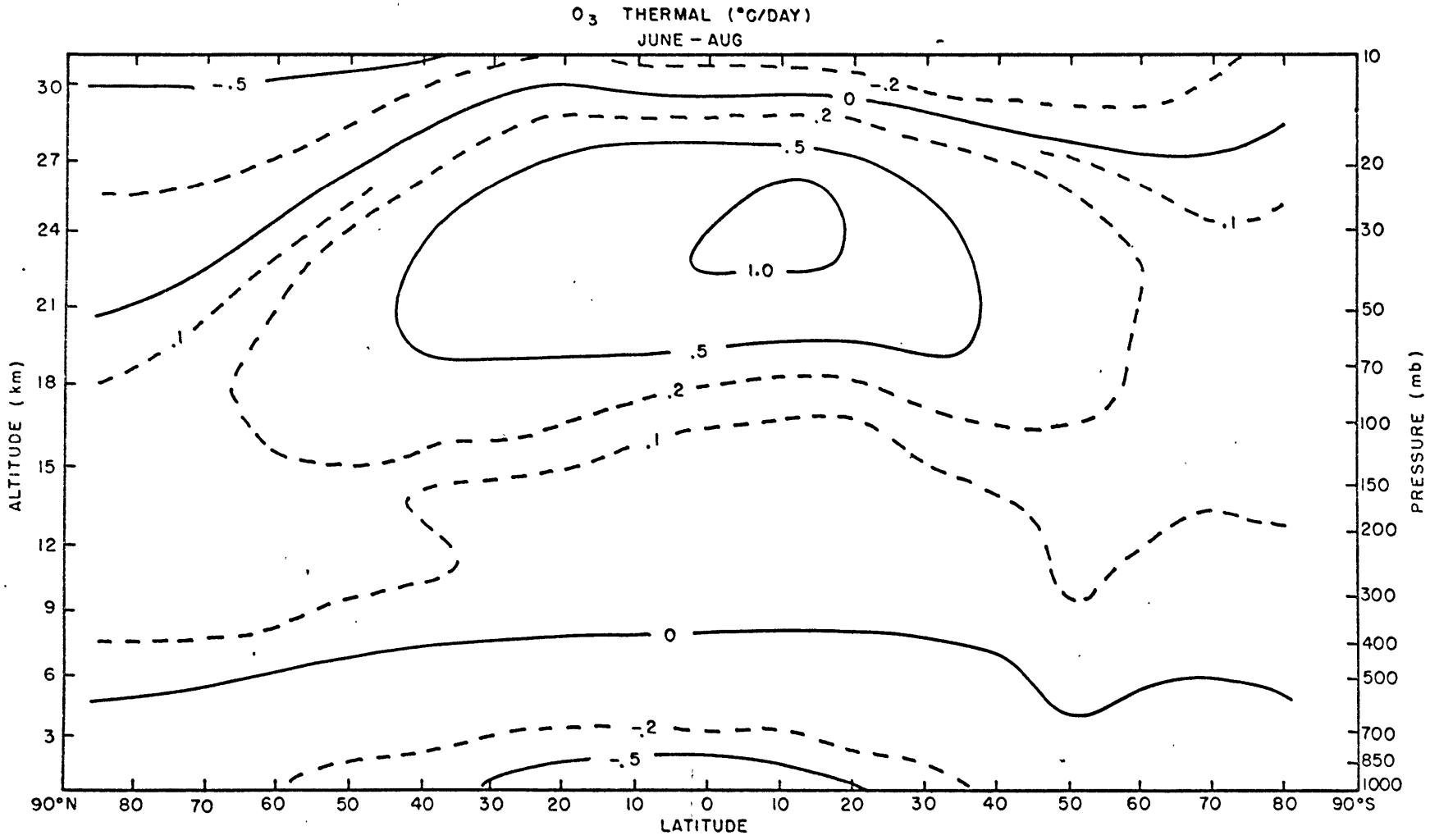
O_3 THERMAL (°C/DAY)
JUNE – AUG
ALTITUDE (km)
PRESSURE (mb)
LATITUDE
90°N
80
70
60
50
40
30
20
10
0
10
20
30
40
50
60
70
80
90°S
30
27
24
21
18
15
12
9
6
3
10
20
30
50
70
100
150
200
300
400
500
700
850
1000
-.5
.5
1.0
.2
.1
0
-.2
-.1

Figure 14.

mixing ratio with increasing mixing ratios with height (see Figs. 2 and 4). It is the gradient of the ozone mixing ratio which determines the region of maximum thermal heating since the temperature gradient above the tropical tropopause has only small latitudinal variations within a season. Note the shift of the region of maximum thermal heating into the S.H. in June-August which follows the region of maximum vertical gradients of ozone. In the stratosphere in middle and high latitudes of both hemispheres, thermal cooling occurs which varies with the mixing ratios and temperature field (e.g. high latitudes N.H. in December-February compared with high latitudes S.H. in June-August).

A.3 Carbon Dioxide

Presented in Figs. 15 and 16 is the global thermal cooling by the 15μ band of carbon dioxide for December-February and June-August. Like ozone, overlap with water vapor has been taken into account and tropospheric cooling is predominantly that due to water vapor although carbon dioxide cooling is important near the surface. Of particular note again is the thermal heating which occurs at the tropical tropopause because of the warmer temperatures above and below the tropopause. Thermal heating results from a convergence of thermal flux into this region with more heating at the tropopause in December-February associated with the colder tropopause. Above the tropical tropopause thermal cooling increases rapidly with height associated with the increase of temperature. For the stratosphere in both hemispheres there is an increase of cooling with height with the minimum

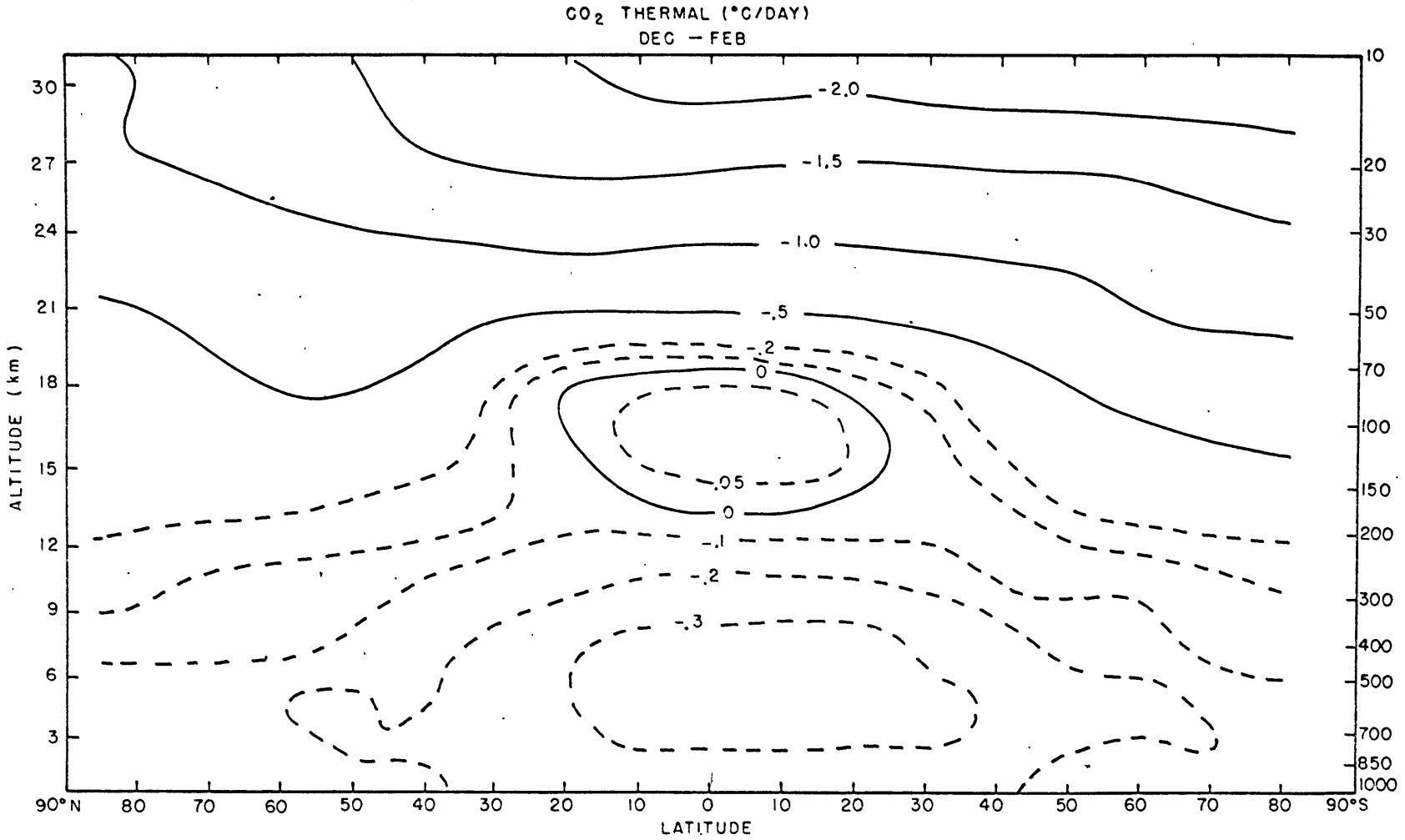
CO_2 THERMAL (°C/DAY)
DEC – FEB
-2.0
-1.5
-1.0
-.5
-.2
0
.05
0
-.1
-.2
-.3
ALTITUDE (km)
30
27
24
21
18
15
12
9
6
3
PRESSURE (mb)
10
20
30
50
70
100
150
200
300
400
500
700
850
1000
90°N 80 70 60 50 40 30 20 10 0 10 20 30 40 50 60 70 80 90°S
LATITUDE

Figure 15.

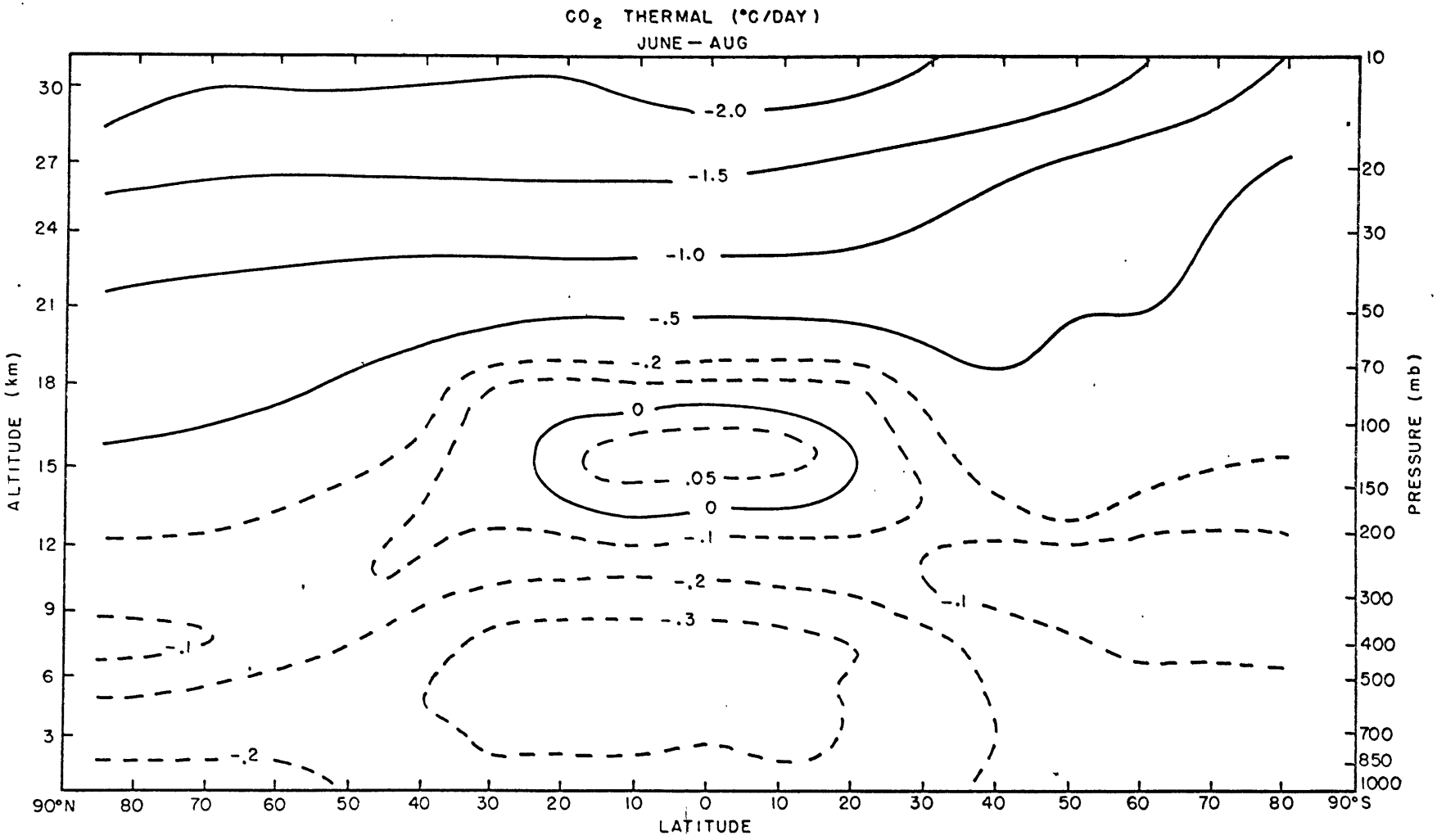
CO_2 THERMAL (°C/DAY)
JUNE — AUG
ALTITUDE (km)
PRESSURE (mb)
LATITUDE
90°N
80
70
60
50
40
30
20
10
0
10
20
30
40
50
60
70
80
90°S
30
27
24
21
18
15
12
9
6
3
10
20
30
50
70
100
150
200
300
400
500
700
850
1000
-2.0
-1.5
-1.0
-.5
-.2
0
.05
0
-.1
-.2
-.3
-.1
-.1
-.2

Figure 16.

cooling occurring in the S.H. winter which is associated with the colder temperatures.

A.4 Net Thermal Cooling

Four seasons of net thermal cooling are given in Figs. 17-20. In the troposphere it is water vapor that dominates the cooling rates. Maximum cooling rates occur in low latitudes with the region of maximum cooling (-2°C/day isoline) following the warmer hemisphere. In the troposphere in middle and high latitudes there is generally less net thermal cooling in the S.H. season than in the comparable N.H. season. The inhomogeneity in the cooling rates in middle and high latitudes reflects the variations in cloud amount and distribution of cloudiness.

The tropical tropopause has a small net thermal heating for all seasons due to thermal heating by ozone and carbon dioxide and the minimum cooling rates by water vapor. Above the tropical tropopause there is substantial thermal heating by ozone but both carbon dioxide and water vapor give increased cooling with height resulting in net thermal cooling.

In the stratosphere in middle and high latitudes for both hemispheres, there is only weak compensation by ozone to the thermal cooling by carbon dioxide and water vapor and net thermal cooling increases with height everywhere. The pronounced temperature differences between the winter hemispheres in the stratosphere is quite evident with much less cooling in the S.H. winter than in the N.H. winter.

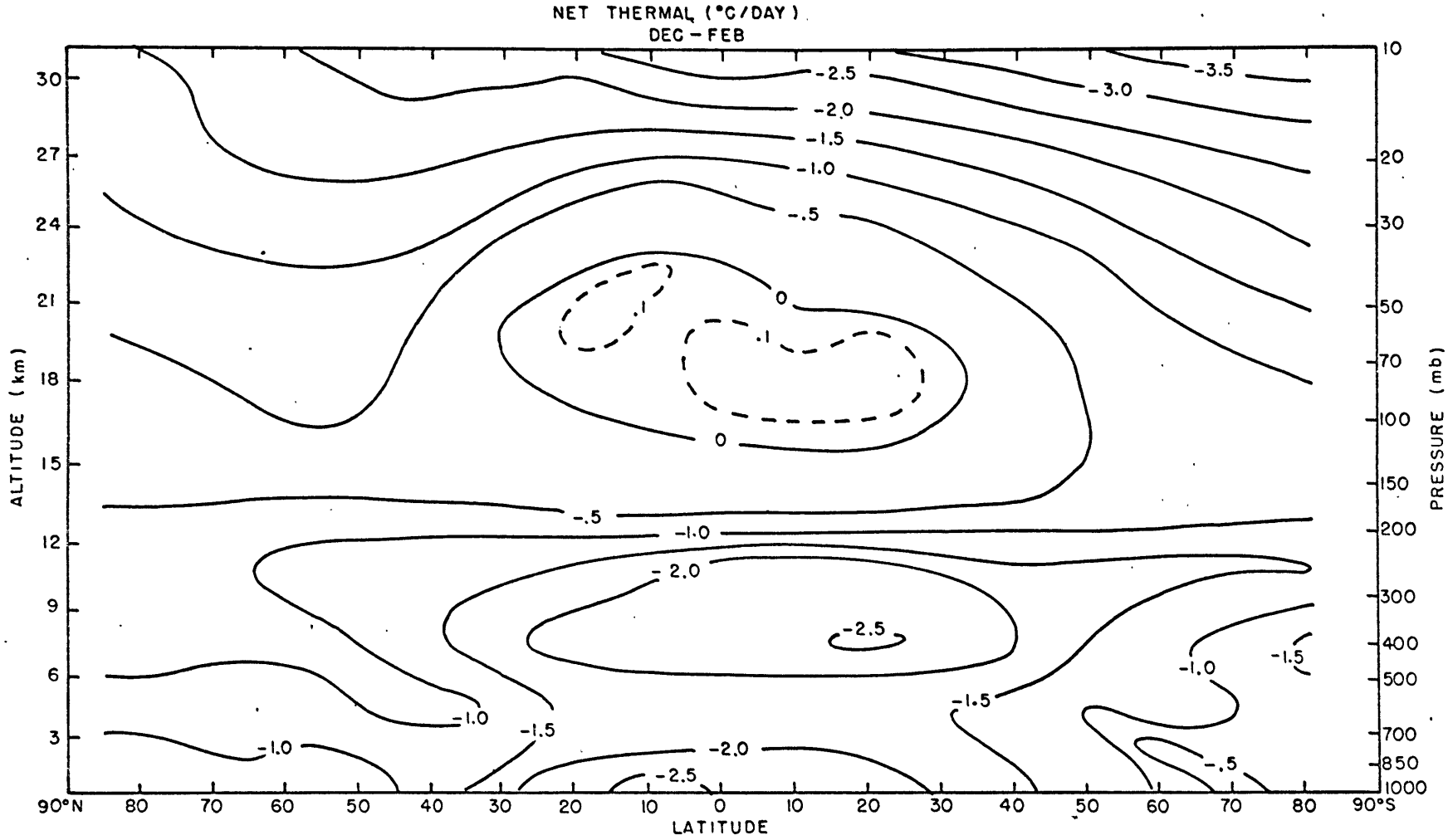
NET THERMAL (°C/DAY)
DEC - FEB
ALTITUDE (km)
PRESSURE (mb)
LATITUDE
90°N
80
70
60
50
40
30
20
10
0
10
20
30
40
50
60
70
80
90°S
30
27
24
21
18
15
12
9
6
3
10
20
30
50
70
100
150
200
300
400
500
700
850
1000
-2.5
-3.0
-3.5
-2.0
-1.5
-1.0
-.5
0
.1
-.1
-.5
-1.0
-2.0
-2.5
-1.5
-1.0
-1.5
-1.0
-1.5
-2.0
-2.5
-.5

Figure 17.

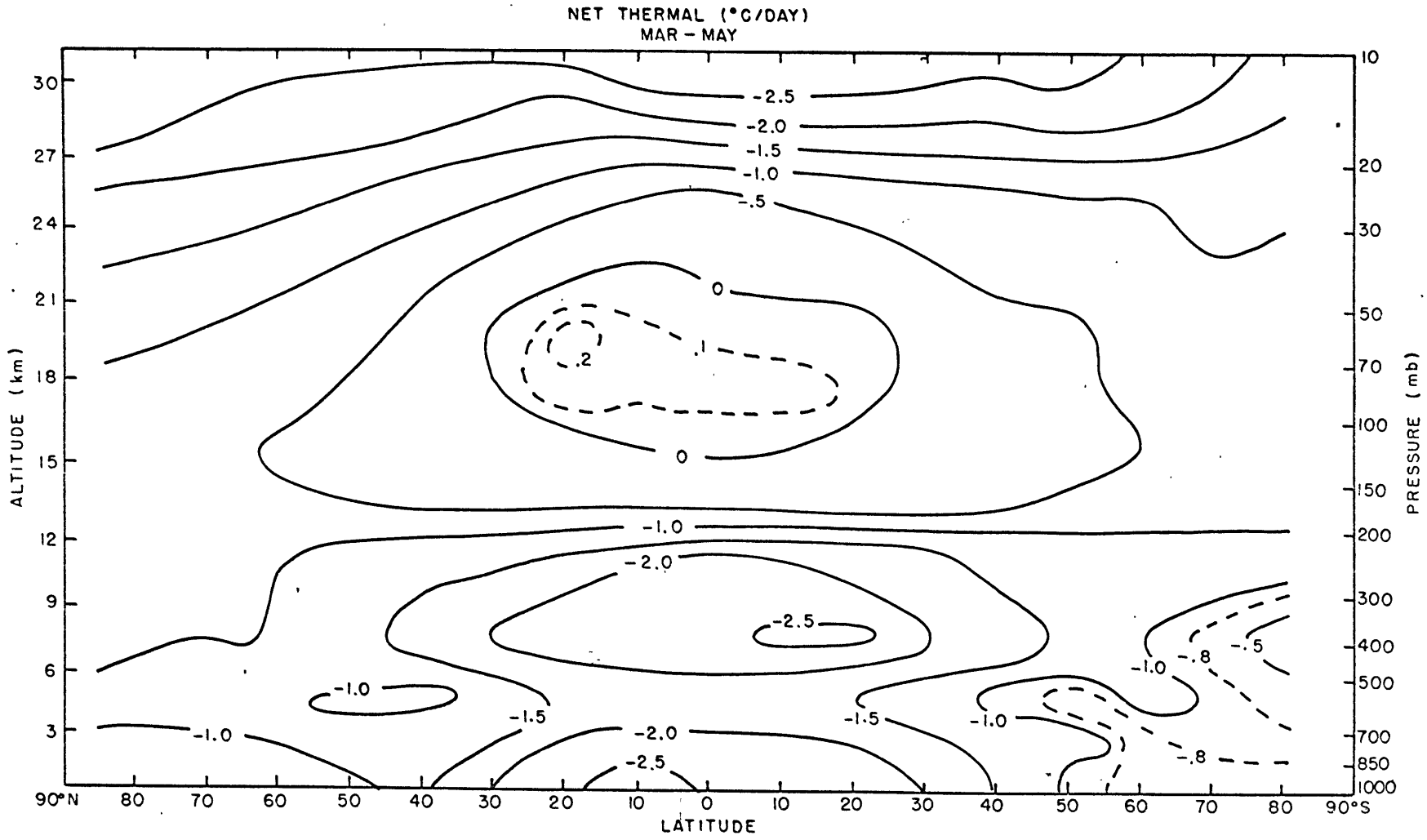
NET THERMAL (°C/DAY)
MAR – MAY
ALTITUDE (km)
PRESSURE (mb)
LATITUDE
90°N
90°S
-2.5
-2.0
-1.5
-1.0
-.5
0
.1
.2
-.8

Figure 18.

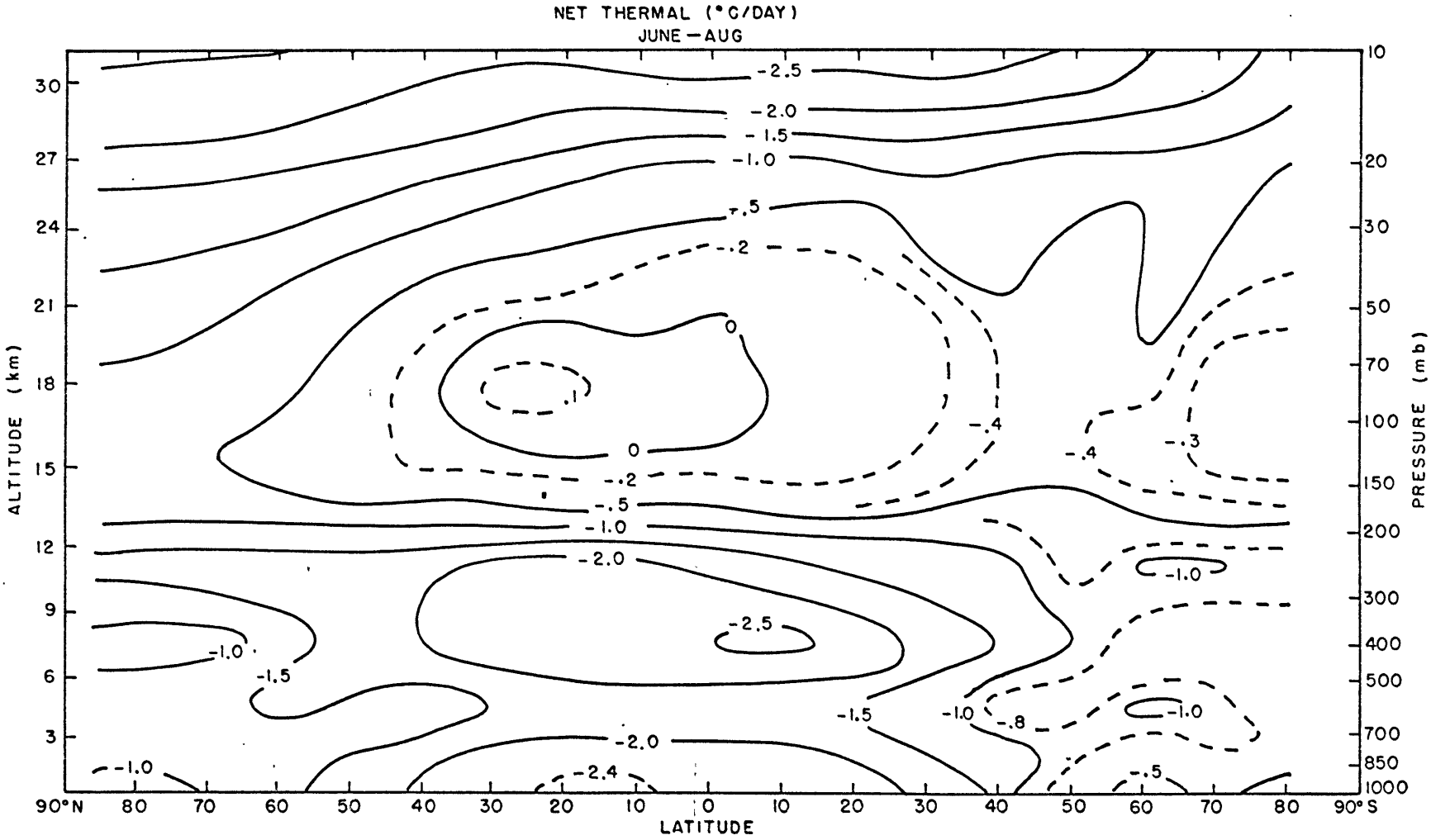
NET THERMAL (°C/DAY)
JUNE—AUG
ALTITUDE (km)
PRESSURE (mb)
LATITUDE
90°N
80
70
60
50
40
30
20
10
0
10
20
30
40
50
60
70
80
90°S
30
27
24
21
18
15
12
9
6
3
10
20
30
50
70
100
150
200
300
400
500
700
850
1000
-2.5
-2.0
-1.5
-1.0
-.5
-.2
0
.1
0
-.4
-.2
-.5
-1.0
-2.0
-2.5
-1.0
-1.5
-2.0
-2.4
-1.0
-1.5
-1.0
-.8
-1.0
-.5
-.4
-.3
-1.0

Figure 19.

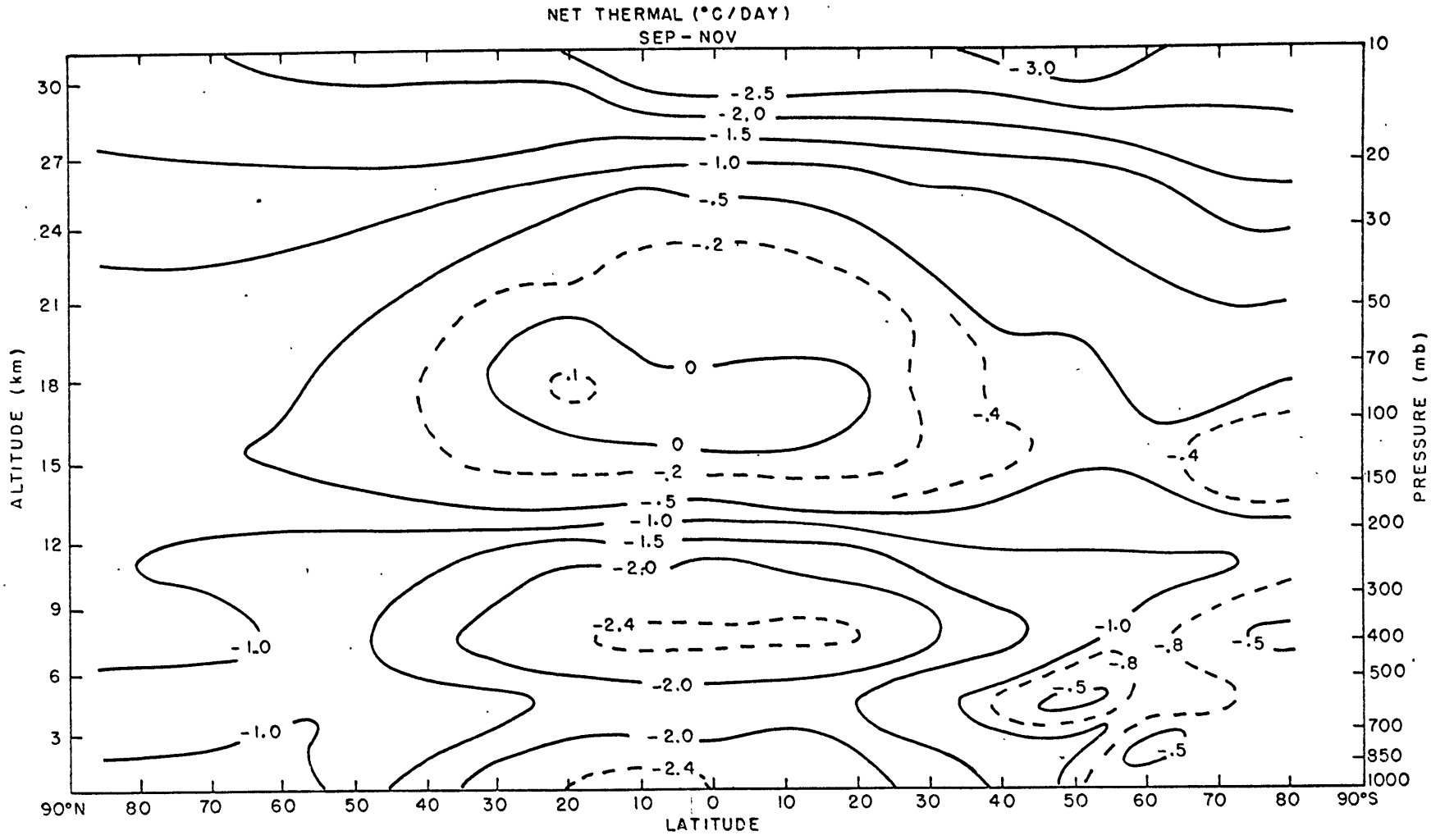
NET THERMAL (°C/DAY)
SEP - NOV
ALTITUDE (km)
PRESSURE (mb)
LATITUDE
90°N
90°S
-3.0
-2.5
-2.0
-1.5
-1.0
-.5
-.2
-.1
0
-.4
-2.4
-.8

Figure 20.

B. Solar Heating

B.1 Ozone

Presented in Figs. 21 and 22 is the solar heating due to ozone for December-February and June-August. Ozone heating is important only in the stratosphere and depends very closely on the magnification factor and duration of sunlight, i.e. solar geometrical factors. Maximum heating occurs in the summer hemisphere in high latitudes with increased heating with height.

B.2 Water Vapor, Carbon Dioxide and Molecular Oxygen

Presented in Figs. 23 and 24 is the solar near infrared heating by water vapor, carbon dioxide and molecular oxygen for December-February and June-August. In the troposphere the near infrared solar heating is maximum in the summer hemisphere due to solar geometry. Heating in the tropics is associated with the high water vapor content; whereas, heating in the middle and high latitudes is due to absorption by middle and low clouds. In the stratosphere the heating rates increase with height above 100 mb due to solar geometry.

C. Total Radiative Heating

Four seasons of total radiative heating are presented in Figs. 25-28. In the troposphere in low latitudes there is radiative cooling because the thermal cooling by water vapor dominates over the solar near infrared heating. This region contains the most extensive cooling especially near the surface and above 500 mb. Tropospheric inhomo-

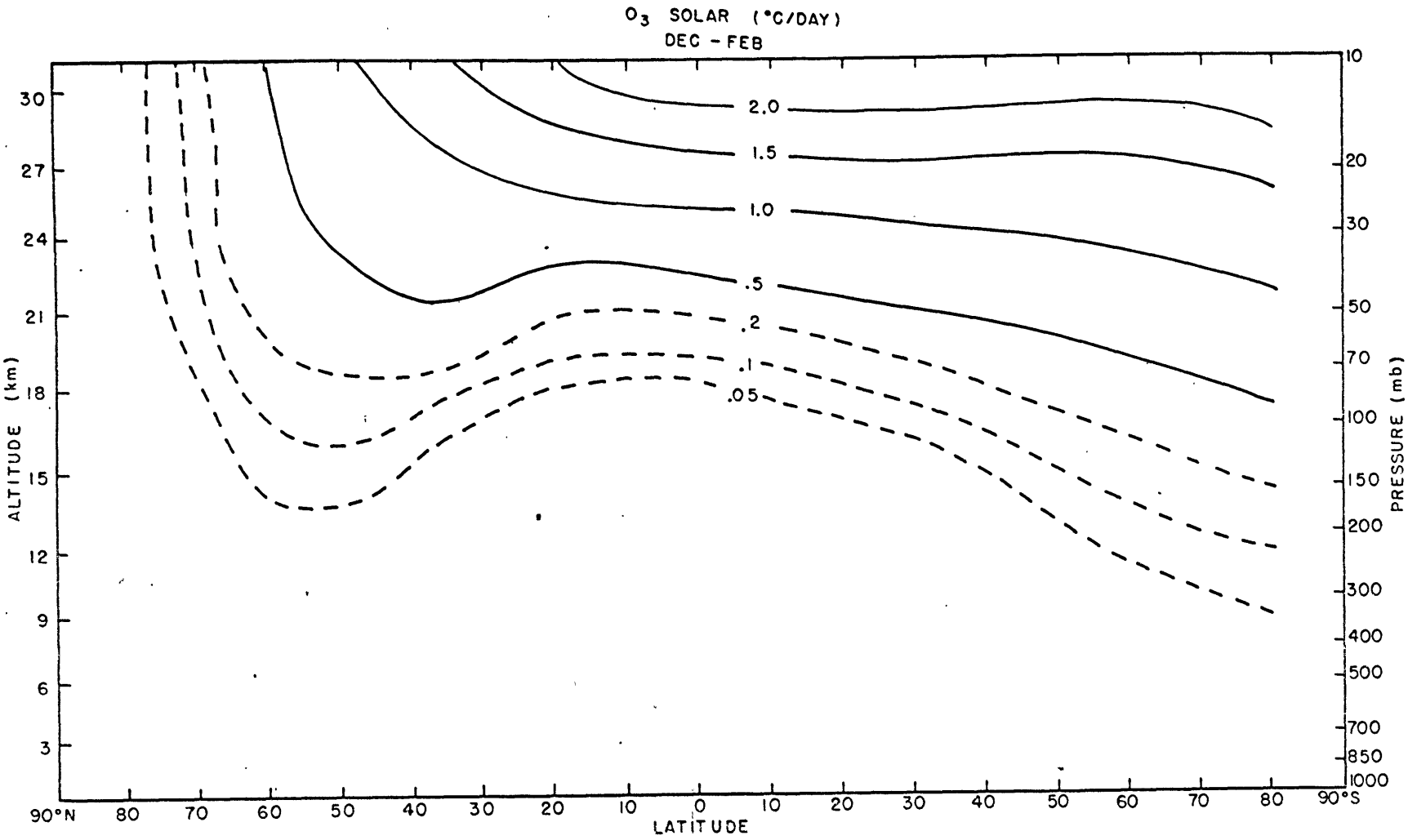
O_3 SOLAR (°C/DAY)
DEC - FEB
2.0
1.5
1.0
.5
.2
.1
.05
ALTITUDE (km)
30
27
24
21
18
15
12
9
6
3
PRESSURE (mb)
10
20
30
50
70
100
150
200
300
400
500
700
850
1000
90°N 80 70 60 50 40 30 20 10 0 10 20 30 40 50 60 70 80 90°S
LATITUDE

Figure 21.

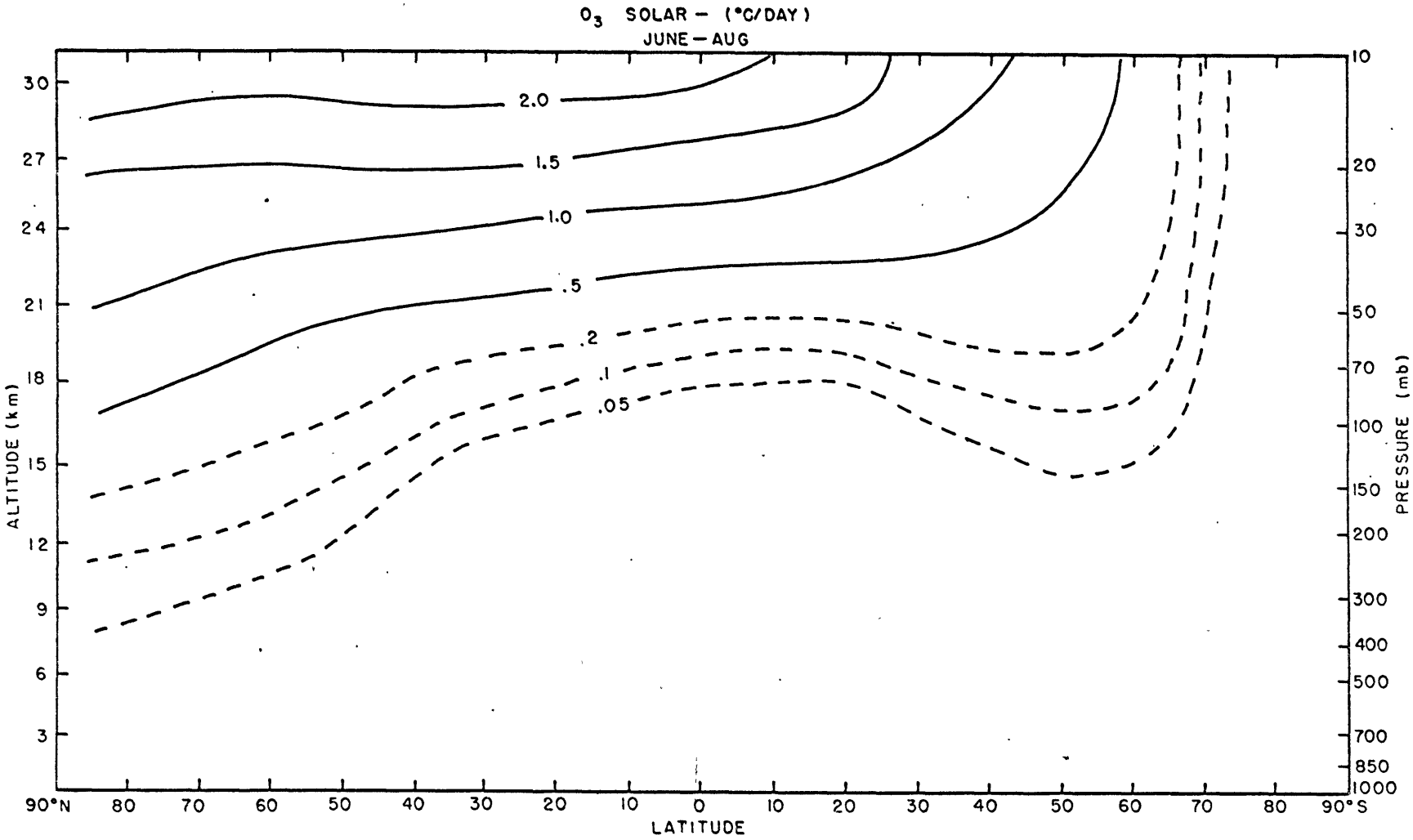
O_3 SOLAR – (°C/DAY)
JUNE – AUG
2.0
1.5
1.0
.5
.2
.1
.05
ALTITUDE (km)
30
27
24
21
18
15
12
9
6
3
PRESSURE (mb)
10
20
30
50
70
100
150
200
300
400
500
700
850
1000
90°N
80
70
60
50
40
30
20
10
0
10
20
30
40
50
60
70
80
90°S
LATITUDE

Figure 22.

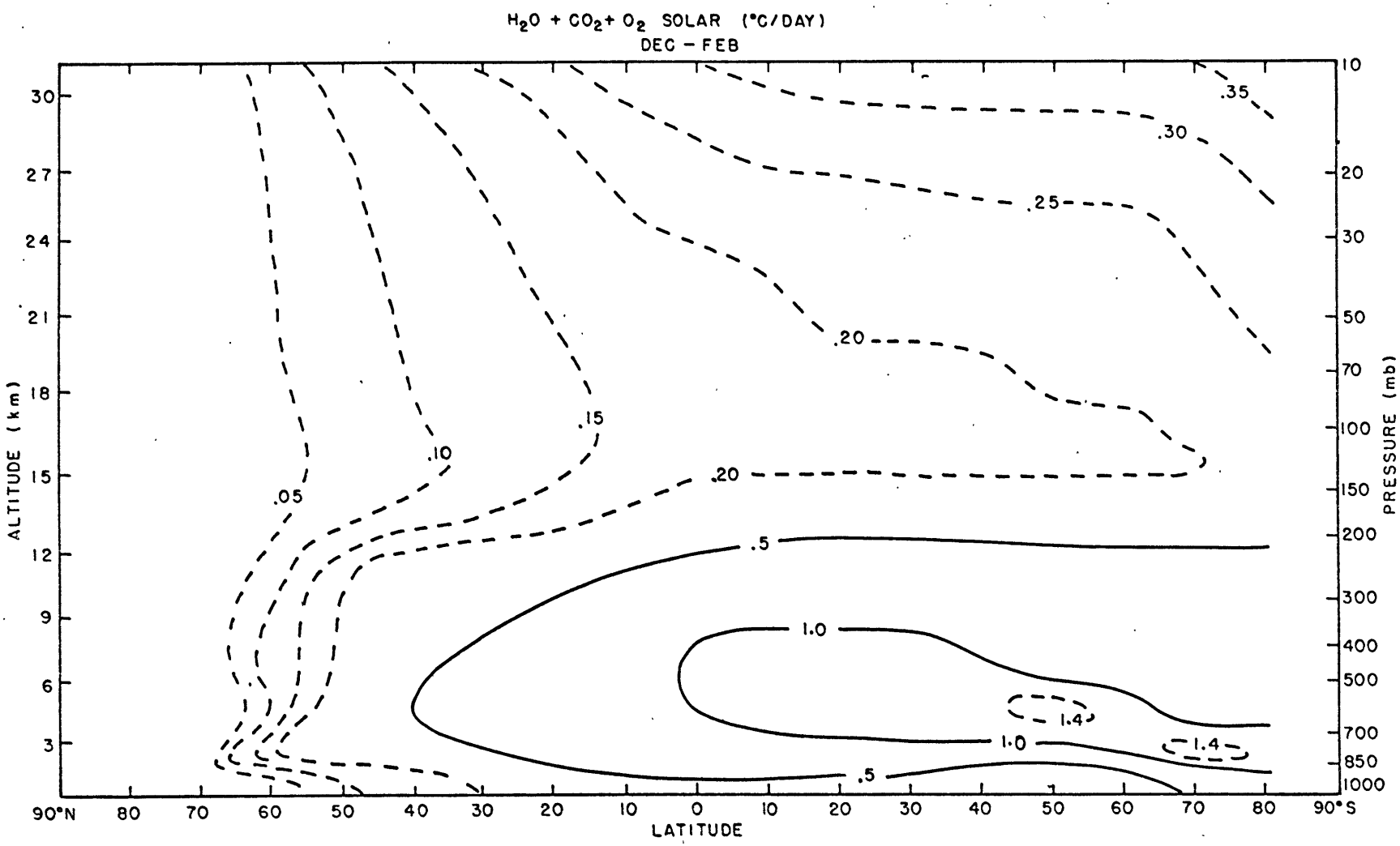
$H_2O + CO_2 + O_2$ SOLAR (°C/DAY)
DEC – FEB
ALTITUDE (km)
PRESSURE (mb)
LATITUDE
90°N
80
70
60
50
40
30
20
10
0
10
20
30
40
50
60
70
80
90°S
30
27
24
21
18
15
12
9
6
3
10
20
30
50
70
100
150
200
300
400
500
700
850
1000
.35
.30
.25
.20
.15
.10
.05
.20
.5
1.0
1.4
1.0
1.4
.5

Figure 23.

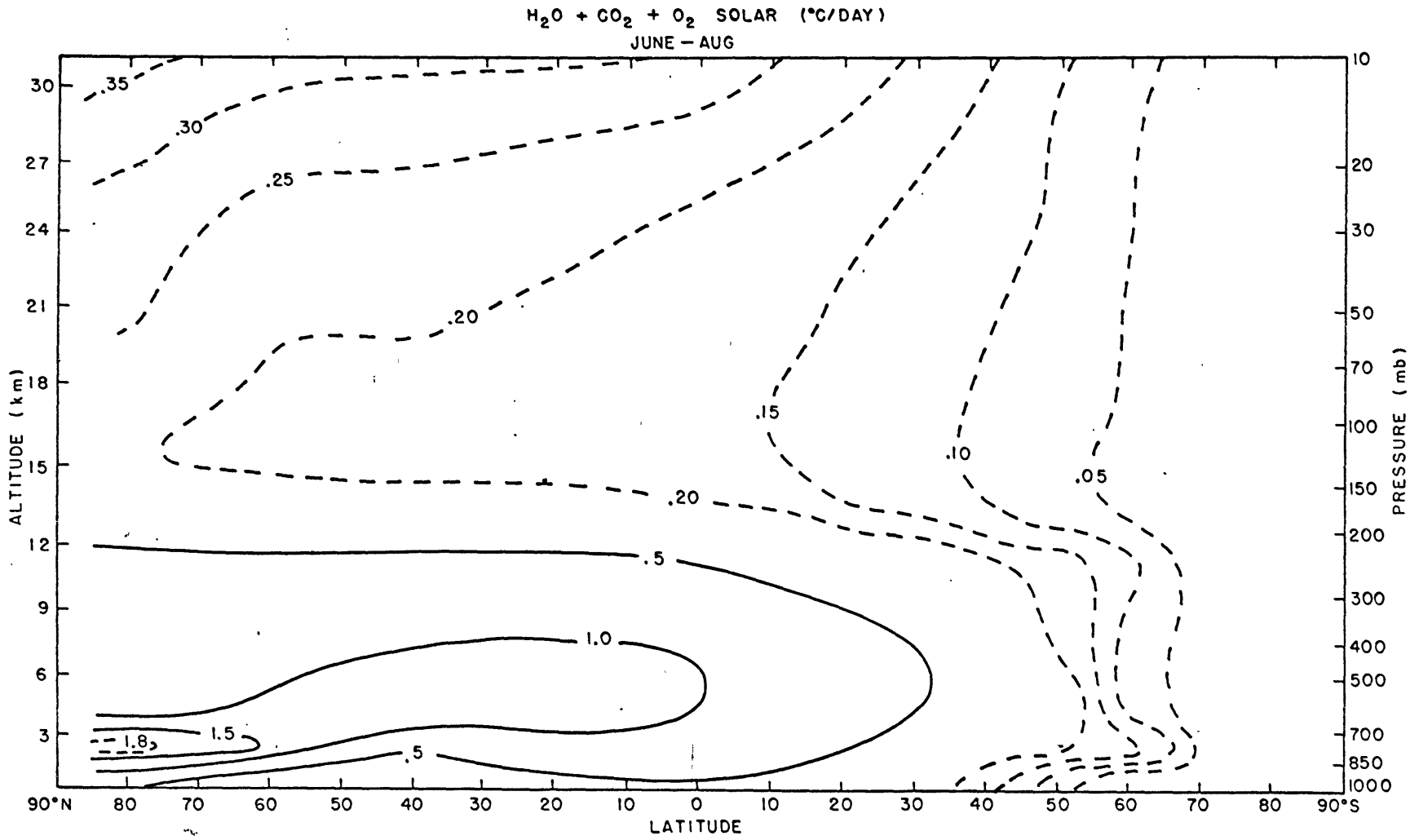
$H_2O + CO_2 + O_2$ SOLAR (°C/DAY)
JUNE – AUG
ALTITUDE (km)
PRESSURE (mb)
LATITUDE
90°N
90°S
.35
.30
.25
.20
.15
.10
.05
.5
1.0
1.5
1.8

Figure 24.

geneity in the heating rates in middle and high latitudes results from variations in thermal cooling and solar near infrared heating associated with clouds. There is radiative heating in these latitudes which varies with the solar declination angle due to solar near infrared absorption by clouds and relative minima in radiative cooling are also caused by clouds as noted in Section IV A.

There is extensive radiative heating in the tropical stratosphere which does extend partially into the mid-latitude stratosphere. Near the tropical tropopause there is slight thermal and solar heating. Above the tropical tropopause solar heating by ozone coupled with solar near infrared heating increases faster with height than the increase of thermal cooling. The region of maximum radiative heating is shifted upwards away from the tropical tropopause and is controlled principally by both thermal and solar heating due to ozone.

The high latitude stratosphere for both hemispheres shows cooling for all seasons with the differences in the high latitude radiative heating fields reflecting the differences in temperature between the hemispheres. The winter hemispheres show the most pronounced differences with the colder hemisphere showing the smallest cooling.

D. Comparison with Previous Theoretical Computations

In the last decade monthly mean radiative heating rates in the N.H. troposphere have been obtained by Davis (1963), Rodgers (1967a) and Katayama (1966, 1967) and in the N.H. stratosphere by Davis, Kennedy (1964) and Rodgers. Katayama examined three dimensional mean

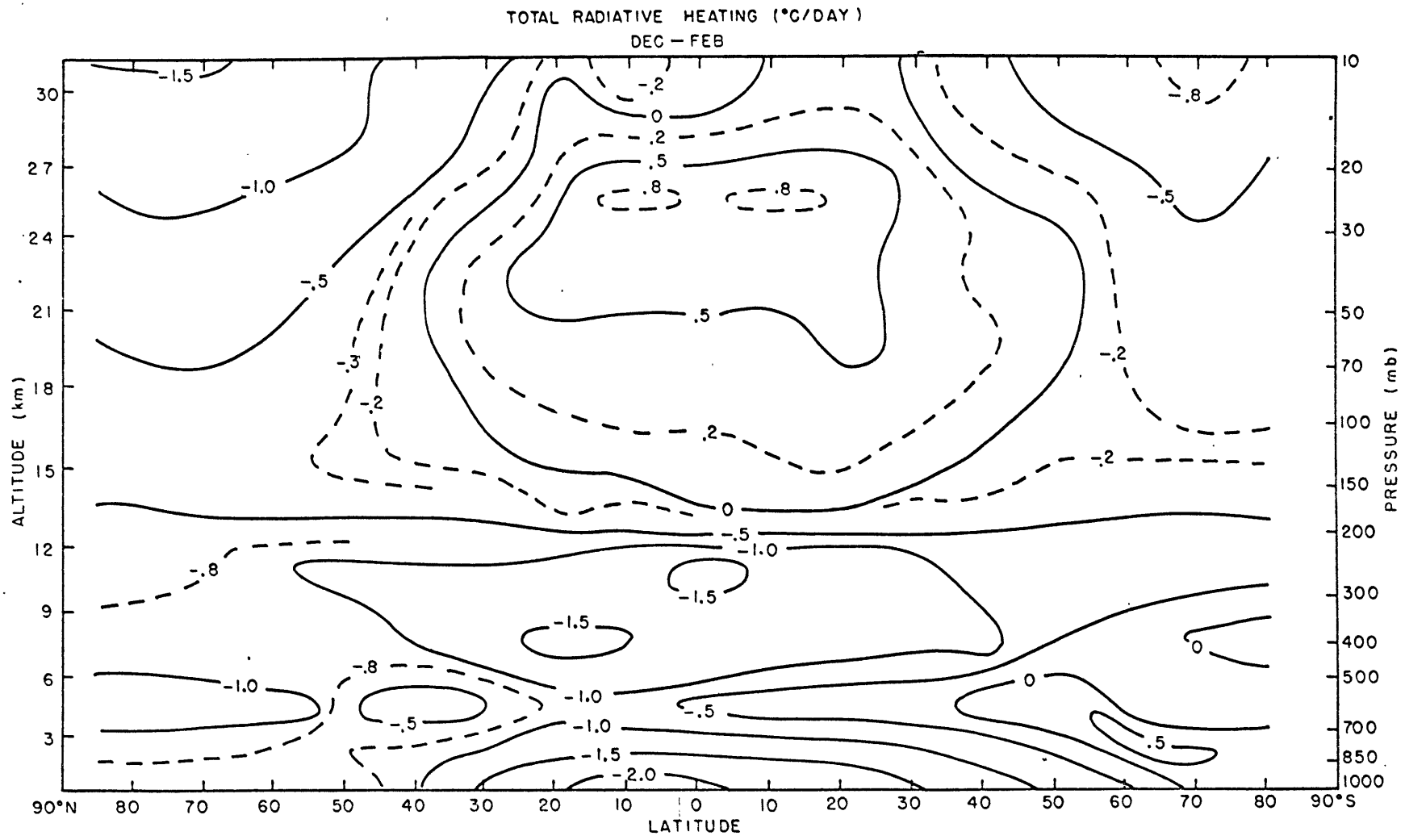
TOTAL RADIATIVE HEATING (°C/DAY)
DEC – FEB
ALTITUDE (km)
PRESSURE (mb)
LATITUDE
90°N
80
70
60
50
40
30
20
10
0
10
20
30
40
50
60
70
80
90°S
30
27
24
21
18
15
12
9
6
3
10
20
30
50
70
100
150
200
300
400
500
700
850
1000
-1.5
-1.0
-.5
-.3
-.2
-.8
0
.2
.5
.8

Figure 25.

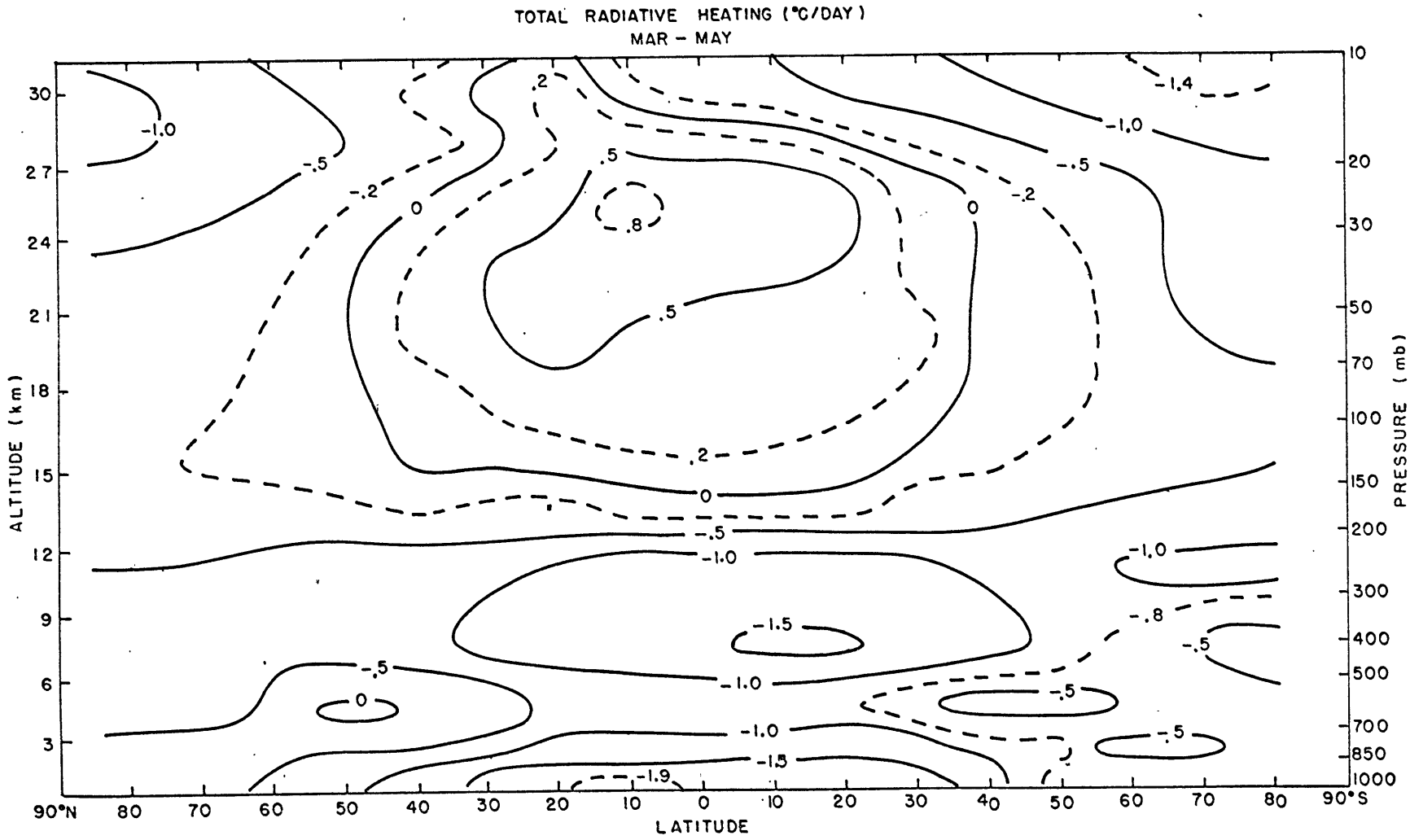
TOTAL RADIATIVE HEATING (°C/DAY)
MAR – MAY
ALTITUDE (km)
PRESSURE (mb)
LATITUDE
90°N
80
70
60
50
40
30
20
10
0
10
20
30
40
50
60
70
80
90°S
30
27
24
21
18
15
12
9
6
3
10
20
30
50
70
100
150
200
300
400
500
700
850
1000
-1.0
-.5
-.2
0
.2
.5
.8
-1.4
-1.5
-1.9

Figure 26.

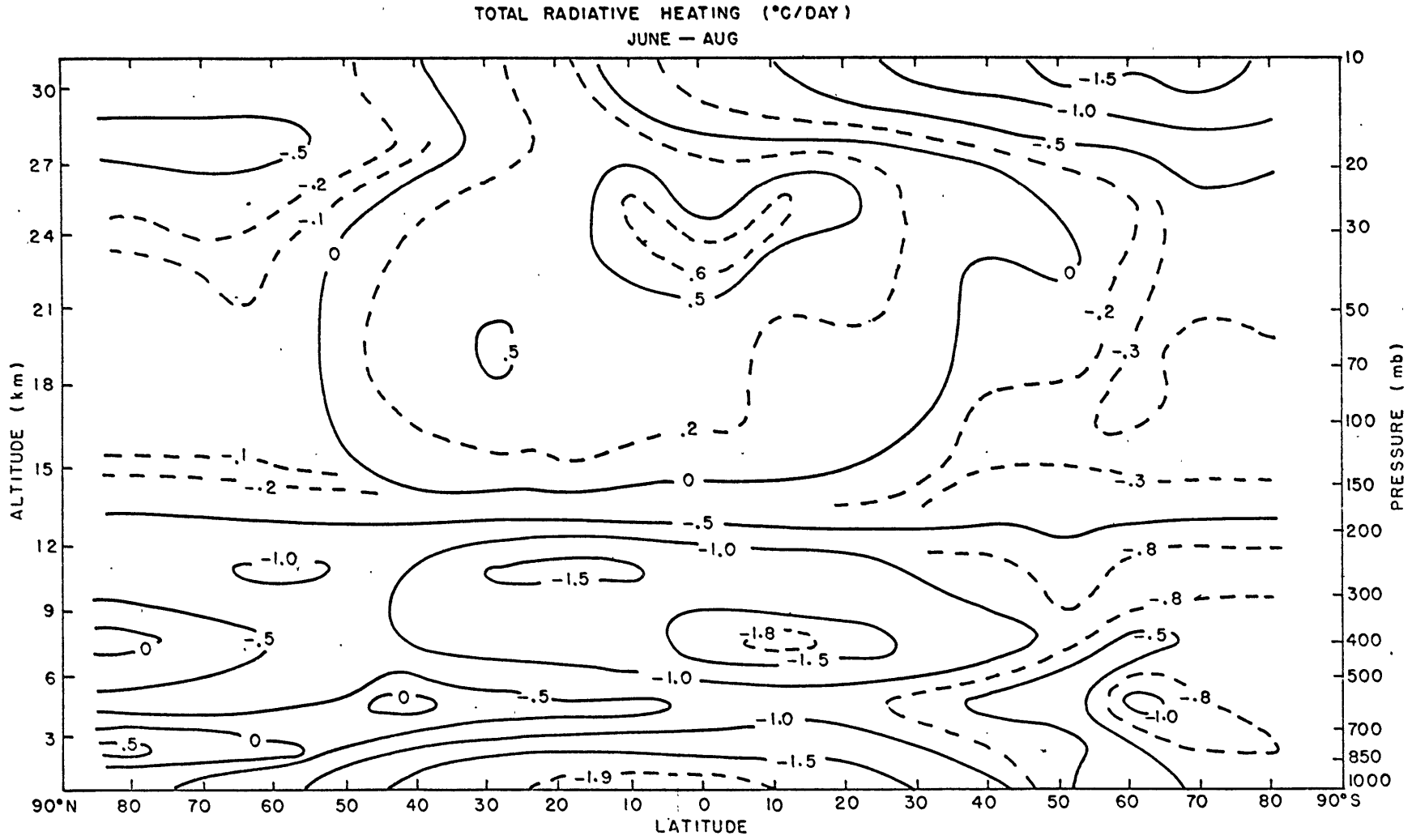
TOTAL RADIATIVE HEATING (°C/DAY)
JUNE — AUG
ALTITUDE (km)
PRESSURE (mb)
LATITUDE
90°N
90°S
30
27
24
21
18
15
12
9
6
3
10
20
30
50
70
100
150
200
300
400
500
700
850
1000
80
70
60
50
40
30
20
10
0
10
20
30
40
50
60
70
80
-1.5
-1.0
-.5
-.2
-.1
0
.6
.5
.2
-.3
-.8
-1.8
-1.9

Figure 27.

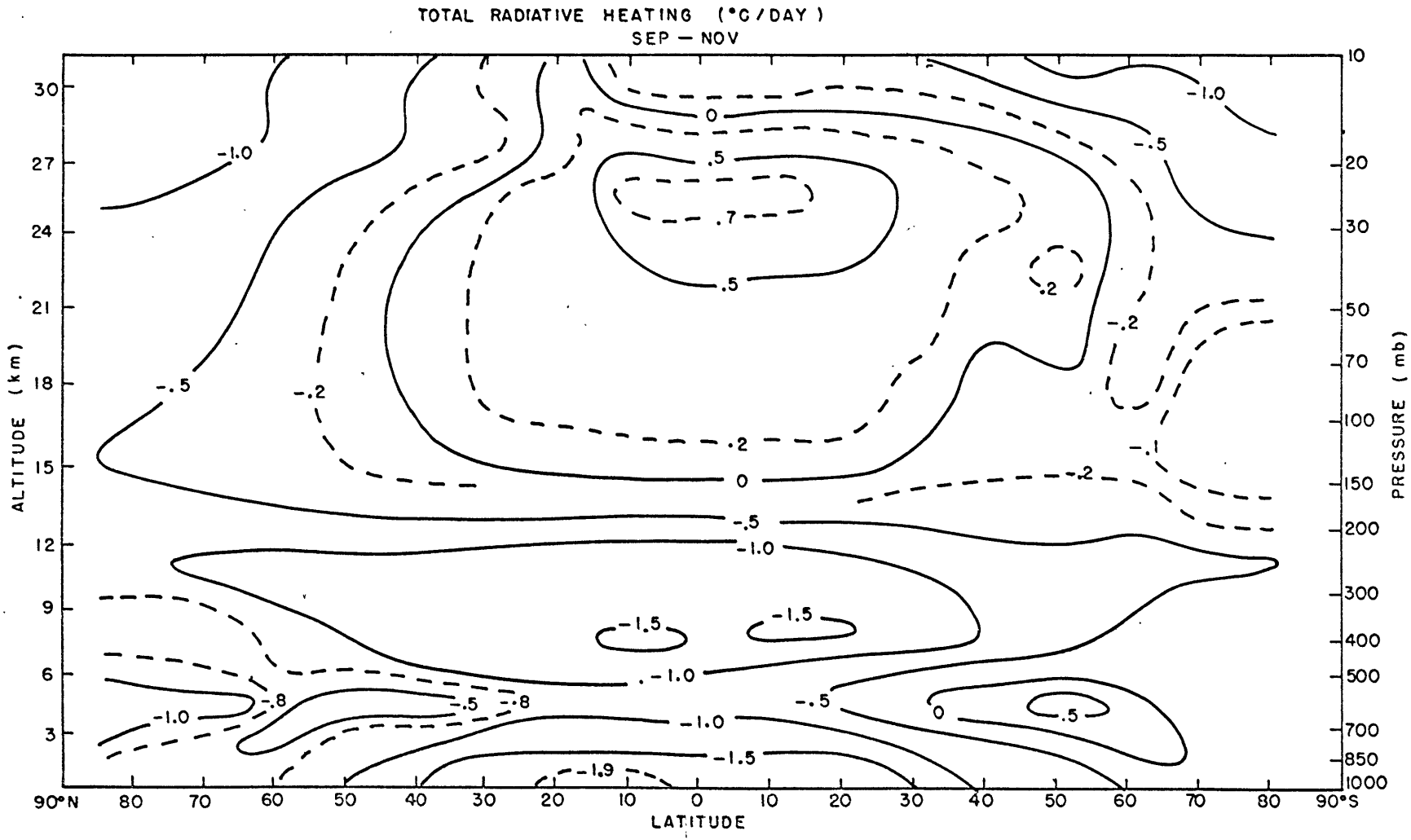
TOTAL RADIATIVE HEATING (°C/DAY)
SEP — NOV
ALTITUDE (km)
PRESSURE (mb)
LATITUDE
90°N
80
70
60
50
40
30
20
10
0
10
20
30
40
50
60
70
80
90°S
30
27
24
21
18
15
12
9
6
3
10
20
30
50
70
100
150
200
300
400
500
700
850
1000
-1.0
0
-.5
.5
.7
.2
-.2
-.1
-1.5
-.8
-1.9

Figure 28.

radiative heating rates for January and July; whereas, the other researchers obtained zonal mean radiative heating rates for January, April, July and October.

D.1 Northern Hemisphere Troposphere

Qualitatively the present results for thermal cooling compare well with Davis who finds maximum cooling in low latitudes and strong cooling above the tropospheric clouds. The magnitudes are different when seasonal and center month profiles are compared. Rodgers finds significantly more thermal cooling in high latitudes due to the use of water vapor emissivities (Rodgers 1967b) which accentuate the cloud boundaries. The effect of integrating over many spectral intervals for water vapor is to smooth the cooling profile. Katayama presents longitudinal cross sections of thermal cooling and it appears that he also finds more cooling in low latitudes.

The only tropospheric cross sections of solar heating are longitudinal cross sections by Katayama. In January he finds more heating in low latitudes, whereas in July there is extensive heating in higher latitudes. Tnis is qualitatively the same pattern as found in this study although the present study gives somewhat higher heating rates in high latitudes for the summer. Tabulated data by Rodgers also show considerable heating in high latitudes in July and little heating in January.

D.2 Northern Hemisphere Stratosphere

More stratospheric detail and slightly larger thermal cooling

rates are evident in the present results when compared with Davis' results. This is probably due to better specification of the stratospheric temperature and ozone profiles.

The solar heating rates obtained in the present study are much larger than those obtained by Davis but are quite consistent with solar heating rates found by Kennedy and Rodgers. The total stratospheric heating rates of Kennedy, Rodgers and the present study are qualitatively similar although the seasonal profiles have more heating in low latitudes and more cooling in high latitudes. A noteworthy point of the present study is the nearly global cooling for all seasons along the 10 mb surface. This is significantly more cooling than found by Kennedy and Rodgers. Total radiative heating at this level depends on the radiative parameters above as well as below 30 km. As an example, Hering et al. (loc. cit.) report that a 20% error in the ozone mixing ratio at 10 mb results in a 10% error in the ozone heating at 10 mb and 50% uncertainty in the amount of ozone between 5-0 mb results in a 12% uncertainty in ozone heating at 10 mb. Although our knowledge of the temperature field above 30 km is increasing, there is still a great dearth of information on the upper level ozone distribution. This problem is also pertinent to computations of radiative heating in the upper stratosphere and mesosphere.

E. Comparison with Satellite Measurements

The net radiation available to the earth-atmosphere system (defined here as RNEA) has been measured by several meteorological satellites (e.g. Raschke 1968, Vonder Haar 1968) and can be readily compared with theoretical values of RNEA at 5 mb. An updated set of curves for RNEA was made available by Dr. Vonder Haar (private communication) and includes data processed as of August, 1969 from the first and second generation satellites (all TIROS data through 1965 and Nimbus II and ESSA III data for 1966). Comparison between the theoretical computations and satellite observations is given in Fig. 29. Theory consistently overestimates the amount of energy available to the earth-atmosphere system in the warmer hemisphere which is undoubtedly due to the inability to accurately specify the cloud and surface albedos. Using mean cloud and surface albedos is not accurate enough for studying the radiation available to the earth-atmosphere system. It should be noted that there is an imbalence for the satellite measurements such that too much energy is available to the earth-atmosphere system.

In addition to overestimating the amount of energy available to the earth-atmosphere system, theory probably yields too much solar absorption by clouds in the troposphere and too little reflected radiation absorbed in the stratosphere. However, according to Hering et al. (loc. cit.) the contribution of the reflected solar flux to the total solar heating rates at 10 mb is about 10%. Thus, underestimating the earth-atmosphere albedo results in only minor errors in the total

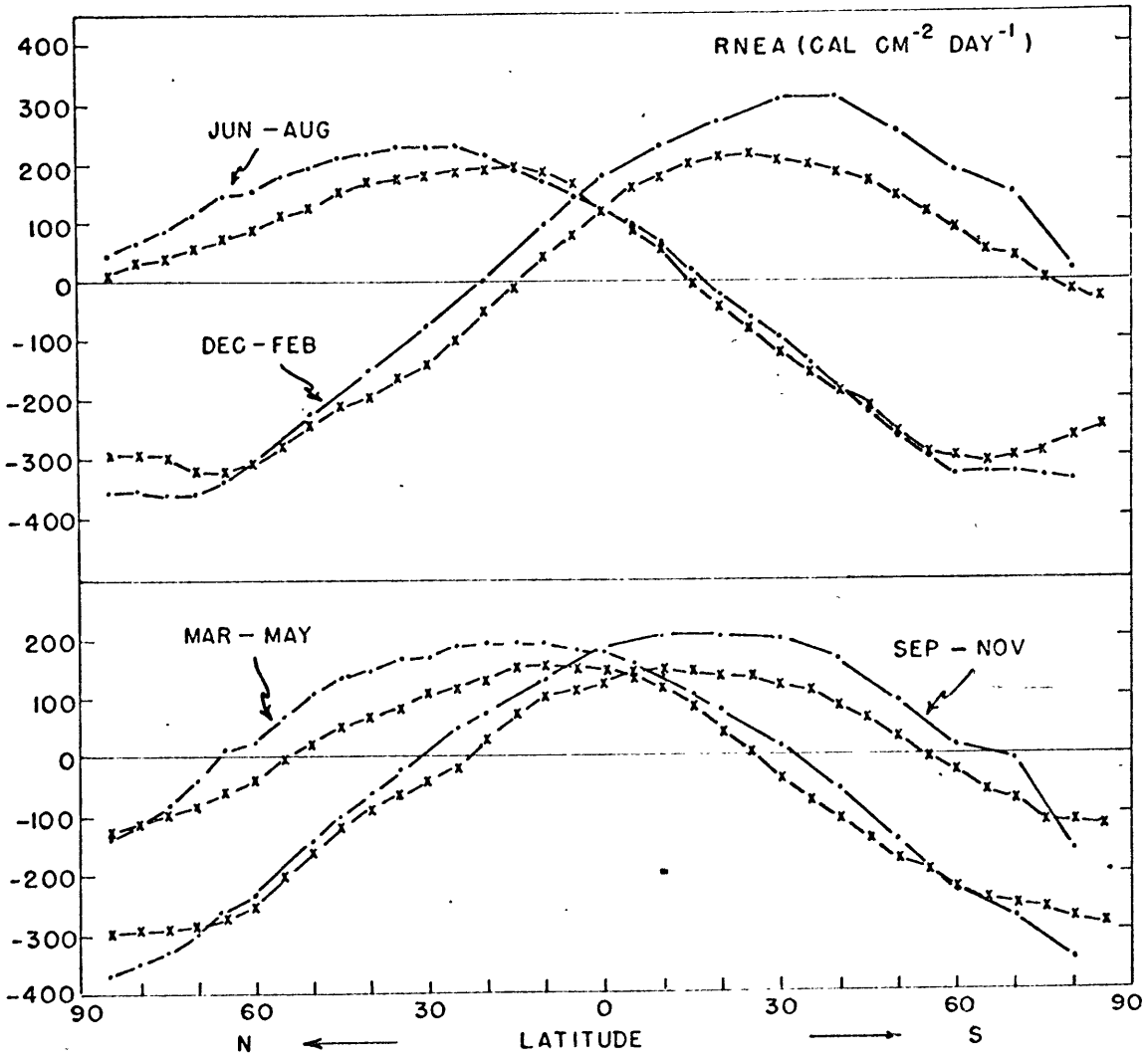

Figure 29. Comparison of RNEA for satellite (x-x) and theory (• - •). Units: Cal cm^{-2} day^{-1}.

solar heating rates at 10 mb. Much more uncertainty arises from insufficient information on the ozone distribution above 30 km (see Section IV.D).

Much more work, both observational and theoretical, is needed to either parameterize or construct better physical models of solar heating in the troposphere. At this time observations are not even able to give a definitive magnitude of the total solar radiation absorption by clouds. Measurements of total absorption by clouds range from 3% by Cheltzov (1952) as reported by Kondratiev (loc. cit.) to as much as 27% by Fritz and Mac Donald (1951). Solar heating in a cloudy atmosphere remains as a significant problem with further research required.

V. The Role of Radiation in the General Circulation of the Lower Stratosphere

A. Approximate Solutions of Thermal Cooling in the Lower Stratosphere

The interactions between the field of radiation and the field of motion are very complex. Radiative heating depends in a nonlinear manner on many parameters including temperature, clouds, water vapor, ozone, carbon dioxide and the optical properties of clouds and the ground. However, knowledge of radiative heating, especially the variation with longitude, is of paramount importance in understanding the energy budget of the lower stratosphere and must be pursed in spite of the complex problems that arise.

There have been several studies of radiative heating in the lower stratosphere based on the theory of radiative transfer. However, it has only been since around 1960 that sufficient observations of ozone have become available to correctly portray its vertical distribution. Prior to 1960 the profiles of ozone which were used, for example Ohring (1958), differed considerably from current observations. Since 1960 there have been the studies of Davis (1963), Kennedy (1964) and Rodgers (1967a). However, because of the lack of observational data and the large amount of time involved in numerically solving for radiative transfer, these studies sought only the zonal mean radiative heating for the N.H. for January, April, July and October. In addition to identifying the zonal mean radiative sources

and sinks of energy, the results of these studies were also used in estimating the Generation of Zonal Available Potential Energy by Kennedy (loc. cit.), Oort (1964) and Richards (1967).

The need to go beyond mean zonal profiles of radiative heating is obvious but the amount of work required becomes very large if numerical integration from first principles is required for each profile. To simplify numerical solutions of the thermal radiative transfer equations, an approximation known as the "Curtis-Matrix" method has been used.

Curtis (1956) originally proposed a solution for thermal radiative transfer which allowed the separation of the dependence on temperature from the dependence on absorber distribution. Rodgers and Walshaw (1966) outlined the use of the Curtis-Matrix method and Rodgers (1967a) employed this method in obtaining numerical solutions of thermal radiative transfer. Consider the thermal radiative transfer equation in the following form (see Section II):

$$F(z) = \int_{z'} B(z')\, d\mathcal{T}(z,z')$$

A numerical solution for this equation might be

$$F(z) \simeq \sum_i \frac{(B_i + B_{i+1})}{2}\left(\mathcal{T}_i - \mathcal{T}_{i+1}\right)$$

The form of the solution is $B_i A_j$ for suitable definitions of A_j.

The subscript i represents ordinates of integration whereas initially B is only specified at reference levels z' in the atmosphere. If the Planck function between reference levels is represented by an interpolation formula, then the solution reduces to a linear combination of the Planck function values.

$$F_z(\Delta\nu_r) = \sum_{z'} B_{z'}(\Delta\nu_r)\, A_{z,z'}(\Delta\nu_r)$$

The Curtis Matrix $A_{z,z'}$ is a function of temperature, pressure, absorber distribution and spectral interval $\Delta\nu_r$. The variation with temperature enters through the absorptivity of the absorbing gases. For a wide band, such as the 15μ band of CO_2, the dependence of the absorptivity on temperature is small except in the band wings. Goody (1964a) comments that the variation of the Curtis Matrices for CO_2, computed with and without a temperature effect on the mean line intensity, was small. For O_3 the dependence on temperature is also small according to Plass (1956). Rodgers and Walshaw (loc. cit.) computed thermal cooling with and without temperature effects on the Curtis Matrices and found only small variations for a large temperature range. Rodgers and Walshaw considered absorption by H_2O, CO_2 and O_3.

Effectively the dependence on temperature has been separated from the dependence on absorber distribution. Calculations of radiative flux for new Planckian profiles but the same absorber distribu-

tions are readily carried out without recalculating the transmissivities.

In the lower stratosphere a considerable saving of computational time can further be accomplished by the use of emissivity for calculating radiation fluxes due to water vapor. Rodgers (1967b) investigated the use of emissivity for water vapor in the troposphere and lower stratosphere and found this approximation to give the same order of accuracy as the diffuse approximation if the emissivities are fitted to calculated or accurately measured atmospheric fluxes rather than laboratory measurements. The water vapor emissivity has the form:

$$\mathcal{E}(u) = \sum_{n=1}^{4} a_n u^{n/2} \qquad u < v$$

$$= \sum_{n=0}^{4} b_n (\log u)^n \qquad u > v$$

$$u = \int c(p) \frac{p_s}{g} p \, dp \qquad (g\ cm^{-2})$$

where the parameter v delineates between weak and strong absorption. Note that different emissivities must be used for upward and downward fluxes. The equations for infrared transfer due to water vapor at some height z in the atmosphere become:

$$F^{\downarrow}(z) = \int_{\infty}^{z} B(z') \frac{d\mathcal{E}^{\downarrow}(z, z')}{dz'} dz'$$

$$F^{\uparrow}(z) = \int_{z}^{0} B(z') \frac{d\mathcal{E}^{\uparrow}(z,z')}{dz'} dz' + B(g)\left\{1 - \mathcal{E}^{\uparrow}(z,0)\right\} \qquad (5.1)$$

$F^{\uparrow}(Z)$ and $F^{\downarrow}(Z)$ are the upward and downward fluxes of infrared radiation due to water vapor, B(z') is the Planck function at height z' equal to σT^4 and $\mathcal{E}(z,z')$ is the emissivity of the water vapor between z and z'. CO_2 and O_3 also absorb in the infrared and overlap of CO_2 and O_3 with H_2O must be taken into account. The overlap of O_3 and H_2O is especially important in the lower stratosphere where complete absorption by ozone does not occur for even moderate path lengths. Proper consideration of the overlap of O_3 and H_2O for a spectral interval $\Delta\nu_r$ yields the following additional set of equations which must be added to eqs. (5.1).

$$F^{\downarrow}_{O_3}(\Delta\nu_r, z) = \int_{\infty}^{z} B(\Delta\nu_r, z') \frac{d}{dz'}\left[\mathcal{E}_{O_3}(\Delta\nu_r, z, z')\, T_{H_2O}(\Delta\nu_r, z, z')\right] dz'.$$

$$F^{\uparrow}_{O_3}(\Delta\nu_r, z) = \int_{z}^{0} B(\Delta\nu_r, z') \frac{d}{dz'}\left[\mathcal{E}_{O_3}(\Delta\nu_r, z, z')\, T_{H_2O}(\Delta\nu_r, z, z')\right] dz'$$

$$- B(\Delta\nu_r, g)\, \mathcal{E}_{O_3}(\Delta\nu_r, z, 0)\, T_{H_2O}(\Delta\nu_r, z, 0) \qquad (5.2)$$

For this study only the O_3 9.6 μ and the CO_2 15 μ bands are considered in addition to the water vapor spectrum. The use of water vapor emissivities (eqs. 5.1) coupled with additional equations (eqs. 5.2) for the 9.6 μ and 15 μ bands, reduces the Curtis Matrix solution to a sum over three spectral intervals.

$$F(z) = \sum_{r=1}^{3} \sum_{z'} B_{z'}(\Delta\nu_r) A_{z,z'}(\Delta\nu_r) \qquad (5.3)$$

Curtis Matrices were obtained using the monthly mean radiative parameters outlined in Section III for 10 pressure levels (200-, 150-, 100-, 70-, 50-, 30-, 20-, 15-, 10- and 5 mb) from 85°N-20°N for all twelve months of the year – a total of 5,040 column matrices each containing $\sim$ 25 elements. Thermal cooling is computed by finite-differencing the thermal flux to give the mean thermal cooling between two pressure surfaces.

$$C = \frac{g}{c_p} \frac{\Delta F(p)}{\Delta p}$$

B. Approximate Solutions of Solar Heating in the Lower Stratosphere

Hering et al. (1967) have found that solar heating by ozone in the lower stratosphere varies more strongly with the solar zenith angle and duration of sunlight than with absorber amount. They found that the time variations of <u>total solar heating</u> in the lower stratosphere could be adequately represented by linear regression equations

of the form:

$$H(lat,p) = a(p) \times n\,\overline{M}^{-1/2} + b(p)$$

$$n\,\overline{M}^{-1/2} = A(lat) + B(lat)\cos(2\pi t/365)$$

where a and b are regression constants at p = 10-, 15- and 25 mb, n is the number of daylight hours, $\overline{M}$ is the average magnification factor over the daylight hours and t is the number of days after the summer solstice. Encouraged by their results, linear regression equations of the form:

$$H(lat,p) = C_0(lat,p) + C_1(lat,p)\cos(2\pi t/365) \qquad (5.4)$$

were derived for levels 10 and 30 mb from 85°-20°N. Fig. 30 gives the variation at 10 mb of solar heating with time at several latitudes based on the mean radiative heating obtained in Section IV. The cosine variation is obvious. Eq. (5.4) gives good agreement in low and middle latitudes but systematic departures do occur in the warmer months at high latitudes.

C. Estimating Vertical Motions from the First Law of Thermodynamics

In dynamical studies where observational data are used, one approach in obtaining vertical motions is to compute such motions from the first law of thermodynamics. This, however, requires

knowledge of the non-adiabatic heating which is primarily due to radiation and the release of latent heat of condensation. Previous studies such as Jensen (1961), Barnes (1962), Oort (loc. cit.) and Miller (1966) have used the first law of thermodynamics but have neglected the non-adiabatic heating, arguing that the effect of non-adiabatic heating was small in comparison to dynamical heating. For the lower stratosphere the individual change of pressure ($\omega = dp/dt$) obtained from the first law of thermodynamics and the equation of state is:

$$\omega = \frac{\frac{\partial T}{\partial t} + \vec{V}_p \cdot \nabla_p T}{\frac{R}{c_p}\frac{T}{P} - \frac{\partial T}{\partial P}} - \frac{\frac{1}{c_p} Q}{\frac{R}{c_p}\frac{T}{P} - \frac{\partial T}{\partial P}} \qquad (5.5)$$

where T is temperature, P is pressure in mb and Q/cp is the non-adiabatic heating due to radiation. All other symbols are defined in the appendix. Numerical solutions for ω have been obtained for an extended period of time in the lower stratosphere and the data sources and their manipulation are discussed below.

Daily temperature and geopotential data from 90^{o}-15^{o}N, sfc-10 mb for 1964 were obtained from Asheville, N.C. and the National center for Atmospheric Research, Boulder, Colorado on the standard NWP octagonal grid. These data were interpolated to a latitude-longitude grid and geostrophic winds were computed from 150-10 mb. Use of geostrophic winds should be a good approximation in these

higher levels where low wavenumbers dominate the flow patterns. All terms in eq. (5.5) except for Q/cp could be evaluated from the geopotential and temperature fields. To evaluate Q/cp both the thermal cooling and solar heating must be evaluated.

Thermal cooling is readily obtained using Curtis Matrices (eq. 5.3) provided the adjusted Planckian profiles $B_z, (\Delta\nu_r)$, are obtained. The Planckian profiles depend on temperature and cloud cover since clouds are allowed for by adjusting the temperature field. Mean monthly maps of total cloud amount for 1964 were available as outlined in Section III and included both latitudinal and longitudinal variations. The total cloud amount was distributed into amounts of high, middle and low cloud amount based on the Wisconsin study in low and middle latitudes and London's (1957) study in high latitudes. Mean cloud tops were used within a latitude circle and varied only with latitude and month of year.

Daily hemispheric temperature maps were available for the following levels: surface, 850-, 700-, 500-, 300-, 200-, 150-, 100-, 50-, 30- and 10 mb. Temperature profiles were linearly interpolated in log (pressure) to obtain additional levels where needed. For example, each Curtis Matrix contained elements at 70-, 20- and 15 mb.

The adjusted Planckian profiles also depend on the high level ($<$ 10 mb) temperatures. For 1964 no daily synoptic maps of temperature were available above 10 mb but Western Hemispheric maps of temperature were available once a week during 1964 (Staff, Upper Air

Branch N.M.C. 1967) for 5-, 2- and 0.4 mb. Grid point data were extracted from these maps and grouped together into several latitude bands ($20^{o}N$-$35^{o}N$, $40^{o}N$-$60^{o}N$, $65^{o}N$-$85^{o}N$) in order to increase the sample size. For each month two parameter prediction equations for each latitude band were derived and have the form:

$$T(5\,mb) = a_o\,T(10\,mb) + a_1\,T(30\,mb)$$

$$T(2\,mb) = b_o\,T(10\,mb) + b_1\,T(30\,mb)$$

where T(p) is the temperature at pressure level p. These equations were used to estimate the daily hemispheric temperatures at 5 and 2 mb and can only portray the large scale temperature patterns. However, because of the persistence of large scale features to great heights (e.g. the warm Aleutian high), it is important to estimate the high level temperature fields. Monthly mean temperatures were used at 0.5 and 0.1 mb which varied only with latitude.

Hemispheric profiles of thermal flux were computed using Curtis Matrices and the adjusted Planckian profiles at 200-, 150-, 100-, 70-, 50-, 30-, 20-, 15-, 10- and 5 mb. Thermal cooling was obtained at 9 intermediate levels by finite differencing the thermal flux and linearly interpolated in log (pressure) to give thermal cooling at 150-, 100-, 50-, 30- and 10 mb.

To obtain solar heating, linear regression equations (see Section V B.) were used at 30 and 10 mb which give time and latitude variations but not longitudinal variations. In the warmer months in

high latitudes the monthly mean solar heating rates were used as the linear regression equations depart significantly from the actual time variations of the solar heating. For 150-, 100- and 50 mb the monthly mean solar heating was used since the time changes are small.

Because of the strong dependence of stratospheric thermal cooling on the temperature field (see Section IV), the use of mean absorber distributions coupled with daily hemispheric temperature profiles should give a good representation of hemispheric thermal cooling in the lower stratosphere. When Curtis Matrices are used the assumption is made that the absorber distribution within a period of a month varies with latitude and height but not longitude. For H_2O and CO_2 this assumption is quite good but ozone does have significant longitudinal variations in middle and high latitudes because of the redistribution by the large scale eddies. However, middle latitudes is the region of minimum thermal cooling by ozone as can be seen from Figs. 13 and 14. In higher latitudes and higher levels, CO_2 dominates the thermal cooling.

Since solar heating in the lower stratosphere is mainly dependent on the solar zenith angle and duration of sunlight, longitudinal variations in ozone should not incur significant errors in the total solar heating rates. Overall there is of course considerable uncertainty in the absolute values of the total radiative heating primarily because of the longitudinal variations in ozone.

Examples of the mean total radiative heating along $60^{o}N$ for January and July are presented in Fig. 31 with the differences between

the months reflecting the large seasonal differences between the winter and summer temperature profiles along 60°N.

Vertical motions were computed from eq. (5.5) for each day of 1964 using daily hemispheric fields of temperature, geopotential and radiative heating for 85°N-20°N for the following levels: 150-, 100-, 50-, 30- and 10 mb. The vertical motions so computed represent a 24 hr. average of the large scale vertical motion field.

D. Diagnostic energy equations for the lower stratosphere

The energy cycle of the global atmosphere consists of three parts: generation of available potential energy by non-frictional heating, conversion of available potential energy into kinetic energy by reversible adiabatic processes and dissipation of kinetic energy by friction. A discussion by the author of the background and general equations for available potential energy is contained in Newell et al. (1970a).

Although available potential energy is defined only for the entire atmosphere, it is possible to treat the contribution of a limited region to the available potential energy of the entire atmosphere.

$$A_j = \frac{c_p}{2} \int_{M_j} \gamma T'^2 \, dM$$

Where M_j is the mass of the limited region. This formulation of

available potential energy is based on the approximate equations developed by Lorenz (1955). To gain further insight into the physical processes in the atmosphere, the fields of mass and temperature are further resolved into the amounts associated with the zonal average and the amounts associated with the eddies. Thus the zonal available potential energy (AZ) and the eddy available potential energy (AE) become

$$AZ = \frac{c_p}{2} \int_{M_j} \gamma [T]^{*2} dM$$

$$AE = \frac{c_p}{2} \int_{M_j} \gamma T^{*2} dM$$

Likewise the zonal kinetic energy (KZ) and eddy kinetic energy (KE) become

$$KZ = \frac{1}{2} \int_{M_j} \left([u]^2 + [v]^2 \right) dM$$

$$KE = \frac{1}{2} \int_{M_j} \left(u^{*2} + v^{*2} \right) dM$$

The energy balance equations for each type of energy have the form:

$$\frac{\partial AZ}{\partial t} = GZ - CZ + CA + BAZ$$

$$\frac{\partial AE}{\partial t} = GE - CE - CA + BAE$$

$$\frac{\partial KZ}{\partial t} = CZ + CK + B\phi Z + BKZ - DZ$$

$$\frac{\partial KE}{\partial t} = CE - CK + B\phi E + BKE - DE \qquad (5.6)$$

For a polar cap bounded by two pressure surfaces P_1 and P_2 ($P_1 < P_2$) and a lateral boundary $\varphi = \varphi_s$, the energy conversions and boundary fluxes become:

$$GZ = \int_{M_j} \gamma [Q]'' [T]'' \, dM$$

$$GE = \int_{M_j} \gamma [Q^* T^*] \, dM$$

$$CE = -\int_{M_j} [\omega^* \alpha^*] \, dM$$

$$CZ = -\int_{M_j} [\omega]'' [\alpha]'' dM$$

$$CK = \int_{M_j} [u^* v^*] \cos\varphi \frac{\partial}{\partial \varphi} \left(\frac{[u]}{a \cos\varphi} \right) dM$$

$$+ \int_{M_j} [u^* \omega^*] \frac{\partial [u]}{\partial p} \, dM$$

$$CA = c_p \int_{M_j} \gamma [v^* T^*] \frac{1}{a} \frac{\partial [T]}{\partial \varphi} \, dM$$

$$+ c_p \int_{M_j} \frac{1}{p^\chi} [\omega^* T^*] \frac{\partial}{\partial p} \left(\gamma p^\kappa [T]'' \right) dM$$

$$B\phi Z = BV\phi Z + B\omega\phi Z$$

$$= \int_0^{2\pi} \int_{P_1}^{P_2} [v][\phi]'' a \cos\varphi_s \frac{dp}{g} d\lambda$$

at $\phi = \phi_s$

$$- \int_{M_j} \frac{\partial}{\partial p} [\omega]'' [\phi]'' dM$$

$$B\phi E = BV\phi E + B\omega\phi E$$

$$= \int_0^{2\pi} \int_{P_1}^{P_2} [v^* \phi^*] a \cos\varphi_s \frac{dp}{g} d\lambda$$

at $\phi = \phi_s$

$$- \int_{M_j} \frac{\partial}{\partial p} [\omega^* \phi^*] dM$$

$$BAZ = BAZH + BAZV$$

$$= \int_0^{2\pi} \int_{P_1}^{P_2} \frac{\gamma c_p}{2} \left\{ 2[v^* T^*][T]'' + [v][T]''^2 \right\} a \cos\varphi_s \frac{dp}{g} d\lambda$$

at $\phi = \phi_s$

$$-\int_{M_j} \frac{\partial}{\partial p}\left(c_p \gamma \left\{2[\omega^* T^*][T]'' + [T]''^2[\omega]\right\}\right) dM$$

$$BAE = BAEH + BAEV$$

$$= \int_0^{2\pi} \int_{P_1}^{P_2} \frac{\gamma c_p}{2}[V T^{*2}]\, a \cos\varphi_s \frac{dp}{g}\, d\lambda$$

at $\varphi = \varphi_s$

$$-\int_{M_j} \frac{\partial}{\partial p}\left(c_p \gamma \frac{[\omega T^{*2}]}{2}\right) dM$$

$$BKZ = BKZH + BKZV$$

$$= \int_0^{2\pi} \int_{P_1}^{P_2} \frac{1}{2}\left[V(u^2 + v^2 - u^{*2} - v^{*2})\right] a \cos\varphi_s \frac{dp}{g}\, d\lambda$$

at $\varphi = \varphi_s$

$$-\int_{M_j} \frac{1}{2}\frac{\partial}{\partial p}\left[\omega\left(u^2 + v^2 - u^{*2} - v^{*2}\right)\right] dM$$

$$BKE = BKEH + BKEV$$

$$= \int_0^{2\pi} \int_{p_1}^{p_2} \frac{1}{2}\left[v(u^{*2}+v^{*2})\right] a \cos\varphi_s \frac{dp}{g} d\lambda$$

at $\varphi = \varphi_s$

$$- \int_{M_j} \frac{1}{2} \frac{\partial}{\partial p}\left[\omega(u^{*2}+v^{*2})\right] dM$$

$$DZ = \int_{M_j} \left\{ [u][F_\lambda] + [v][F_\varphi] \right\} dM$$

$$DE = \int_{M_j} \left[u^* F_\lambda^* + v^* F_\varphi^* \right] dM$$

Here T is temperature and all other symbols are defined in the appendix. The form of the boundary terms is based upon the development by Muench (1965). The zonally averaged continuity equation

$$\frac{1}{a\cos\varphi}\frac{\partial [v]\cos\varphi}{\partial \varphi} = -\frac{\partial [\omega]}{\partial p}$$

was numerically integrated from the North Pole to 20°N to estimate $[v]$ at the lateral boundary since $[v_g] \equiv 0$.

For the global atmosphere the conversion of available potential energy into kinetic energy (CE + CZ) is given by the integral of $\omega\alpha$ over the mass of the atmosphere. For a restricted region, however, the following relations hold:

$$-\int_{M_j} \vec{V}_p \cdot \nabla_p \phi \, dM = -\int_{M_j} \omega\alpha \, dM - \int_{M_j} \nabla_p \cdot \vec{V}_p \phi \, dM - \int_{M_j} \frac{\partial}{\partial p}\omega\phi \, dM \qquad (5.7)$$

The generation of kinetic energy in the limited region may be interpreted as that due to the conversion between available potential and kinetic energy and the redistribution of kinetic energy (boundary terms on r.h.s. of eq. (5.7)). With such an interpretation it is not possible to say that generation of kinetic energy is taking place in the limited region by only considering the conversion between available potential and kinetic energy.

E. Energy Sources for the Lower Stratosphere

A slab in the atmosphere is contrasted with the entire atmosphere in that the energy balance equations for a slab contain boundary terms which may result in energy being brought into a region rather than energy being generated in situ. Both Starr (1960) and White and Nolan (1960) suggested that the lower stratosphere might be dependent on energy brought in from the troposphere rather than energy generated internally.

Evidence from numerous observational and theoretical studies shows that the lower stratosphere is dependent on mechanical work from the troposphere for the maintenance of the kinetic energy budget. This is the pressure work term, 'pw' in geometric coordinates or 'ωz' in pressure coordinates, that arises in the kinetic energy balance equations (eqs. 5.6). The idea that the lower stratosphere is a forced region is further supported by the countergradient flux of sensible heat first discovered by White (1954). This occurs because northward moving parcels of air are sinking and southwards moving parcels are rising relative to isentropic surfaces (Newell 1961, Molla and Loisel 1962, Peng 1965a,b) and is related to the N.H. ozone buildup in high latitudes in the spring.

A number of observational studies have examined the energetics of the lower stratosphere during sudden warmings (Reed et al. 1963, Lateef 1964, Labitzke 1965, Muench loc. cit., Julian and Labitzke 1965, Perry 1967) and additionally there have been a few studies which covered an entire year (Oort loc. cit., Miller loc. cit., Richards

loc. cit.). The picture that emerges is that the lower stratosphere is a forced region with no kinetic energy generated internally. Maintenance of the kinetic energy budget is accomplished by mechanical work from the troposphere. Kinetic energy is converted into available potential energy and radiation is the ultimate sink of this energy. The gross features of the stratospheric energetics are now considered known but more spacial and temporal resolution is needed in order to understand the unique coupling that exists between the lower stratosphere and the troposphere. The present study provides more resolution by examining the energetics of the lower stratosphere on a daily basis including results for the 10 mb level.

Consider now the maintenance of the eddy kinetic energy budget in the lower stratosphere. To offset internal frictional dissipation, KE must be maintained by a conversion from zonal kinetic energy (CK), a direct conversion of eddy available potential energy (CE) and/or boundary energy fluxes into the region (BΦE + BKE). To investigate these processes in detail, the energy balance equations (eqs. 5.6) have been evaluated for each day of 1964 for the region 100-10 mb, 90°N-20°N. In presenting numerical results, eqs. (5.6) have been divided by the surface area of the polar cap.

Like the troposphere the conversion CK (Fig. 33) is principally KE $\longrightarrow$ KZ throughout the year. The conversion CE (Fig. 32) shows an annual variation with significant release of AE occurring only in late November and the winter months. For the other months (March-November) there is no significant conversion of AE $\longrightarrow$ KE. For these periods it

is necessary that energy be brought in through the boundaries. To get proper perspective on this problem, the monthly mean energy conversions and boundary energy fluxes are presented in Table II. It is clear that for all months except January, that the eddy kinetic energy budget is maintained by boundary energy fluxes and that the dominant eddy boundary term is the convergence of the vertical eddy flux of geopotential ($B_{\omega\Phi E}$). The importance of mechanical work at the horizontal boundaries is in agreement with previous investigations.

Daily variations of $B_{\omega\Phi E}$ for 1964 are presented in Fig. 34. During the winter months there are alternating periods of convergence and divergence of vertical energy flux but all other seasons are characterized by convergence of vertical energy flux. Of particular note are the periods of substantial energy flux convergence in early spring and late fall and early winter. Daily variations of the vertical eddy flux of geopotential ($\langle [\omega^* Z^*] \rangle$) through 100 and 10 mb are presented in Fig. 35 and it is evident that the primary energy source for the vertical energy flux is tropospheric in origin.

Certainly the upward propagation of energy from the troposphere is of fundamental importance in maintaining the eddies in the lower stratosphere. Tropospheric wave disturbances are excited by asymmetric topographic and thermal forcing near the surface in addition to baroclinic instability. These low frequency wave disturbances may propagate from the lower atmosphere into the upper atmosphere with the possibility of substantial energy propagation. Using a linearized

Table II

Monthly mean energy contents ($\times 10^7$ ergs cm^{-2}), energy conversions (ergs cm^{-2} sec^{-1}) and boundary terms (ergs cm^{-2} sec^{-1}) for 1964 for 100-10 mb, $90^{\circ}N$-$20^{\circ}N$.

	AZ	AE	KZ	KE
J	6.0	6.8	20.1	11.6
F	6.4	5.1	18.0	7.3
M	9.4	4.0	7.7	8.9
A	7.6	.5	2.6	2.0
M	6.4	.4	1.5	1.2
J	7.9	.5	2.7	1.4
J	8.3	.4	4.3	1.5
A	6.6	.5	3.8	1.5
S	5.1	.5	3.0	1.8
O	4.3	1.3	4.3	2.9
N	4.6	2.8	8.1	7.4
D	5.7	4.2	13.1	10.3

	CZ	CA	CE	CK
J	-191.8	-182.2	135.6	198.8
F	-110.7	-169.8	54.3	65.9
M	-29.4	65.3	-121.2	53.3
A	-32.4	-8.0	-22.1	1.7
M	-23.9	-2.0	-21.8	2.9
J	-40.9	2.5	-14.2	-1.9
J	-44.2	9.7	-11.6	5.3
A	-30.8	12.0	-14.9	6.0
S	-32.5	7.9	-12.4	7.4
O	-16.0	-1.8	-26.5	22.7
N	-58.0	-28.6	-8.4	50.4
D	-109.9	-84.5	48.0	68.4

	GZ	GE	$B\dot{\Phi}Z$	$B\dot{\Phi}E$*
J	-1.5	-82.5	228.0	-16.4
F	-11.0	-61.5	194.6	59.7
M	-78.0	-65.2	53.7	265.8
A	-63.5	-7.6	60.0	39.7
M	-37.7	-5.5	60.6	41.0
J	-39.6	-6.1	77.7	32.0
J	-46.4	-7.1	73.8	19.2

Table II (continued)

A	-45.6	-6.0	63.9	36.1
S	-42.4	-7.0	67.8	23.2
O	-19.6	-14.3	96.9	80.0
N	-12.8	-34.2	137.8	117.9
D	5.8	-50.6	128.6	127.6

	BAZ	BAE	BKZ	BKE
J	7.1	-.2	4.5	-10.4
F	16.4	.1	11.3	4.2
M	7.6	-6.9	-27.6	-8.2
A	8.4	-.8	-6.1	-6.1
M	8.0	-.6	-1.2	-3.2
J	7.5	.4	4.9	1.5
J	6.0	.5	-13.1	-5.3
A	7.8	.5	-2.4	-1.8
S	.9	-.4	-19.8	-5.3
O	2.2	-.5	-10.8	-8.9
N	1.7	-1.2	-12.0	-9.6
D	4.9	-3.5	-12.2	-3.9

	BAEV	BAEH	BAE	BAZV	BAZH	BAZ
J	1.8	-2.0	-.2	-3.3	10.4	7.1
F	.8	-.7	.1	-4.5	20.9	16.4
M	-6.7	-.2	-6.9	-2.4	10.0	7.6
A	-.4	-.4	-.8	.4	8.0	8.4
M	-.6	.0	-.6	4.0	4.0	8.0
J	.5	-.1	.4	9.4	-1.9	7.5
J	.3	.2	.5	7.5	-1.5	6.0
A	.2	.3	.5	5.7	2.1	7.8
S	-.1	-.3	-.4	1.6	-.7	.9
O	-.3	-.2	-.5	.3	1.9	2.2
N	-1.6	.4	-1.2	1.4	.3	1.7
D	-3.3	-.2	-3.5	2.7	2.2	4.9

Table II (continued)

	BKEV	BKEH	BKE	BKZV	BKZH	BKZ
J	1.9	-12.3	-10.4	-12.3	16.8	4.5
F	5.8	-1.6	4.2	-6.8	18.1	11.3
M	-2.5	-5.7	-8.2	-24.7	-2.9	-27.6
A	3.1	-9.2	-6.1	-3.8	-2.3	-6.1
M	.9	-4.1	-3.2	-1.7	.5	-1.2
J	.4	1.1	1.5	2.5	2.2	4.9
J	1.3	-6.6	-5.3	2.5	-15.6	-13.1
A	2.1	-3.9	-1.8	2.3	-4.7	-2.4
S	.4	-5.7	-5.3	.5	-20.3	-19.8
O	-.5	-8.4	-8.9	-8.7	-2.1	-10.8
N	-3.4	-6.2	-9.6	-20.0	8.0	-12.0
D	-3.6	-.3	-3.9	-33.4	21.2	-12.2

	$B\omega\phi E$	$BV\phi E$	$B\phi E$*	$B\omega\phi Z$	$BV\phi Z$	$B\phi Z$
J	-16.4		-16.4	43.5	184.5	228.0
F	59.7		59.7	-1.6	196.2	194.6
M	265.8		265.8	-68.9	122.6	53.7
A	39.7		39.7	11.1	48.9	60.0
M	41.0		41.0	21.1	39.5	60.6
J	32.0		32.0	29.9	47.8	77.7
J	19.2		19.2	27.9	45.9	73.8
A	36.1		36.1	24.8	39.1	63.9
S	23.2		23.2	55.2	12.6	67.8
O	80.0		80.0	23.7	73.2	96.9
N	117.9		117.9	14.5	123.3	137.8
D	127.6		127.6	-34.4	163.0	128.6

*It is not possible to evaluate $BV\phi E$ using geostrophic winds. A qualitative analysis of this term using the Eliassen and Palm approximation (see section V.G and Newell and Richards 1969) indicates there is a loss of energy laterally to the tropical stratosphere in the winter, but a gain of energy by the extra-tropical stratosphere in the warmer months. The latter energy source might be important to the maintenance of the summer eddies.

cartesian model, Charney and Drazin (1961) found for standing waves that the transmissivity of the upper atmosphere increases with increasing wavelength and that only the stationary ultra-long waves should be able to propagate significant energy through the stratosphere. They also found that for zonal winds greater than 38 m sec^{-1} or negative that waves are trapped. This would permit significant energy propagation through the stratosphere only at the equinoxes.

Murakami (1967) investigated the energetics of stationary disturbances in an attempt to assess the relative roles of topographic and diabatic forcing. He found that at 35°N the upward energy transfer is accomplished by topographically induced waves; whereas, at 60°N the thermally induced waves are principally responsible for the upward energy transfer.

Dickinson (1968a) considered stationary waves forced at the lower boundary with spherical geometry and found that there will always be two or more wave modes which can propagate through the stratospheric westerlies. However, winds at thermospheric heights are predicted to have excessively large disturbance amplitudes which is attributed to the lack of horizontal wind shears and diabatic damping. Inclusion of latitudinal wind shears by Dickinson (1968b) shows that the stratospheric westerly jet will act as a wave barrier to disturbances excited in the mid-latitude troposphere, creating a stratospheric wave guide in high latitudes. When Newtonian cooling is introduced (Dickinson 1968c) in a linearized cartesian model,

stationary wave disturbances are highly damped for weak west winds and still damped for west winds below the critical cutoff velocity. The theoretical models developed to date are certainly idealized but they do provide a conceptual framework for discussing vertical energy propagation.

Consider now the maintenance of the zonal kinetic energy budget. Frictional dissipation must be offset by the conversion CK, a direct conversion of zonal available potential energy (CZ) and/or boundary energy fluxes into the region ($B\phi Z$ + BKZ). For KZ there exists no significant period when direct conversion from AZ is possible (Fig. 32). As noted earlier the conversion CK is from KE $\longrightarrow$ KZ and is quite large in the winter (Fig. 33). However, from Table II we see that if there were no boundary energy fluxes, then only during March and October would CK possibly be large enough to offset the loss by CZ and whatever frictional dissipation is taking place. Clearly KZ must also be maintained by boundary energy fluxes and the dominant fluxes from Table II are seen to be $B\omega\phi Z$ and $BV\phi Z$. In the winter months the forcing is primarily lateral forcing at $20^{\circ}N$ from the tropical stratosphere, whereas in the warmer months both lateral and tropospheric forcing are important.

The boundary fluxes $B\omega\phi Z$ and $BV\phi Z$ are very prone to error because of the difficulty in accurately assessing the mean cells ($[\omega]$ and $[v]$). No great accuracy is claimed for these boundary terms as they are probably known only to within a factor of two. Only monthly mean values are presented since daily values show a great

deal of oscillation.

F. Vertical Energy Flux and Convergence in the Lower Stratosphere

Re-examining Fig. 35 it is seen that the vertical energy flux through 100 mb is almost always upwards into the lower stratosphere with major periods of enhanced energy flux occurring in late fall and winter and one period of particularly large and sustained energy flux occurring throughout March. In the winter a substantial amount of this energy passes upward through 10 mb (Fig. 35) particularly in January and is very significant when compared with the energy content of the upper stratosphere (Newell 1966a,b). It is interesting to note that the stratosphere is very open to the upward transmission of energy in late winter although the zonal winds (Fig. 39) in this region are maximum during this time reaching values in excess of 50 m sec^{-1}. Note also that very little energy is propagated upward through 10 mb at the spring equinox and virtually no upward propagation occurred at the fall equinox. These time periods will be discussed in more detail later in this paper.

The change-over from the polar westerlies to the summer easterlies is quite dramatic at 10 mb with virtually no upward propagation of energy during the summer easterlies which became well established in April (Fig. 40). The trapping of wave disturbances by easterlies is well predicted by theory. Tropospheric westerlies protrude upward to about 50 mb in the warmer months (e.g. see April, Fig. 40) and a small but important upward energy flux from the troposphere through

100 mb continues throughout the summer. As predicted by theory this energy flux is trapped by the easterlies above resulting in a continual vertical energy convergence during the warmer months.

To investigate the latitudinal variations, monthly mean vertical energy fluxes have been obtained for 100-, 50-, 30- and 10 mb and are presented in Table III. In the winter most of the upward energy flux takes place between 45^{o}-75^{o}N with the peak fluxes occurring between 60^{o}-65^{o}N. This is also the region of the largest westerlies as can be seen from Table IV. It is clear that in the winter a substantial amount of energy passes upward into the upper stratosphere in high latitudes. Of particular note is the downward flux of energy through 10 mb in the very high latitudes which increases from January to March. The source of this downward energy flux is possibly the upper baroclinic stratospheric westerly vortex (Fig. 38).

The dramatic change from substantial upward energy propagation in March to virtually no propagation at all above 50 mb in April is shown clearly in Table III. From Table IV we see that this change occurs when the westerly vortex is replaced by the summer easterlies as noted previously. In the fall a weak polar cyclonic vortex is established in high latitudes with anticyclonic flow in low and middle latitudes. The tropospheric energy flux increases throughout the fall but a considerable fraction of the energy flux is absorbed.

Table III

$\overline{[\omega^* z^*]}$ (ergs cm^{-2} sec^{-1}).

Lat	J	F	M	A	M	J	J	A	S	O	N	D
					1964 - 100 mb							
85	21	52	67	18	-1	-9	4	0	-3	10	-41	27
80	104	-5	26	21	-4	-17	5	-1	-9	-14	-102	-41
75	-125	-195	-306	-12	-13	-5	-2	-5	-15	-62	-159	-108
70	-498	-196	-625	-36	-28	1	-18	-11	-25	-109	-216	-72
65	-702	-204	-779	-28	-30	-16	-22	-22	-38	-143	-236	85
60	-701	-317	-878	-23	-22	-30	-24	-32	-53	-180	-260	-44
55	-547	-379	-788	-35	-23	-19	-28	-23	-51	-218	-342	-497
50	-356	-336	-568	-39	-39	-18	-38	-48	-35	-213	-372	-788
45	-201	-248	-390	-68	-58	-36	-28	-71	-21	-112	-332	-659
40	-99	-114	-232	-83	-64	-27	0	-39	-19	-15	-155	-275
35	-78	9	-54	-68	-70	-32	-12	-10	-26	-40	-59	-30
30	-5	26	-27	-41	-56	-64	-40	-50	-17	-50	-74	-9
25	24	-1	-47	-21	-30	-55	-22	-57	-12	-16	-58	-59
20	-15	5	-43	-1	-29	-41	-6	-21	-6	4	-34	-65
					1964 - 50 mb							
85	-42	61	427	0	0	-1	1	0	0	5	-37	-1
80	-162	78	806	-1	0	0	5	0	1	0	-121	-84
75	-443	-101	407	-5	-1	2	5	0	-1	-28	-234	-217
70	-693	-265	-183	-9	-4	3	0	0	-8	-58	-297	-226
65	-726	-360	-649	-10	-3	1	-4	-2	-16	-78	-264	-128
60	-621	-386	-933	-6	-3	-2	-6	-6	-19	-82	-223	-197
55	-588	-321	-854	-1	-4	-6	-6	-8	-20	-77	-204	-423
50	-442	-205	-506	-4	-5	-7	-4	-7	-17	-62	-178	-468
45	-183	-95	-196	-7	-6	-7	-1	-3	-9	-29	-106	-276
40	-55	-37	-54	-10	-5	-8	-3	-1	-3	-7	-44	-97
35	-22	-13	-15	-8	-3	-7	-8	-2	-4	-4	-17	-22
30	-3	-4	-6	-3	-2	-6	-9	-3	-4	-5	-7	-9
25	1	-1	-2	-3	-2	-4	-5	-4	-4	-3	-2	-6
20	-1	-1	-1	-3	-1	-2	-3	-3	-3	-1	-2	-2

Table III (continued)

Lat	J	F	M	A	M	J	J	A	S	O	N	D
					1964 - 30 mb							
85	-84	121	468	-1	0	0	1	0	1	1	16	2
80	-291	234	977	-2	1	1	3	0	2	-5	30	-101
75	-552	65	655	-3	0	2	3	0	1	-14	-60	-325
70	-776	-251	-26	-2	0	2	-1	0	-4	-35	-215	-391
65	-883	-473	-543	-3	-1	0	-4	-1	-10	-44	-236	-256
60	-853	-442	-785	-3	-2	-2	-4	-3	-10	-45	-179	-247
55	-699	-308	-685	-2	-2	-4	-4	-4	-9	-44	-150	-365
50	-408	-180	-417	1	-2	-4	-3	-3	-8	-32	-112	-351
45	-155	-76	-170	2	-2	-5	-3	-2	-4	-11	-50	-178
40	-54	-23	-45	0	-2	-5	-4	-1	-2	-2	-20	-54
35	-19	-6	-13	-3	-2	-3	-4	-1	-1	-1	-11	-14
30	-5	-2	-7	-3	-1	-1	-3	0	0	-1	-7	-4
25	-1	0	-3	-2	-1	-1	-4	0	1	-1	-2	-2
20	0	1	0	-1	0	0	-1	0	2	0	-1	0
					1964 - 10 mb							
85	99	216	252	1	0	0	0	0	1	0	-1	3
80	142	434	588	1	1	0	0	1	2	-10	-30	-63
75	-208	247	570	1	0	-1	-1	0	2	-24	-155	-238
70	-728	-103	283	0	-1	-2	-3	-1	-2	-26	-289	-353
65	-921	-360	-104	0	-1	-1	-3	-1	-5	-19	-283	-247
60	-842	-419	-378	0	-1	-1	-3	-1	-6	-13	-176	-133
55	-633	-304	-414	-1	-1	-1	-2	-1	-5	-10	-67	-149
50	-310	-151	-274	-1	-1	-1	-2	0	-4	-6	-32	-170
45	-111	-61	-130	-2	-1	-2	-2	0	-2	-2	-25	-102
40	-39	-22	-63	-2	-1	-1	-1	-1	-1	-1	-13	-34
35	-13	-4	-27	0	0	0	-1	-1	-1	0	-4	-8
30	-4	-1	-7	1	0	0	0	0	0	1	-5	-1
25	-2	-1	-2	1	0	0	-1	0	0	0	-2	0
20	-1	2	-1	0	0	1	-1	0	0	1	0	0

Table IV

Mean Zonal Wind (m sec^{-1})

Lat	J	F	M	A	M	J	J	A	S	O	N	D
						1964 - 100 mb						
85	7	7	4	-1	2	1	2	0	1	3	2	4
75	12	12	7	0	3	1	3	0	3	6	5	7
75	17	17	9	1	4	1	3	1	4	8	8	10
70	21	20	10	3	4	1	3	2	5	9	10	13
65	22	20	11	5	5	2	4	3	7	10	13	15
60	21	19	12	7	6	3	4	5	9	11	14	16
55	19	18	13	9	7	4	6	7	11	13	16	17
50	19	18	16	12	9	5	8	10	14	16	18	18
45	21	20	18	14	10	8	9	11	16	18	19	19
40	24	24	22	16	12	9	8	10	15	18	20	20
35	26	26	24	17	12	9	3	5	10	16	20	22
30	26	26	24	17	12	6	-2	-1	4	10	18	23
25	23	22	22	15	9	1	-6	-7	-2	5	15	22
20	16	16	17	13	5	-5	-8	-12	-7	1	9	18
						1964 - 50 mb						
85	11	10	4	-1	0	-1	0	-1	1	4	4	7
80	19	19	7	-1	0	-1	0	-1	2	7	8	12
75	27	26	9	-1	0	-2	-1	-1	3	9	11	16
70	32	31	10	0	0	-3	-1	-1	4	10	13	19
65	32	31	10	0	0	-3	-2	-1	5	10	14	20
60	28	27	10	1	1	-3	-2	0	6	10	14	20
55	23	22	11	2	1	-3	-2	1	6	10	14	19
50	19	17	10	3	1	-3	-2	1	6	10	14	17
45	15	13	10	3	1	-3	-3	-1	5	9	12	14
40	13	10	9	3	0	-3	-5	-3	3	7	10	11
35	11	9	8	3	-1	-5	-8	-6	-1	5	8	8
30	9	7	7	3	-2	-7	-11	-10	-5	1	6	7
25	6	5	5	3	-3	-9	-14	-14	-9	-2	3	6
20	3	3	4	1	-6	-13	-18	-18	-13	-6	0	5

Table IV (continued)

Lat	J	F	M	A	M	J	J	A	S	O	N	D
					1964 - 30 mb							
85	15	13	3	-1	-1	-1	-1	-1	2	5	7	10
80	20	24	5	-2	-1	-3	-2	-2	3	8	11	17
75	35	34	7	-2	-2	-4	-3	-3	4	10	14	21
70	40	39	8	-2	-2	-5	-4	-3	5	11	15	24
65	39	38	8	-2	-2	-6	-4	-3	5	11	16	25
60	34	32	8	-2	-2	-6	-5	-2	5	10	15	24
55	27	25	8	-2	-2	-6	-5	-2	5	10	15	23
50	20	17	7	-3	-2	-7	-6	-3	4	9	13	19
45	13	11	6	-2	-2	-7	-8	-4	3	8	11	14
40	9	6	4	-1	-3	-7	-10	-7	0	6	9	10
35	6	4	4	0	-3	-8	-12	-10	-4	3	8	7
30	5	2	3	1	-4	-10	-14	-13	-8	0	5	4
25	4	2	4	2	-6	-13	-18	-17	-12	-4	2	3
20	3	1	4	1	-10	-17	-20	-21	-16	-7	-1	3
					1964 - 10 mb							
85	20	20	0	-1	-2	-3	-3	-2	2	6	10	14
80	36	35	1	-2	-3	-5	-5	-3	4	11	17	24
75	48	48	3	-3	-4	-6	-6	-4	5	14	22	37
70	55	54	5	-4	-5	-7	-7	-4	6	16	24	36
65	55	53	6	-4	-5	-7	-7	-4	7	16	24	37
60	49	45	5	-5	-4	-8	-8	-4	7	15	23	36
55	39	34	4	-6	-4	-9	-9	-4	7	15	21	34
50	27	22	2	-5	-4	-11	-11	-6	6	14	20	32
45	17	13	0	-2	-3	-13	-13	-8	4	12	19	27
40	10	6	1	2	-3	-15	-15	-11	1	11	17	21
35	7	4	2	6	-2	-17	-17	-14	-3	8	16	14
30	7	4	5	9	-2	-19	-19	-17	-8	5	13	9
25	7	4	7	9	-5	-22	-22	-20	-13	-1	8	5
20	6	2	8	5	-11	-27	-27	-25	-19	-8	0	1

G. The Nature of the Seasonal Circulations in the Lower Stratosphere

G.1 Winter (December-February)

The winter circulation in the lower stratosphere during 1964 was characterized by a polar cyclonic vortex and a weaker anticyclone in the area of the Aleutian Islands. This pattern persisted to at least 50 km. Kriester et al. (1964) describe the circulation in the lower stratosphere during January and February, 1964 as being supernormally strong with extremely cold temperatures persisting in the polar cyclone till mid-March. In January a mid-winter warming occurred in the upper stratosphere over Central Europe (Kriester et al. loc. cit., Kriester 1968) but did not penetrate far into the lower stratosphere.

The winter energetics in the lower stratosphere are similar to those in the winter troposphere. In particular

1) There is substantial release of eddy available potential energy (Fig. 32) which occurs in the baroclinic polar cyclonic vortex (Figs. 39 and 41).

2) The horizontal eddies through the Reynolds' stresses convert KE $\longrightarrow$ KZ (Fig. 33).

3) The horizontal eddies also convert AZ $\longrightarrow$ AE (Fig. 33) by redistributing the zonal temperature field into the eddy temperature field.

Unlike the troposphere there is a convergence of vertical energy flux for December and February and a small divergence in January. This convergence of vertical energy flux combined with the release of AE maintain the eddies against frictional dissipation and the Reynolds' stresses. The zonal kinetic energy is maintained against frictional dissipation and loss of KZ $\longrightarrow$ AZ (Fig. 32) by the Reynolds' stresses and boundary forcing, principally lateral forcing by the tropical stratosphere.

Throughout the winter there is a continual conversion of KZ $\longrightarrow$ AZ because of forced sinking of warm air and rising of cold air by the mean cells. The effect of radiation on AZ, however, is quite small (Fig. 36) due to offsetting regions of generation in high latitudes and destruction in low latitudes. In high latitudes the poleward increase in zonal cooling coupled with the poleward decrease of temperature results in generation of AZ; whereas, in low latitudes the equatorward decrease of both zonal cooling and temperature results in destruction of AZ. An energy balance for AZ is achieved by the horizontal eddies converting AZ $\longrightarrow$ AE (Fig. 33). Redistribution of the zonal temperature field results in significant longitudinal variations and radiation acts to destroy the eddy temperature field (Fig. 36), cooling more in the regions that are warmer and less in the regions that are cooler. A large destruction of AE takes place in the Aleutian anticyclone as can be seen from the monthly mean radiative heating rates along 60°N for January (Fig. 31).

In the winter months most of the energy resides in the kinetic energy field rather than the potential energy field (Fig. 37) with larger temporal variations occurring in the eddy forms of energy. The energy contents AE and AZ show a general inverse relationship with each other as do the energy contents KE and KZ. These variations cannot be explained entirely by the conversions CA and CK.

It is of interest to note that the lower stratosphere is actually exporting energy in January even though some of the largest tropospheric energy fluxes occurred in this month. To examine this in more detail, the monthly mean divergence of the vertical energy flux ($-\frac{\partial}{\partial p}\overline{[\omega^* z^*]}$) is presented for January and February in Fig. 39 . It is seen that the polar night jet is an energy source region which is probably due to wave disturbances excited by the intense baroclinic zone in middle and high latitudes (Fig. 41). In February there is a weakening of the baroclinic zone (not shown) and a concomitant decrease in the export of energy.

Although the January tropospheric energy fluxes were not significantly absorbed in the lower stratosphere, we may infer that they were very important to the mid-winter warming that occurred over Central Europe in the upper stratosphere. The upper stratospheric warming began near January 13 (Kriester et al. loc. cit.) about four days after the peak vertical energy fluxes through 10 mb. The temperature at 3.4 mb over Berlin rose to -19.9°C on January 17 and then dropped until January 20. Temperatures began rising over Berlin and the highest stratospheric temperature as of 1964 ever observed by the

Berlin radiosonde station was recorded on January 31: $+1^{\circ}C$ at 3.8 mb.

This upper stratospheric warming is of notable interest because the time variations in the upper level heating closely follow the variations in the energy flux through 10 mb. Estimates by Newell (1966a,b) of the energy contents AZ and KZ for the winter upper stratosphere (32.5 km - 62.5 km) are about 80×10^{5} ergs cm^{-2} for AZ and 240×10^{5} ergs cm^{-2} for KZ. Thus, vertical energy fluxes of the magnitude observed in winter ($>$ 100 ergs cm^{-2} sec^{-1}) are capable of changing the energy content of the upper stratosphere within a couple of days. In view of the extensive upward energy fluxes through 10 mb in the winter, this suggest a greater coupling of the upper stratosphere with the lower atmosphere than has previously been thought possible.

Discussions by the Staff, Upper Air Branch N.M.C. (loc. cit.) of the upper stratospheric maps for 1964, point out a second warming trend in February with pronounced warming occurring in late February at Fort Greely, Alaska and Fort Churchill, Canada which continued into mid-March. Accompanying this warming anticyclonic flow became established over the pole in March but was replaced briefly by westerly flow in April.

The upper stratospheric circulation during fall and early winter of 1964 was characterized by considerable variability in the westerly flow and marked pulsations of the Aleutian anticyclone. In late December there was an intensification of the Aleutian anti-

cyclone and the formation of an Atlantic anticyclone. During this period there was increased warming at Fort Greely, Fort Churchill and Wallops Island, Virginia.

These synoptic variations with periods of increased activity and warming in the upper stratosphere are significant since they generally occur at times of increased vertical energy flux into the upper stratosphere. In view of the magnitude and duration of the winter energy fluxes through 10 mb, we are forced to consider the existence of more coupling of the upper and lower atmospheres.

Although there is significant energy propagation upward from the troposphere, there is also a large downward energy flux through 10 mb in late winter as can be seen by examining the daily vertical energy fluxes through 10 mb for February (Fig. 42). At the beginning of the month there are extensive downward energy fluxes in middle and high latitudes such that the area averaged energy flux through 10 mb is actually downward (Fig. 35). At the end of the month there is another period of downward energy flux in high latitudes with values in excess of 2000 ergs cm^{-2} sec^{-2}. Although area weighting reduces the contribution of high latitudes, this downward energy flux is a significant component of the net vertical energy flux through 10 mb.

Ozone, which is a good trace substance of stratospheric motions, is brought down in the winter from higher levels in low latitudes and accumulates in middle and high latitudes of the N.H. due to the northward transport of ozone by the eddies. This has been explained by Newell (1961, 1963, 1964) as taking place because of the positive

correlation of ω and v such that northward moving ozone rich air parcels are sinking and southward moving ozone poor air parcels are rising relative to mean isentropic surfaces. For January, 1964 there is a region in low latitudes and another in higher latitudes (Fig. 45) where ω and v are positively correlated.

G.2 Spring (March-May)

On March 10, 1964 a spring warming began in the lower stratosphere over Northern Europe (Kriester et al. loc. cit.). Synoptically the Aleutian high intensified and moved poleward and by the end of March easterly flow became permanently established in high latitudes with cyclonic flow in lower latitudes. Accompanying the change in the wind structure was a warming at high latitudes with a poleward zonal temperature gradient established in the region 50-10 mb. The reason for the spring warming was the large and sustained convergence of vertical energy flux that took place during March.

At the beginning of March the enhanced convergence of vertical energy flux went into the kinetic energy field as KE and the conversion CK (KE $\longrightarrow$ KZ) increased. However, because of the duration and magnitude of the energy convergence, forced vertical (KE $\longrightarrow$ AE) and horizontal (AE $\longrightarrow$ AZ) motions were established which increased the zonal temperature gradient as is evidenced by the rapid increase in AZ during March. Continued increase of the convergence of vertical energy flux resulted in steeper forced motions which increased the transfer of energy into the potential energy field, i.e. temperature field. However, changes in the temperature field are coupled with

changes in the wind field through the thermal wind equation. Hence by mid-March at 10 mb extensive easterlies covered most of the Western hemisphere and the polar cyclone had weakened, resulting in a rapid decrease in the Reynolds' stresses. The forced motions continued throughout the remainder of the month although decreasing as the eddy boundary forcing decreased. By the end of the month substantial warming of the polar regions had taken place with a reversal of the high latitude zonal temperature gradient from that of January (Fig. 46).

The spring warming of 1964 was characterized by forced eddy motions and not by barotropic or baroclinic instability as suggested by Murray (1960) and Charney and Stern (1962). At the end of February there is a short period where K.E. increases because of the conversions AE $\longrightarrow$ KE and KZ $\longrightarrow$ KE. However, at the beginning of March both of these conversions reverse.

To investigate further the forced motions during March, the monthly mean temperatures, eddy heat fluxes and the integrand of CA are presented in Fig. 46. Note in January that the eddy heat fluxes transfer heat down the temperature gradient in high latitudes thereby redistributing the zonal temperature field into the eddy temperature field and increase AE. However, in March the zonal mean temperature gradient is reversed and the northward transfer of sensible heat by the eddies results in a countergradient heat flux which builds up the zonal temperature gradient and increases AZ.

The spring maximum in total ozone in high latitudes is intimately linked to this countergradient heat flux since both phenomena occur because of the forced motions established by the large convergence of vertical energy flux. The need to transfer energy from KE $\longrightarrow$ AE and AE $\longrightarrow$ AZ is accomplished by sinking of northward moving parcels of air and the rising of southward moving parcels of air relative to the mean isentropic surfaces. This is shown clearly by comparing the regions of forced vertical motions (Fig. 41), the regions of the countergradient heat flux (Fig. 46) and the covariance between ω and v (Fig. 45). In March virtually the whole lower stratosphere shows a positive correlation of ω and v with increased values over those that occurred in January. Indeed for 1964 the spring maximum in ozone did occur in March. This verifies the prediction by Newell (1964) that the spring warming and the spring ozone maximum are manifestations of the same phenomenon – enhanced tropospheric energy flux.

An interesting problem arises in March in that a great deal of the upward propagating energy through 100 mb was absorbed even though weak mean zonal westerlies existed during this period (Fig. 40). It appears that the spacial distribution of the wind field is very important in the trapping of upward propagating disturbances.

The daily vertical energy fluxes through 10 mb and the daily zonal winds are presented in Figs. 43 and 44. At the beginning of March there is substantial upward energy flux in middle latitudes but a very large downward energy flux occurred in high latitudes

resulting in significant convergence of vertical energy flux. As time progresses and the tropospheric energy flux continues, the energetics become forced with substantial energy going into the potential energy field. This is reflected in the increase of easterlies or decrease of the zonal mean westerlies (Fig. 44). As the Aleutian system expands and covers more area, less of the surface at 10 mb becomes open for upward transmission of energy from 100 mb. By mid-March from synoptic maps it is found that half of the N.H. is covered by anticyclonic flow which reduces the zonal westerlies to zero (Fig. 44). The easterlies continue to expand and occupy more area and very little energy flux is transmitted upwards through 10 mb. Once the forced motions are started by enhanced energy flux convergence, they in turn modify the wind field which traps more of the upward propagating energy.

The propagation of energy through 100-, 50-, 30- and 10 mb is shown in Fig. 47 and it is seen that the trapping progresses downward with time during March as the wind structure at each level changes from westerlies to easterlies.

Although the downward energy flux through 10 mb at the beginning of March does increase the vertical energy flux convergence, it is the duration of the tropospheric energy flux that apparently brings about the spring warming. In January the baroclinic polar night jet (Fig. 41) was an energy source region (Fig. 39); whereas, in March this region became a large energy sink (Fig. 40) with forced vertical motions (Fig. 41).

During the spring warming AE, KE and KZ decrease significantly but AZ increases markedly (Fig. 37). The form of the energy is shifted from kinetic to potential energy. In the winter and early March, radiation responds strongly to the eddy temperature field destroying AE as noted previously. With the significant shift to AZ, differential zonal radiative heating is established (Fig. 36) in an attempt to balance the sharp increase in AZ. At the end of March AZ decreases but remains the largest form of energy throughout the warmer months. The maintenance of the kinetic energy budget for April and May is similar to that of the summer months which is discussed below.

G.3 Summer (June-August)

In the summer the synoptic situation is that of a warm anticyclone centered on the North Pole above 50 mb with very little day to day variation. Tropospheric westerlies protrude into the lower stratosphere up to about 50 mb resulting in a small but continual upward energy flux from the troposphere which is entirely trapped by the easterlies above. Thus during summer KE and KZ are both maintained by mechanical work accompanied by forced vertical motions which increase AE and AZ. There is also a forced conversion of AE $\longrightarrow$ AZ and radiation destroys AZ.

Consider briefly the maintenance of the energy balance for a layer containing only easterly flow such as the 30-10 mb layer in the summer months. Since easterly flow inhibits vertical energy propaga-

tion, we know that eddy boundary forcing is negligible. For July the monthly mean energy cycle is the following:

$$(B\omega\phi Z + BV\phi Z) \longrightarrow KZ \longrightarrow AZ \longrightarrow GZ$$

The eddy forms of energy are negligible and the kinetic energy and potential energy blances are maintained by forced motions. This is the typical energy cycle for a layer containing only easterly flow (50-10 mb) in the summer months.

G.4 Fall (September-November)

At the beginning of September the synoptic situation is similar to that of the summer circulation with tropospheric westerlies protruding slightly upward through 100 mb and easterlies above. However, by the end of September a weak cyclonic vortex has been established by radiational cooling in high latitudes with anticyclonic flow in low and middle latitudes. In October and November the westerly flow increases at 100 mb and 10 mb with slightly weaker westerly flow in the region 50-30 mb (see Table IV).

The energetics for September are essentially those of the summer months. However, in October the tropospheric energy flux begins to increase, all of which is essentially absorbed in the lower stratosphere. This results in an increase of KE and the conversion of KE $\longrightarrow$ KZ. The forced vertical motions which convert KE $\longrightarrow$ AE also increase. In addition there is also a small conversion of AZ $\longrightarrow$ AE. In response to the increase in the eddy temperature field,

GE increases as radiation acts to destroy AE. KZ also increases at this time because of the conversion CK and increased lateral forcing. Both AZ and GZ decrease during October.

In November there is a significant increase in the upward tropospheric energy flux which is largely absorbed in the lower stratosphere. KE increases markedly showing a maximum peak at the time of maximum convergence of vertical energy flux. CK also increases significantly. There are sizeable periods when baroclinic release of AE takes place and the horizontal eddies maintain AE by the conversion of AZ $\longrightarrow$ AE. GE continues to increase and GZ continues to decrease as AZ reaches minimum values during the fall.

In the fall the energy source for the eddy motions was the large absorption of tropospheric energy flux. This is somewhat perplexing since the fall is characterized by relatively weak westerly winds which should permit maximum penetration if the vertical propagation of energy is controlled primarily by the wind field. Note that in December that even larger absorption took place with predominantly westerly flow throughout the lower stratosphere.

H. The Annual Energy Cycle for the Lower Stratosphere

The annual energy conversions and contents are shown in Fig. 48. The annual mean values were obtained by averaging the daily values for 1964. The driven or forced nature of the circulation is very apparent. Both KE and KZ rely on mechanical work for maintenance of the kinetic

energy budget. Forced motions, principally CZ, transfer energy into the available potential energy field where radiation is the ultimate sink. Although it is clear that the lower stratosphere is a driven region, note that CA and CK are in the same direction as in the troposphere.

As a residual DE is +22.7 ergs cm^{-2} sec^{-1} and DZ is +76.7 ergs cm^{-2} sec^{-1}. DZ is probably too large because of the difficulty is accurately specifying BΦZ.

I. Vertical Motions and Negative Viscosity

In the troposphere and lower stratosphere there are regions where the horizontal eddies transport angular momentum towards latitudes of higher angular momentum and in the lower stratosphere there are regions where the eddies transport sensible heat towards latitudes of higher temperature. Starr (1968) has described this phenomena as a type of negative viscosity. It is possible with the present study to further ask whether the vertical motions in the lower stratosphere also participate in countergradient transport. To answer this question the monthly mean horizontal (CKHOR and CAHOR) and vertical (CKVER and CAVER) components of the conversions CK and CA are presented in Table V. Clearly the vertical motions also transport angular momentum vertically towards levels of higher angular momentum. While the vertical motions contribute only 10% to CK on an annual basis for individual months the values reach 70% (April). Note that the horizontal

Table V

Monthly mean energy conversions (ergs cm^{-2} sec^{-1}) for 1964.

	CKHOR	CKVER	CAHOR	CAVER
J	191.9	6.9	-175.8	-6.4
F	54.2	11.7	-166.2	-3.6
M	41.3	12.0	65.1	.2
A	.5	1.2	-8.0	.0
M	1.8	1.1	-1.9	-.1
J	-1.4	-.5	2.6	-.1
J	4.3	1.0	9.6	.1
A	5.1	.9	11.8	.2
S	7.1	.3	7.6	.3
O	20.5	2.2	-2.7	.9
N	46.7	3.7	-26.1	-2.5
D	60.9	7.5	-78.3	-6.2
Annual	36.1	4.0	-30.2	-1.4

and vertical components of CK are always of the same sign. There is also evidence that the vertical motions are transporting heat vertically towards levels of higher temperature (positive values of the component CAVER) although the values are small. Annually the vertical motions contribute only 4% to CA and in general the horizontal motions are more important. The signs of the components tend to be the same.

J. Use of the Adiabatic Assumption in Studying the Energetics of the Atmosphere.

As mentioned in Section V.C several of the previous studies of the energetics of the lower stratosphere have used eq. (5.5) but neglected diabatic heating. To see the effect of this assumption the monthly mean conversions CE and CZ, computed with and without the adiabatic assumption, are presented in Table VI. Use of the adiabatic assumption is very poor for estimating CE and CZ as adiabatic vertical motions yield the wrong magnitudes and frequently the wrong sign.

Although the conversions CE and CZ are poorly estimated when the adiabatic assumption is made, it is possible that the vertical energy fluxes may be fairly well estimated under this assumption. For example, Eliassen and Palm (1961) derived expressions for wave energy fluxes for long quasi-geostrophic waves which were assumed to be stationary and adiabatic. They found that wave energy is transported upwards if the waves transport sensible heat northwards.

Table VI

Monthly mean energy conversions (ergs cm^{-2} sec^{-1}) computed with (ADCE and ADCZ) and without (CE and CZ) the adiabatic assumption for 1964.

	CE	ADCE	CZ	ADCZ
J	135.6	208.0	-191.8	-197.0
F	54.3	111.4	-110.7	-103.5
M	-121.2	-56.5	-29.4	47.5
A	-22.1	-14.5	-32.4	31.1
M	-21.8	-16.3	-23.9	13.4
J	-14.2	-7.9	-40.9	-.8
J	-11.6	-4.3	-44.2	3.3
A	-14.9	-8.7	-30.8	15.5
S	-12.4	-5.3	-32.5	10.6
O	-26.5	-12.6	-16.0	3.1
N	-8.4	98.9	-58.0	-168.5
D	48.0	94.9	-109.9	-122.7
Annual	-1.3	32.3	-60.0	-39.1

In Table VII are compared the area averaged vertical energy fluxes through 100 mb from the present study and estimates by Newell and Richards (1969) using the Eliassen and Palm approximation. The general patterns are the same although the Eliassen and Palm approximation consistently underestimates the magnitude of the vertical energy flux. There are significant differences between the present study and Newell and Richards (not shown here) for the latitudinal variation of the vertical energy flux. In particular, the present study has more upward energy flux in lower latitudes in the winter months and more upward energy flux for all latitudes at 100 mb in the warmer months. Undoubtedly some of the differences can be ascribed to transient waves which are excluded in the Eliassen and Palm approximation. Also the use of linearized equations and the exclusion of diabatic effects restrict the comparison with the actual atmosphere.

The convergence of vertical energy flux from the present study, computed with and without the adiabatic assumption, is compared with values obtained by Newell and Richards using the Eliassen and Palm approximation in Table VIII. In general the adiabatic approximation results in underestimates of $B_{\omega\phi}E$ with January actually giving the wrong sign for the Eliassen and Palm approximation. These comparisons suggest that vertical fluxes estimated using the adiabatic assumption should be used for qualitative but not quantitative analysis.

Table VII

$\langle \overline{[\omega^* z^*]} \rangle$ (ergs cm^{-2} sec^{-1}) at 100 mb for 1964.

	Present Study	Eliassen and Palm
J	-218	-223
F	-136	-127
M	-325	-244
A	-40	-9
M	-41	-13
J	-33	-2
J	-21	-3
A	-36	-5
S	-25	-6
O	-86	-43
N	-177	-90
D	-216	-146

Table VIII

$B\overline{\omega}\overline{\phi}E$ (ergs cm^{-2} sec^{-1}) for 1964 for 100-10 mb, $90^{o}N$-$20^{o}N$.

	Present Study	Present Study Adiabatic	Eliassen and Palm
J	-16	-56	27
F	60	30	55
M	266	273	231
A	40	31	9
M	41	39	13
J	32	11	2
J	19	0	3
A	36	19	5
S	23	8	6
O	80	64	37
N	118	93	62
D	128	90	85

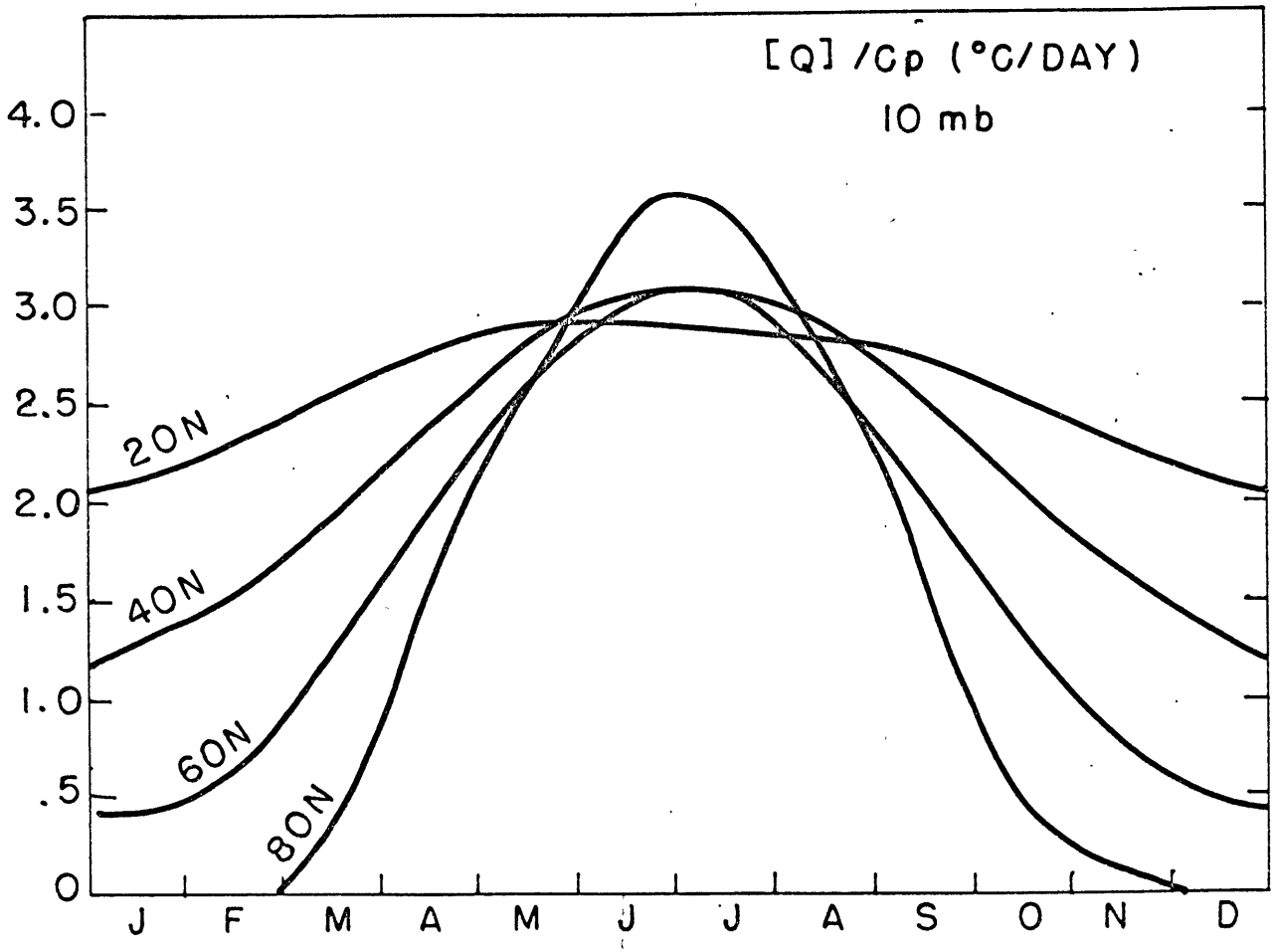
[Q] /Cp (°C/DAY)
10 mb
4.0
3.5
3.0
2.5
2.0
1.5
1.0
.5
0
20N
40N
60N
80N
J
F
M
A
M
J
J
A
S
O
N
D

Figure 30.

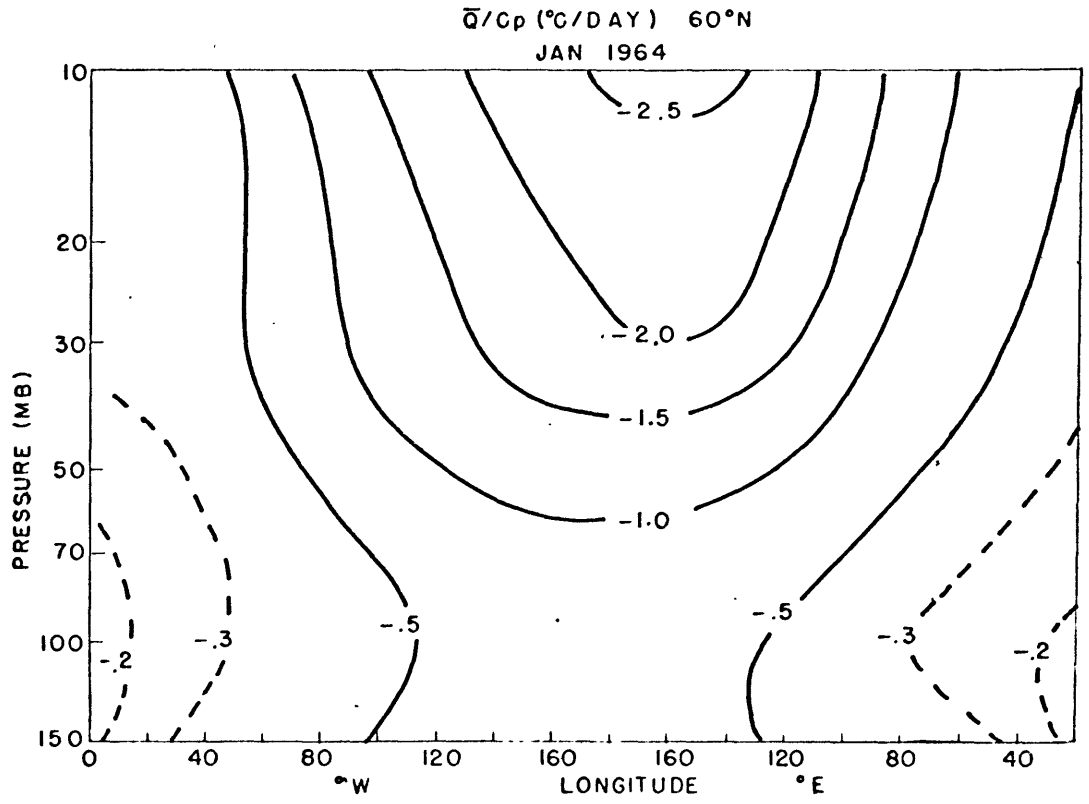
$\bar{Q}$/Cp (°C/DAY) 60°N
JAN 1964
PRESSURE (MB)
10
20
30
50
70
100
150
-2.5
-2.0
-1.5
-1.0
-.5
-.3
-.2
0
40
80
120
160
160
120
80
40
°W
LONGITUDE
°E

(a)

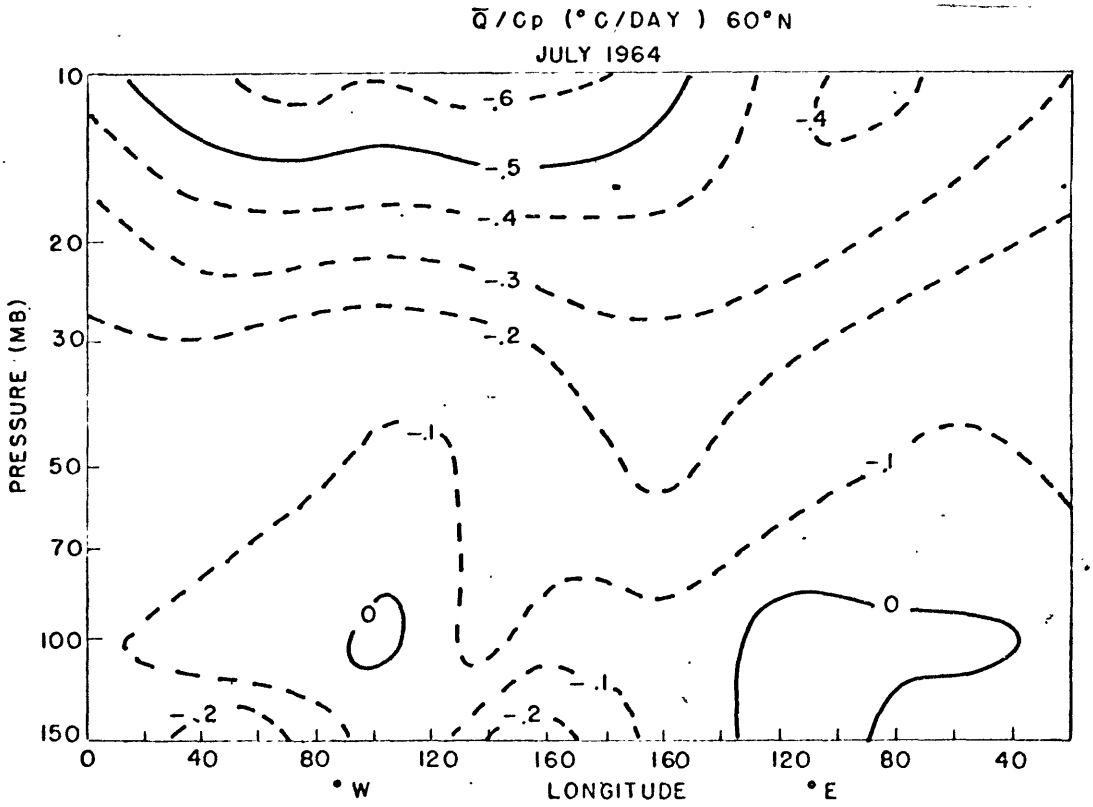
$\bar{Q}$/Cp (°C/DAY) 60°N
JULY 1964
PRESSURE (MB)
10
20
30
50
70
100
150
-.6
-.5
-.4
-.3
-.2
-.1
0
0
40
80
120
160
160
120
80
40
°W
LONGITUDE
°E

(b)

Figure 31.

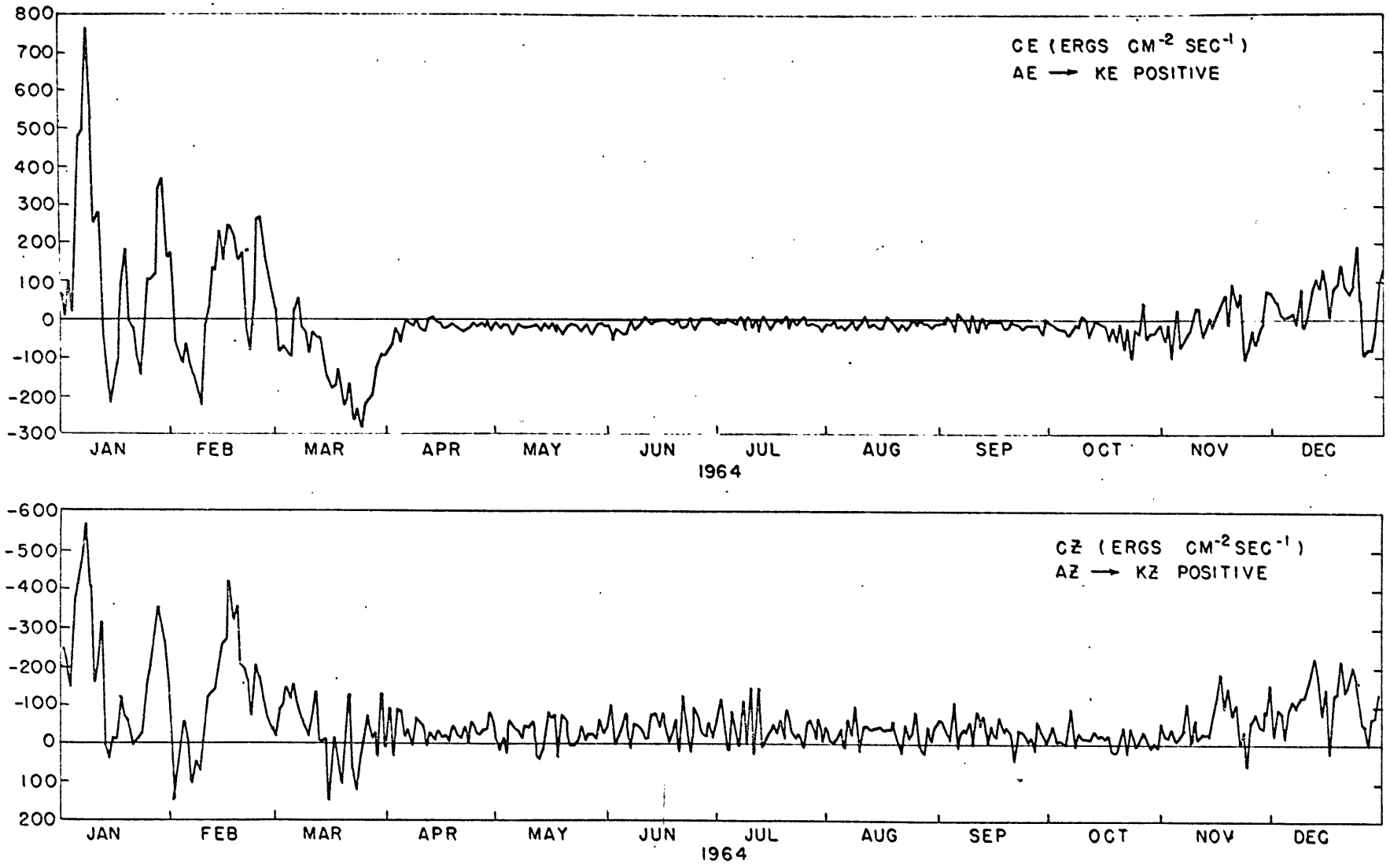
800
700
600
500
400
300
200
100
0
-100
-200
-300
CE (ERGS CM-2 SEC-1)
AE → KE POSITIVE
JAN
FEB
MAR
APR
MAY
JUN
JUL
AUG
SEP
OCT
NOV
DEC
1964
-600
-500
-400
-300
-200
-100
0
100
200
CZ (ERGS CM-2 SEC-1)
AZ → KZ POSITIVE
JAN
FEB
MAR
APR
MAY
JUN
JUL
AUG
SEP
OCT
NOV
DEC
1964

Figure 32.

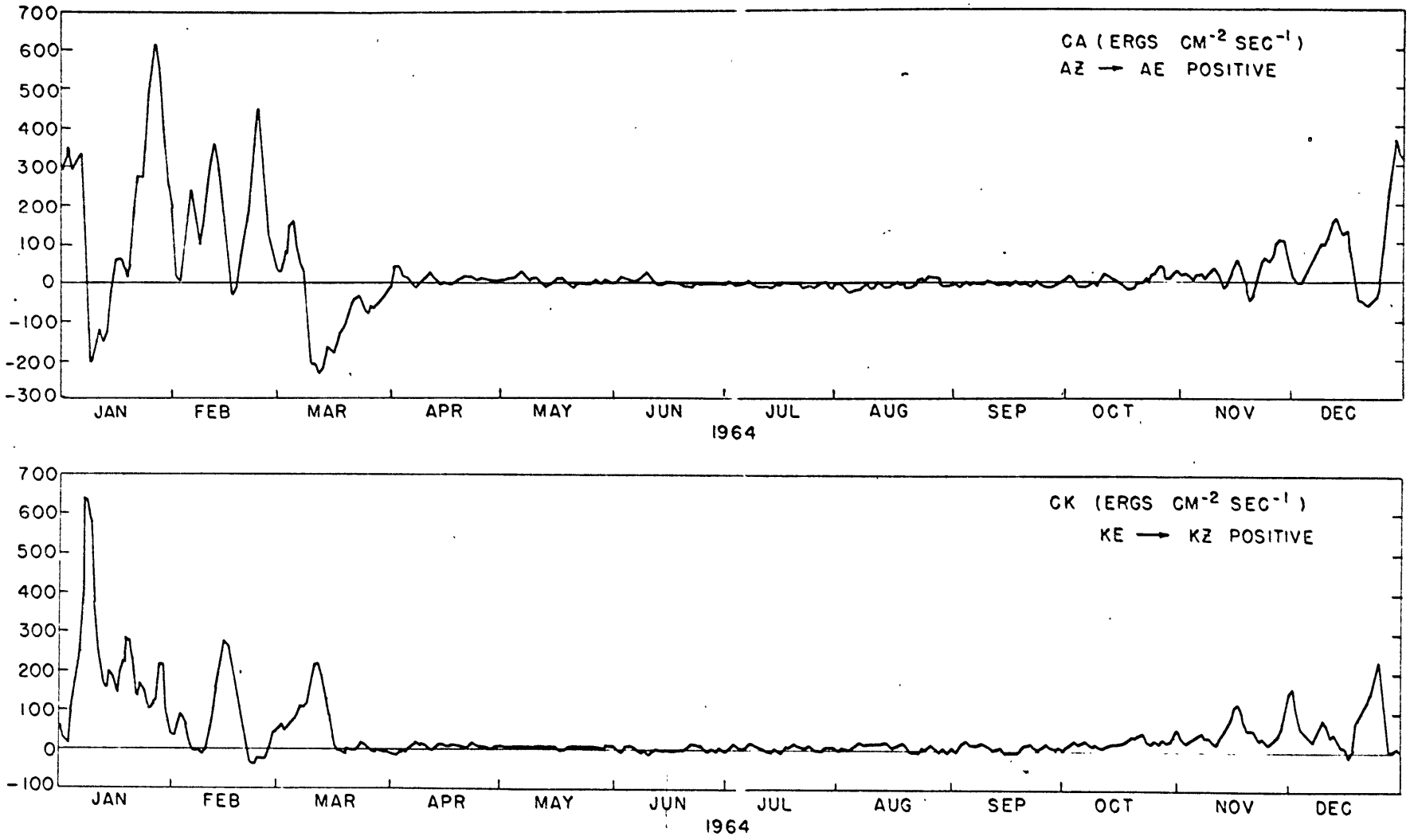
CA (ERGS CM-2 SEC-1)
AZ → AE POSITIVE
700
600
500
400
300
200
100
0
-100
-200
-300
JAN
FEB
MAR
APR
MAY
JUN
JUL
AUG
SEP
OCT
NOV
DEC
1964
CK (ERGS CM-2 SEC-1)
KE → KZ POSITIVE
700
600
500
400
300
200
100
0
-100
JAN
FEB
MAR
APR
MAY
JUN
JUL
AUG
SEP
OCT
NOV
DEC
1964

Figure 33.

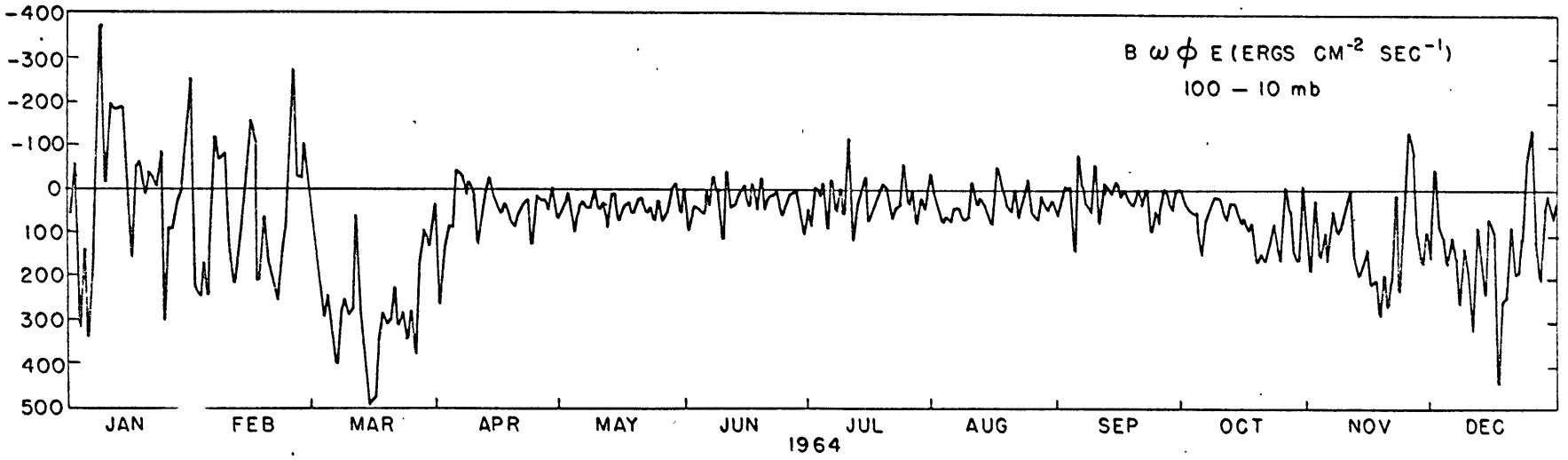
B ω φ E (ERGS CM-2 SEC-1)
100 – 10 mb
-400
-300
-200
-100
0
100
200
300
400
500
JAN
FEB
MAR
APR
MAY
JUN
JUL
AUG
SEP
OCT
NOV
DEC
1964

Figure 34.

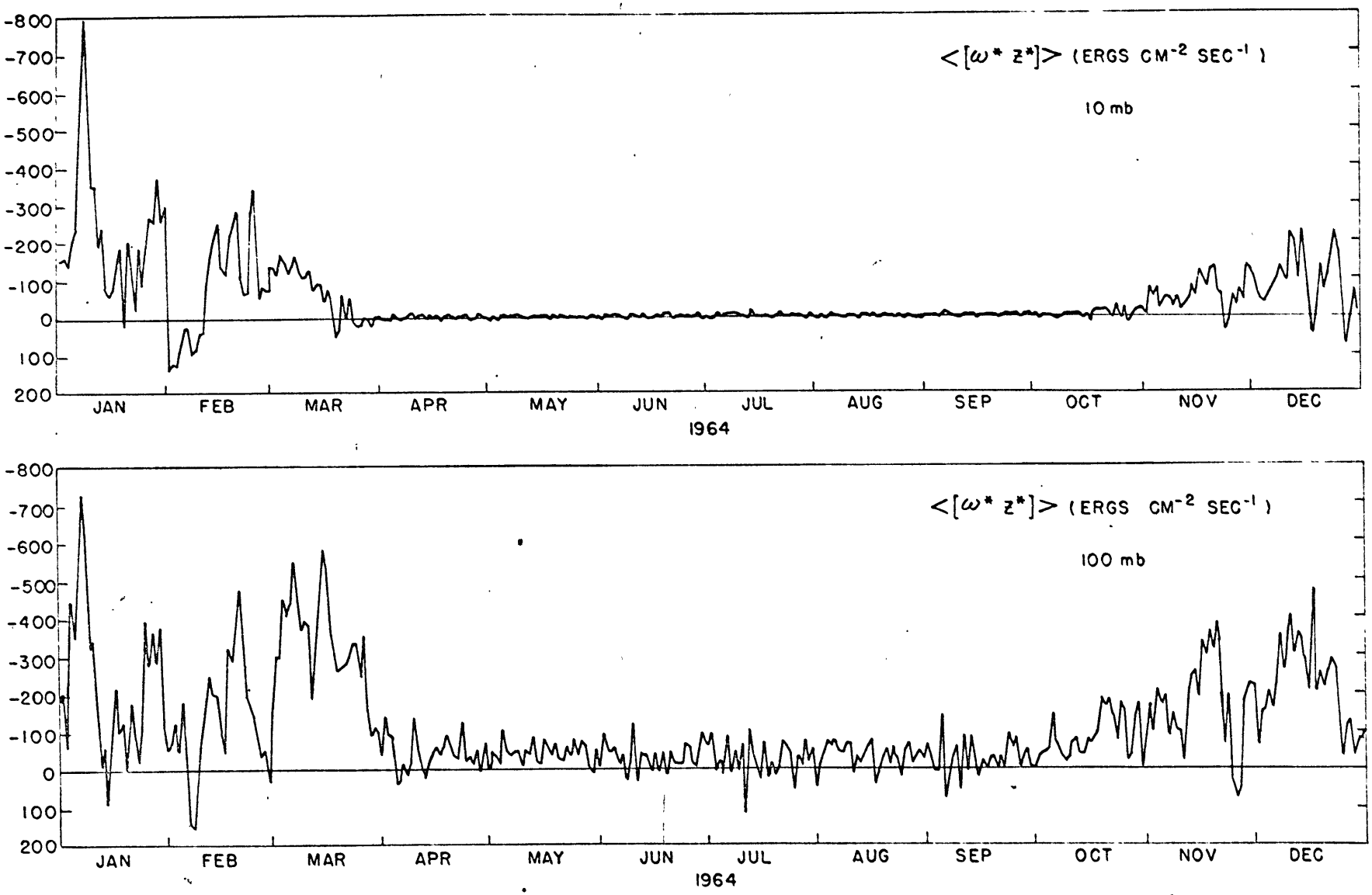
-800
-700
-600
-500
-400
-300
-200
-100
0
100
200
$<[\omega^* z^*]>$ (ERGS CM^{-2} SEC^{-1})
10 mb
JAN
FEB
MAR
APR
MAY
JUN
JUL
AUG
SEP
OCT
NOV
DEC
1964
-800
-700
-600
-500
-400
-300
-200
-100
0
100
200
$<[\omega^* z^*]>$ (ERGS CM^{-2} SEC^{-1})
100 mb
JAN
FEB
MAR
APR
MAY
JUN
JUL
AUG
SEP
OCT
NOV
DEC
1964

Figure 35.

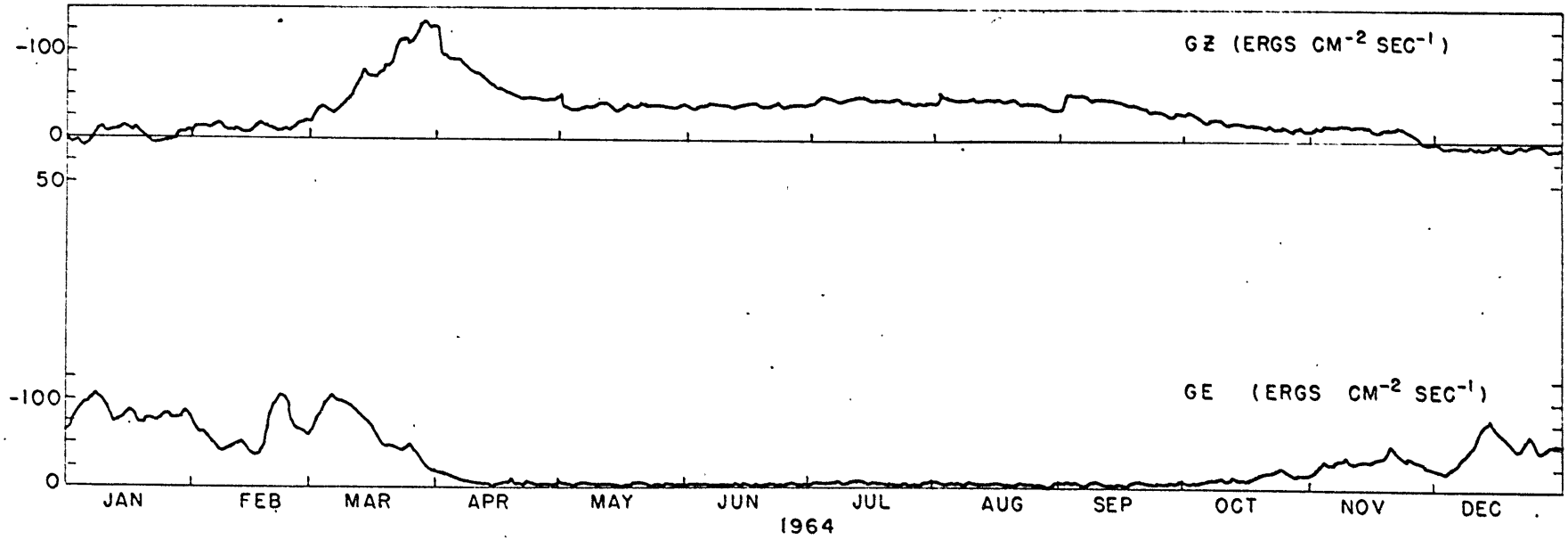
-100
0
50
-100
0
GZ (ERGS CM-2 SEC-1)
GE (ERGS CM-2 SEC-1)
JAN
FEB
MAR
APR
MAY
JUN
JUL
AUG
SEP
OCT
NOV
DEC
1964

Figure 36.

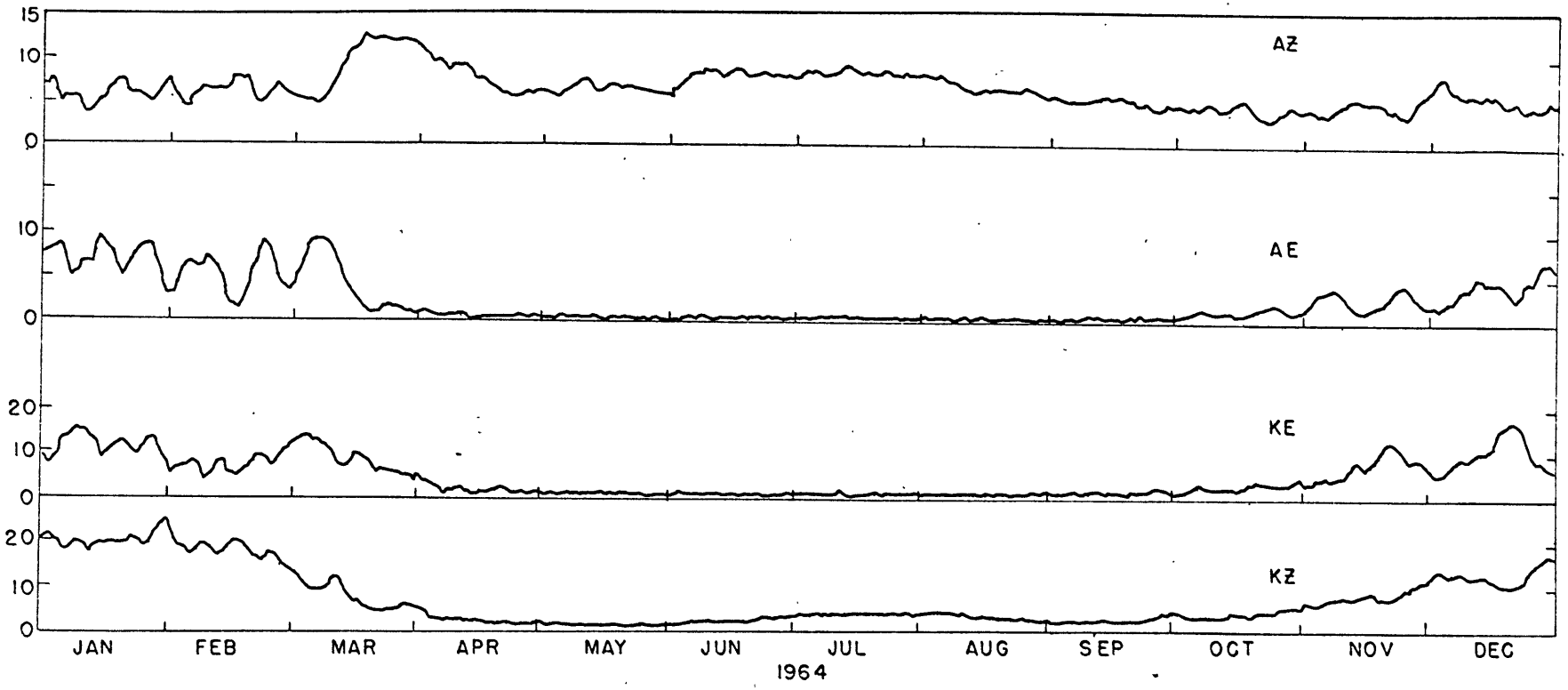
15
10
0
AZ
10
0
AE
20
10
0
KE
20
10
0
KZ
JAN
FEB
MAR
APR
MAY
JUN
JUL
AUG
SEP
OCT
NOV
DEC
1964

Figure 37.

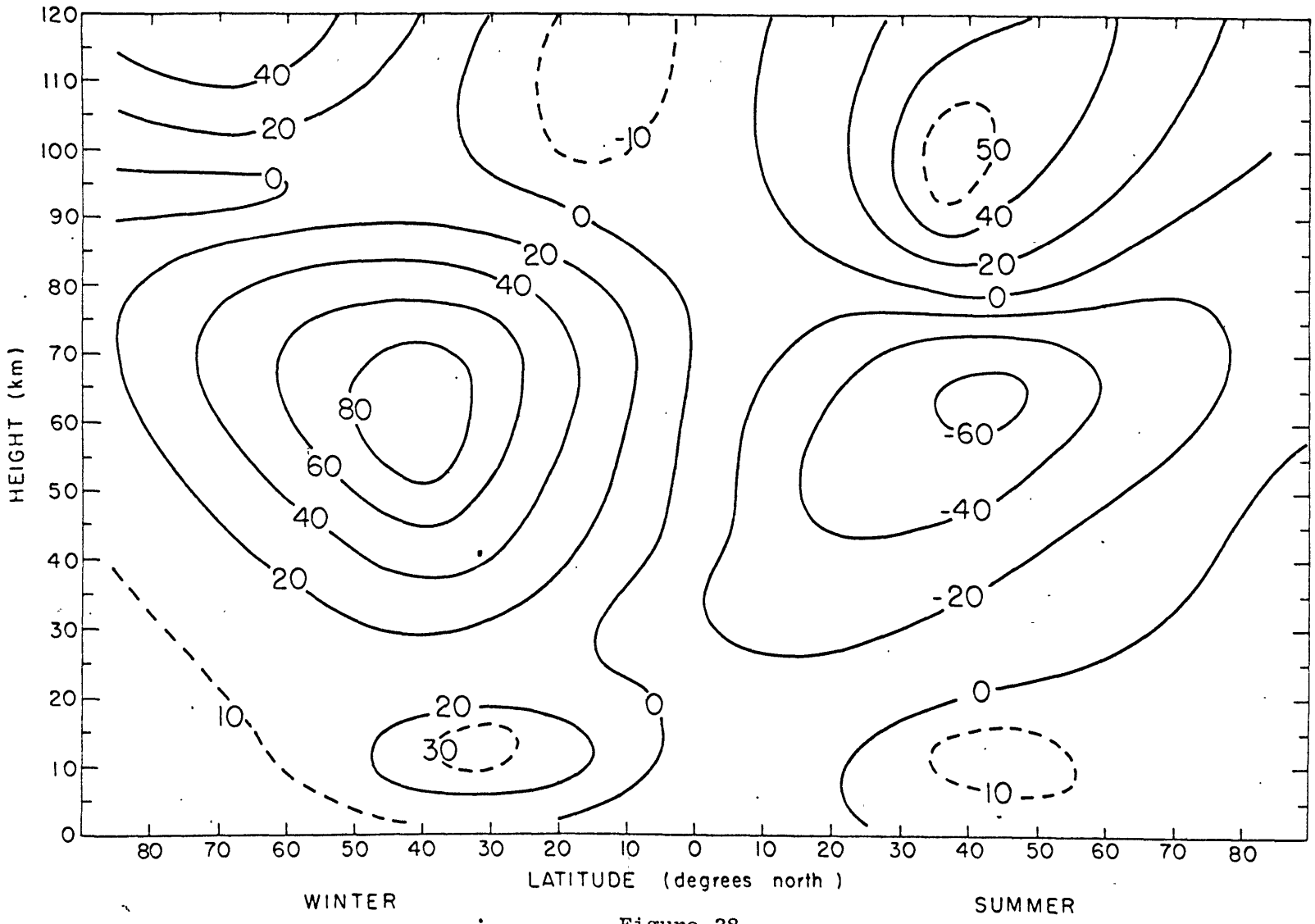
HEIGHT (km)
120
110
100
90
80
70
60
50
40
30
20
10
0
40
20
0
-10
0
20
40
80
60
40
20
10
20
30
0
50
40
20
0
-60
-40
-20
0
-10
80 70 60 50 40 30 20 10 0 10 20 30 40 50 60 70 80
LATITUDE (degrees north)
WINTER
SUMMER

Figure 38.

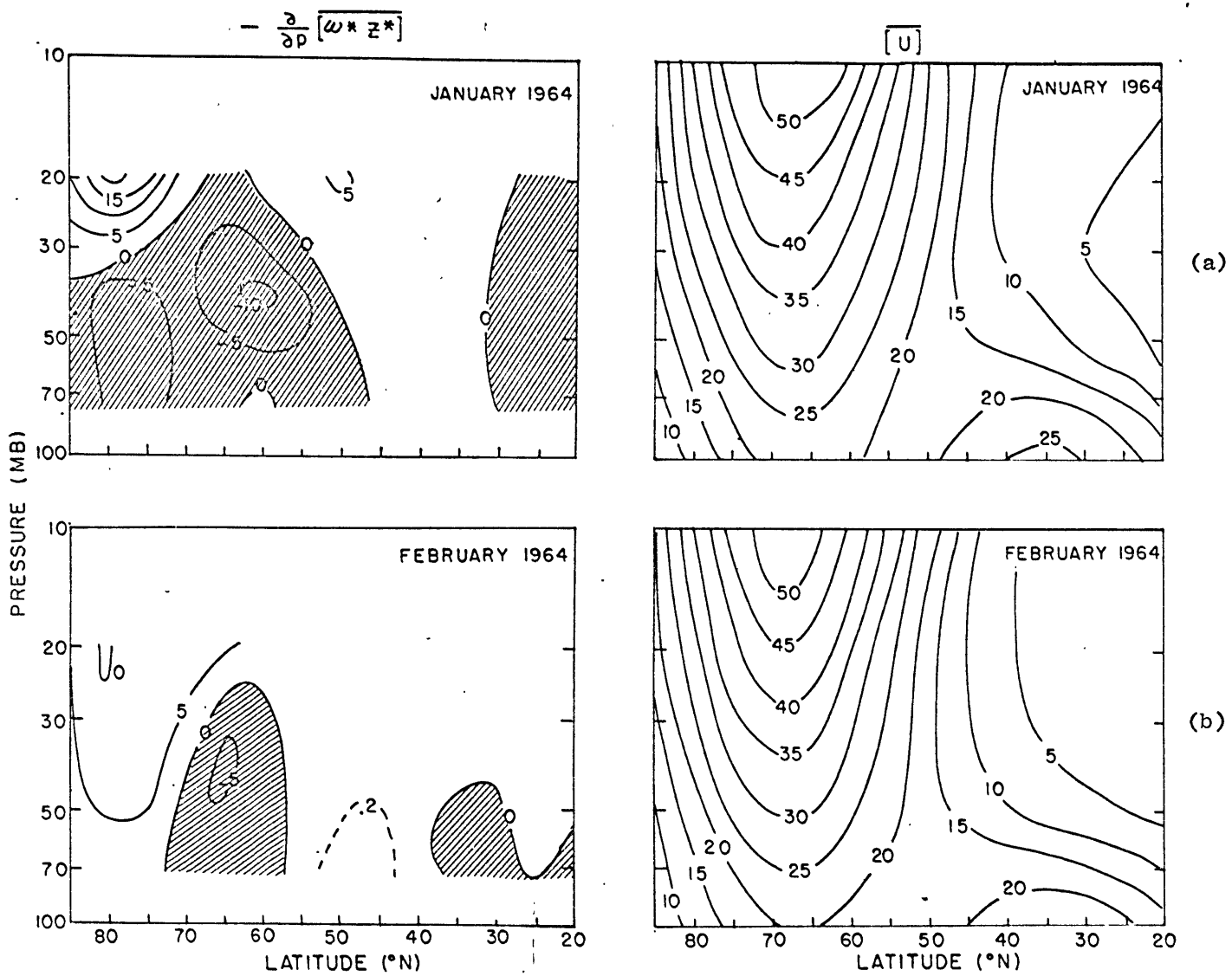
$-\frac{\partial}{\partial p}[\overline{\omega^* z^*}]$
$[\overline{U}]$
JANUARY 1964
FEBRUARY 1964
PRESSURE (MB)
LATITUDE (°N)
(a)
(b)

Figure 39.

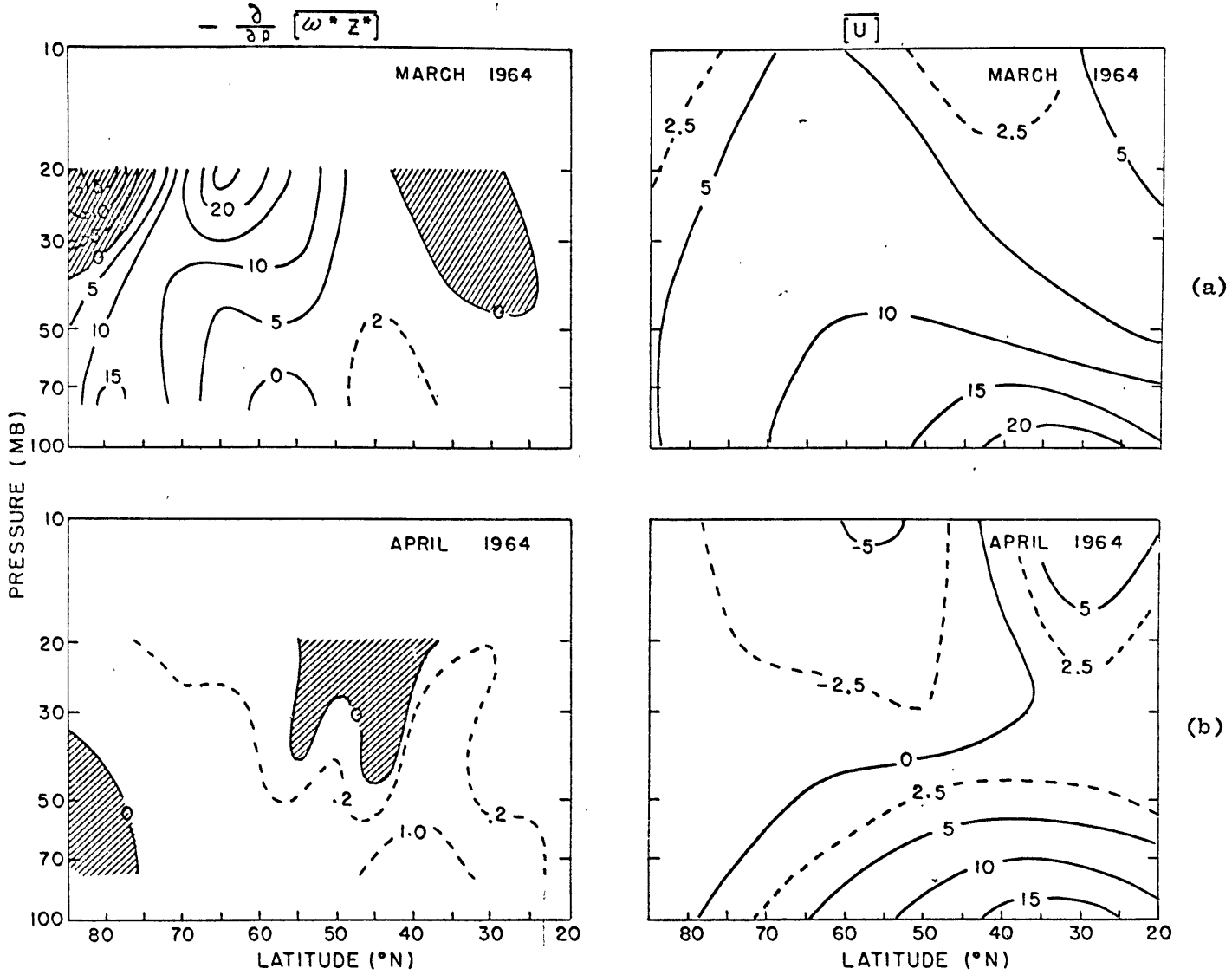
$-\frac{\partial}{\partial p}[\omega^* z^*]$
$[\overline{U}]$
MARCH 1964
APRIL 1964
PRESSURE (MB)
LATITUDE (°N)
(a)
(b)

Figure 40.

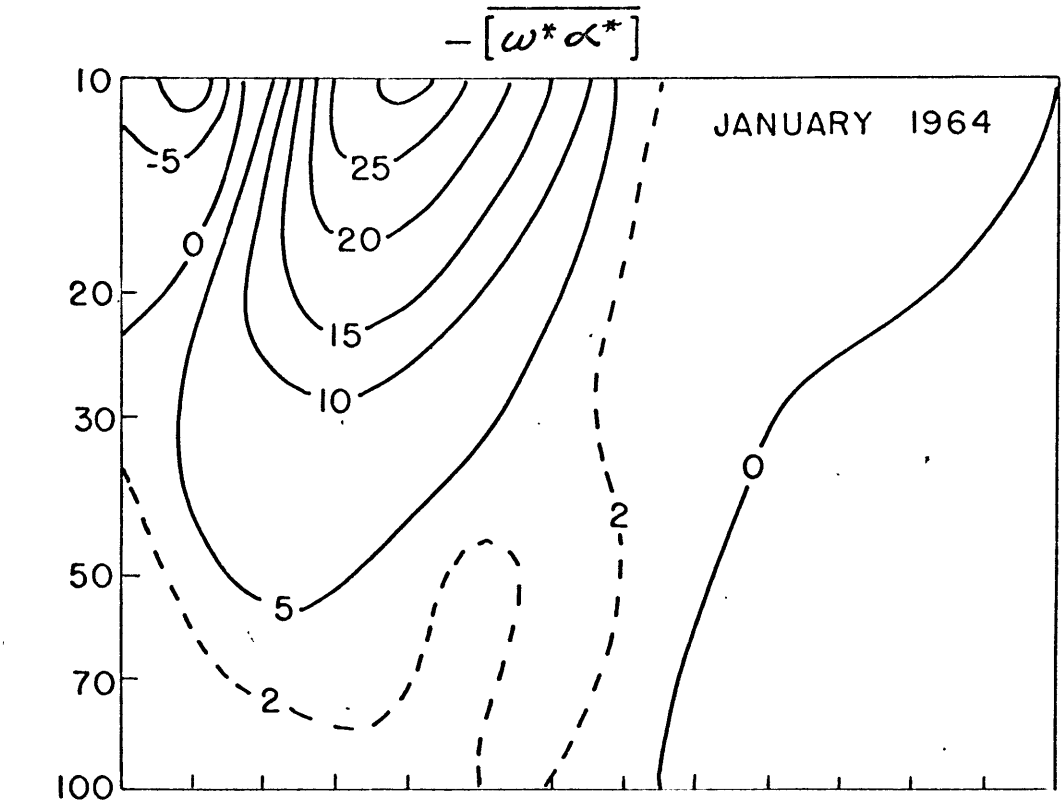
$-[\overline{\omega^* \alpha^*}]$
JANUARY 1964
10
20
30
50
70
100
-5
0
25
20
15
10
5
2
2
0

(a)

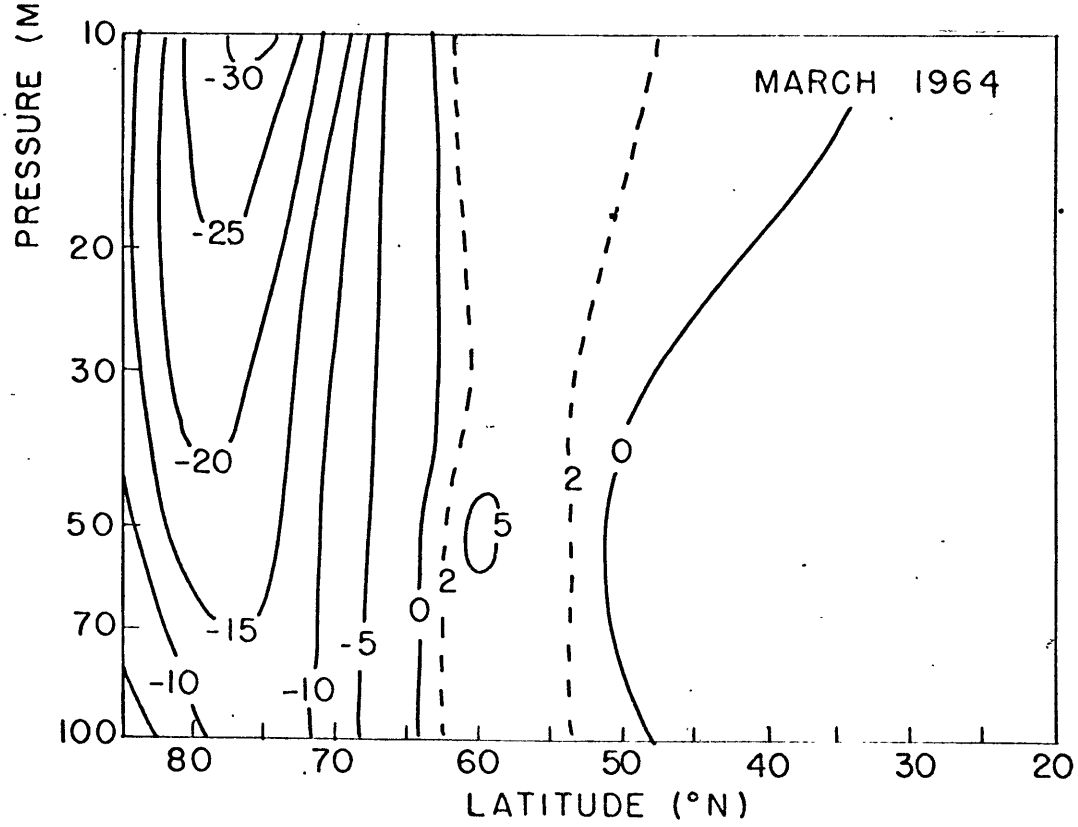
MARCH 1964
PRESSURE (MB)
10
20
30
50
70
100
-30
-25
-20
-15
-10
-10
-5
0
2
5
2
0
80
70
60
50
40
30
20
LATITUDE (°N)

(b)

Figure 41.

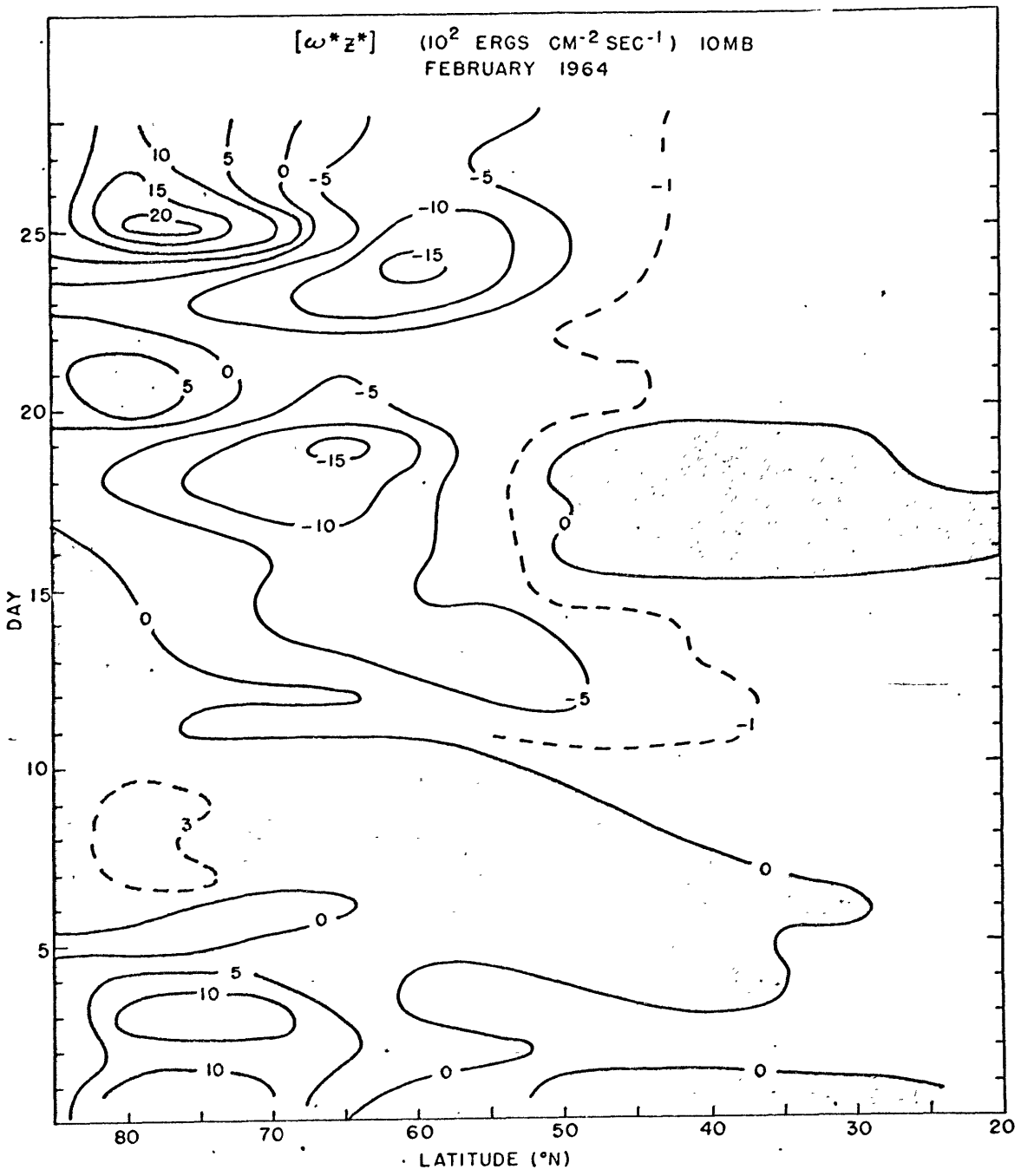
[ω*z*] (10² ERGS CM⁻² SEC⁻¹) 10MB
FEBRUARY 1964
DAY
LATITUDE (°N)
80
70
60
50
40
30
20
25
20
15
10
5

Figure 42.

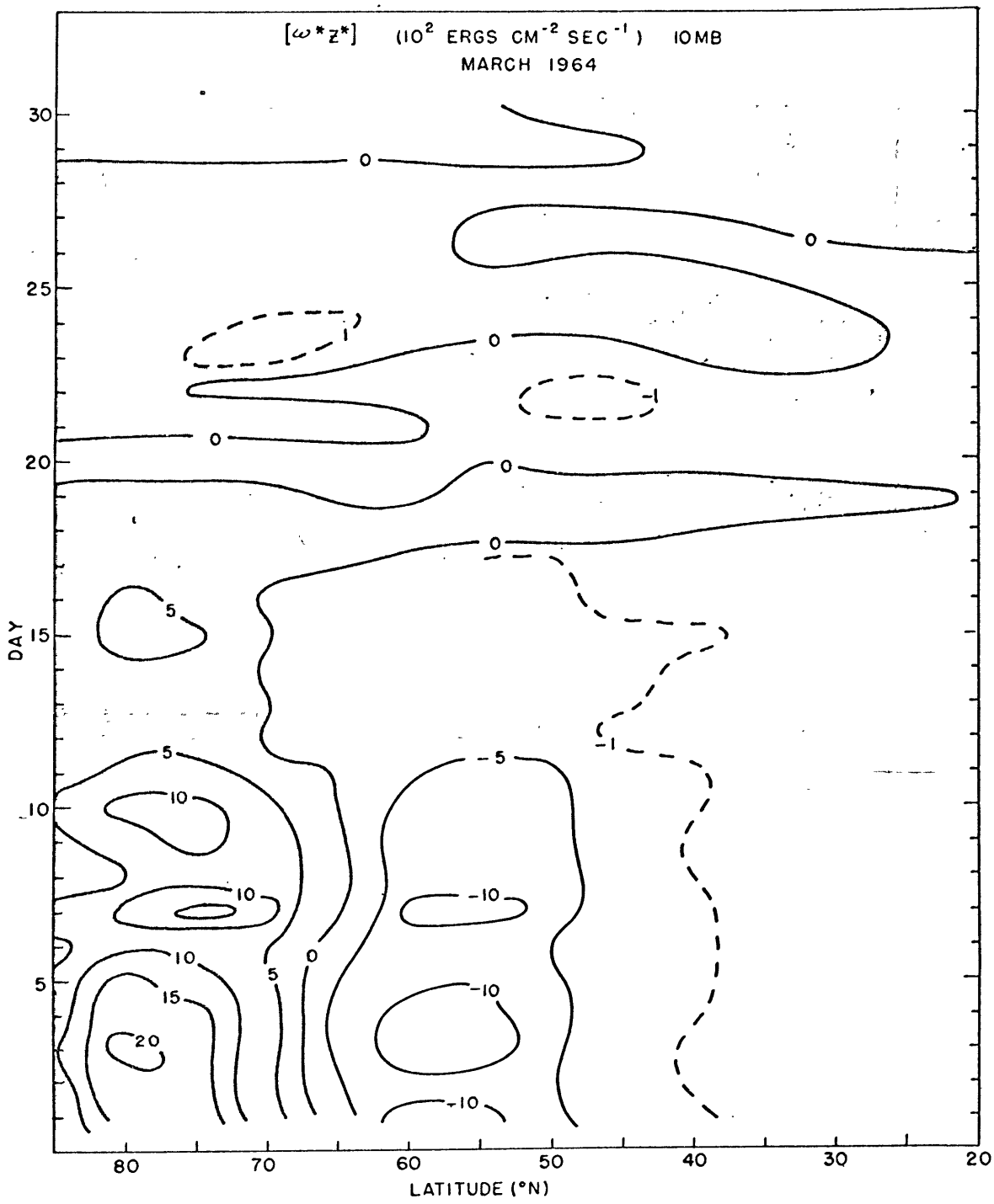
[ω*z*] (10² ERGS CM⁻² SEC⁻¹) 10MB
MARCH 1964
DAY
LATITUDE (°N)
30
25
20
15
10
5
80
70
60
50
40
30
20
0
1
-1
5
10
15
20
-5
-10

Figure 43.

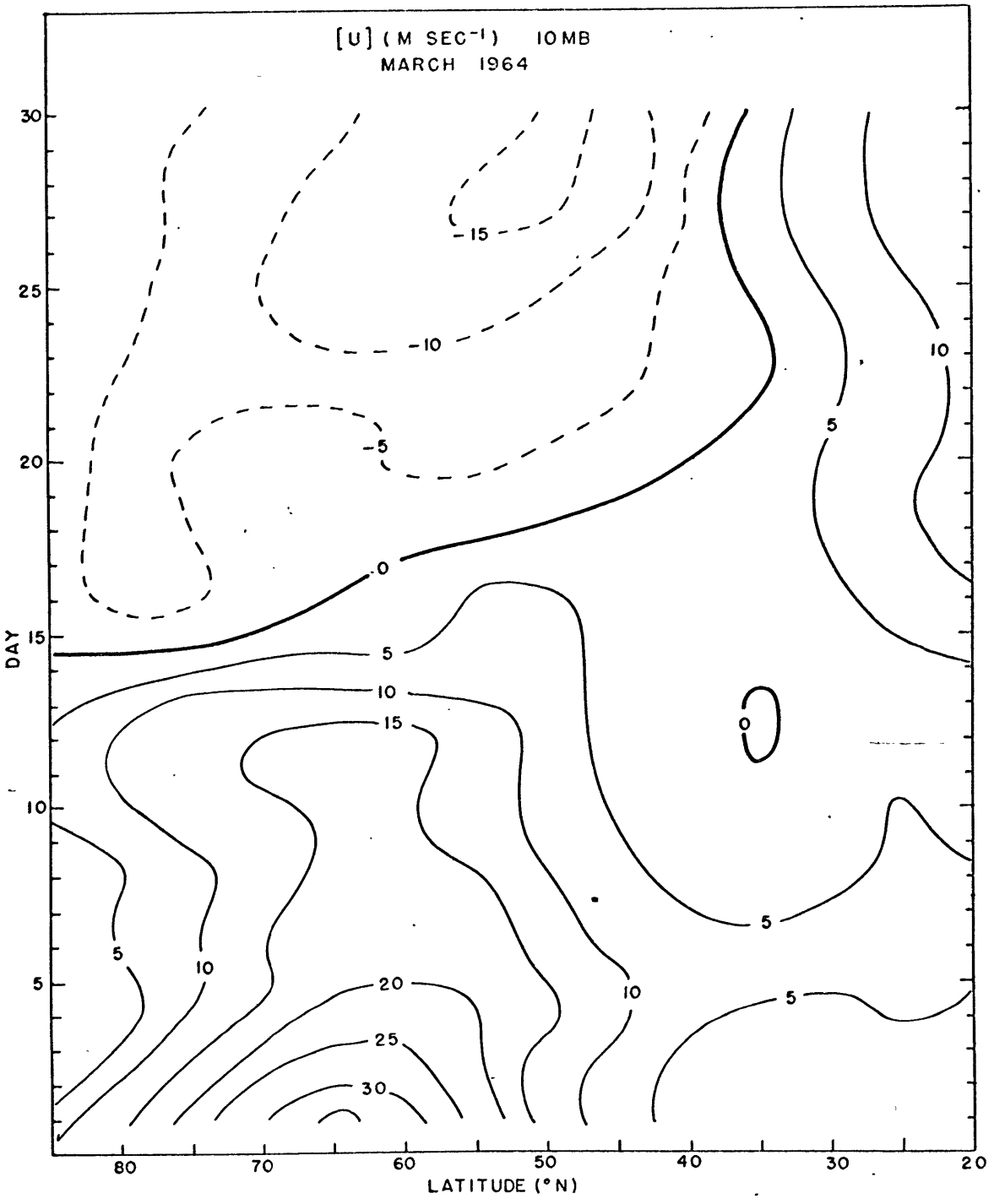
[U] (M SEC⁻¹) 10MB
MARCH 1964
DAY
LATITUDE (°N)
30
25
20
15
10
5
80
70
60
50
40
30
20
-15
-10
-5
0
5
10
15
20
25
30

Figure 44.

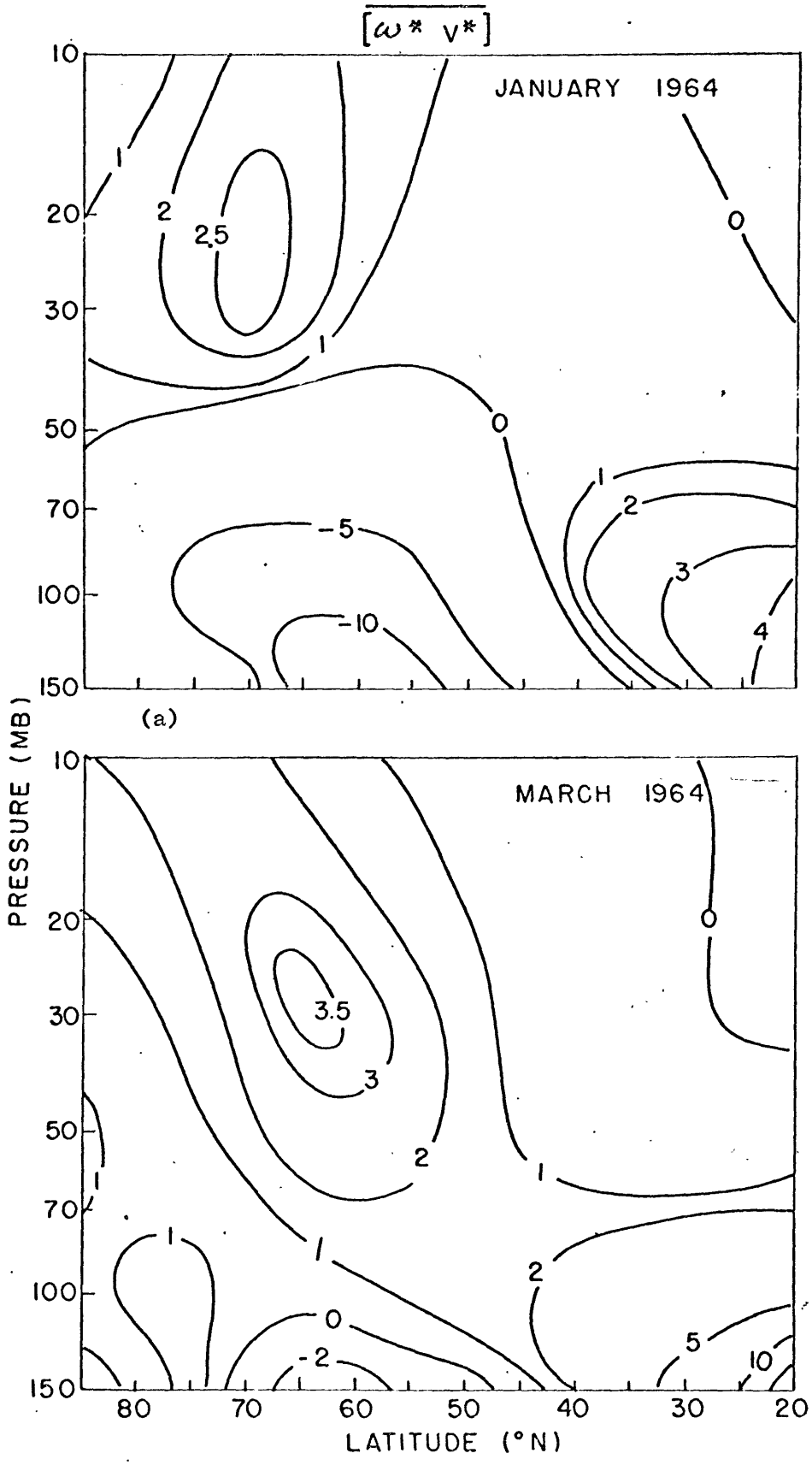
$\overline{[\omega^* v^*]}$
JANUARY 1964
MARCH 1964
PRESSURE (MB)
LATITUDE (°N)
10
20
30
50
70
100
150
80
70
60
50
40
30
20
1
2
2.5
0
-5
-10
3
4
3.5
-2
5
10

(a)

(b)

Figure 45.

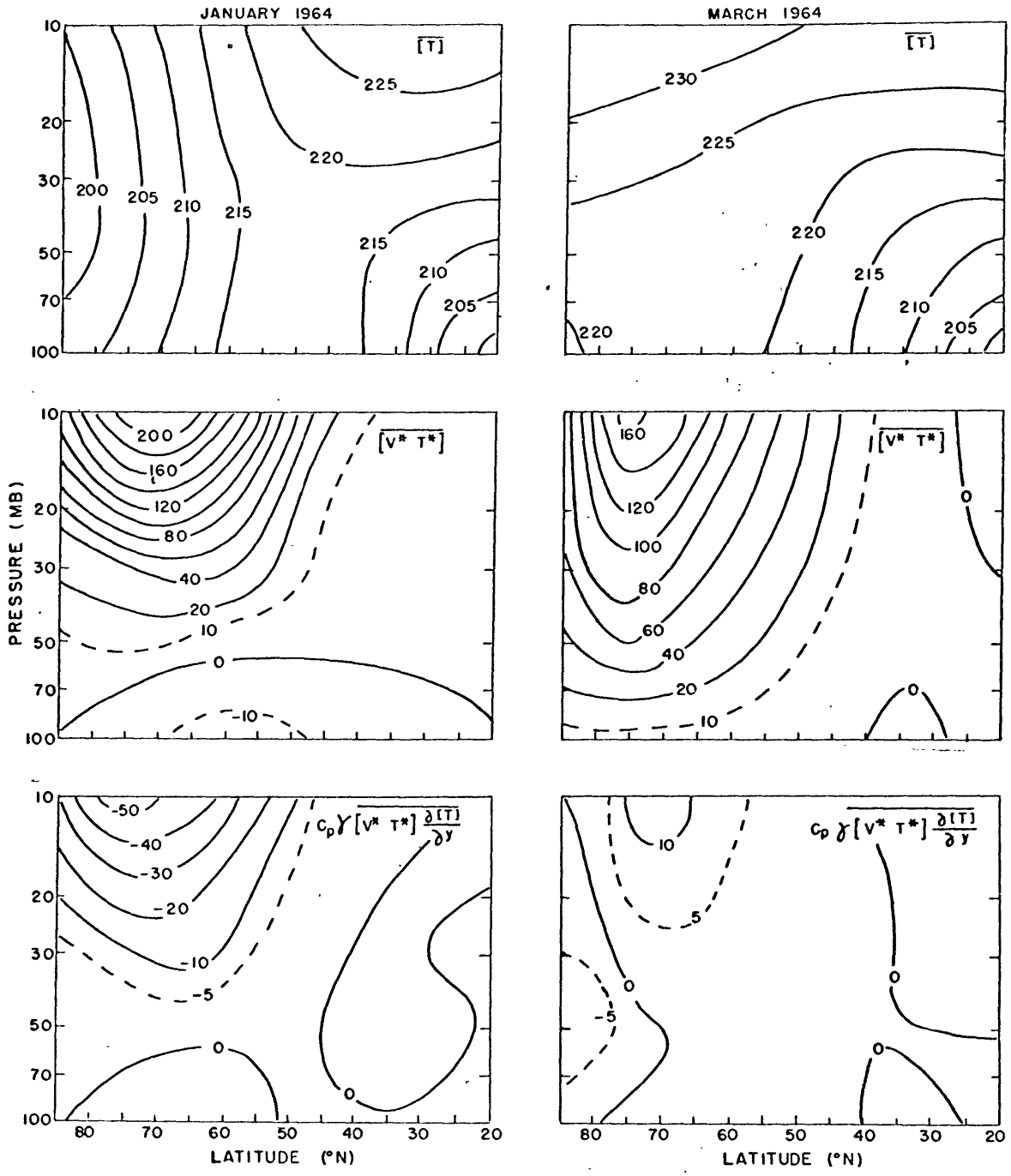
JANUARY 1964
MARCH 1964
[T]
[V* T*]
$c_p \gamma [\overline{V^* T^*}] \frac{\partial [T]}{\partial y}$
PRESSURE (MB)
LATITUDE (°N)
(a)
(b)

Figure 46.

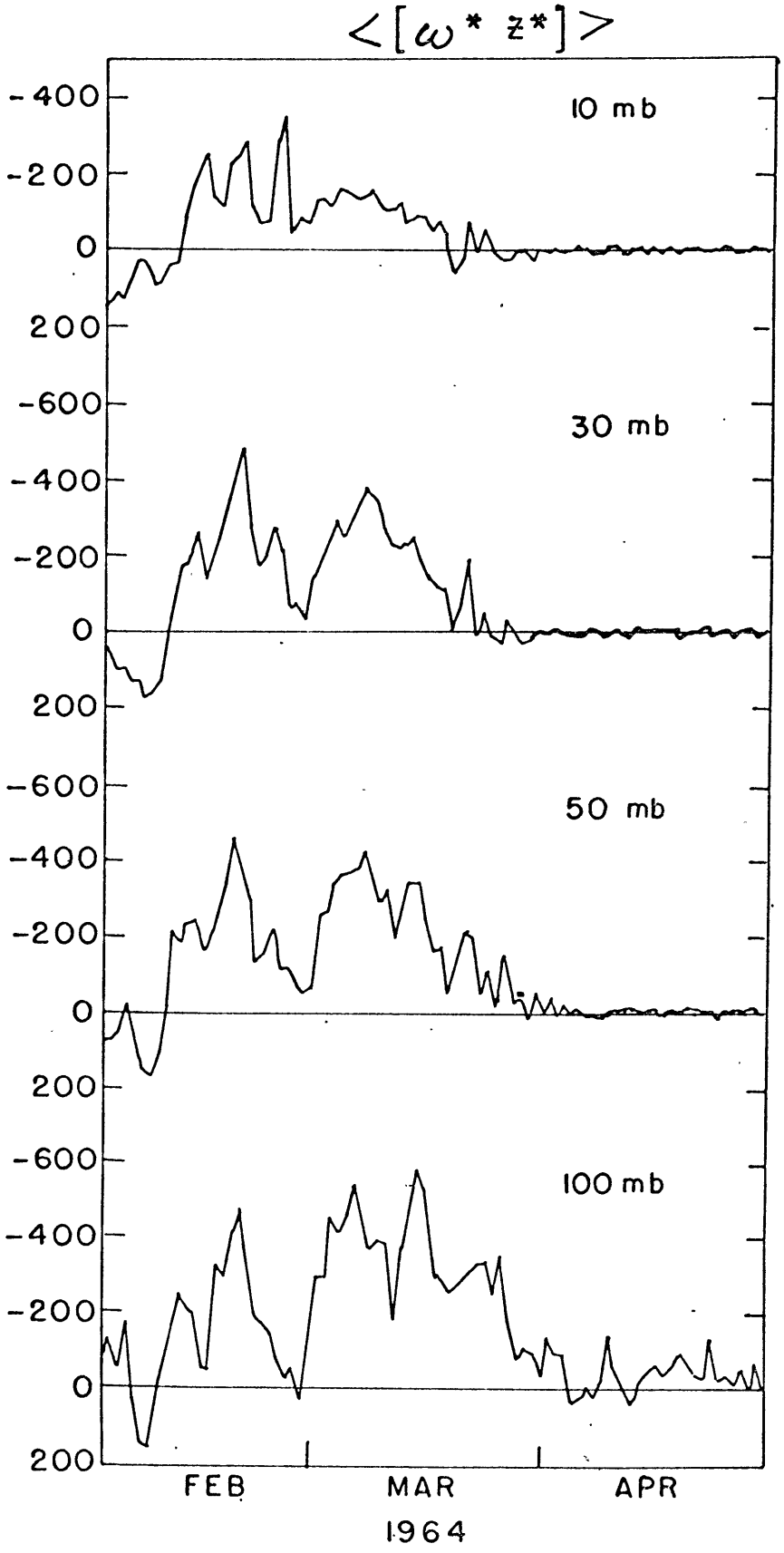
$<[\omega^* \bar{z}^*]>$
10 mb
30 mb
50 mb
100 mb
-400
-200
0
200
-600
FEB
MAR
APR
1964

Figure 47.

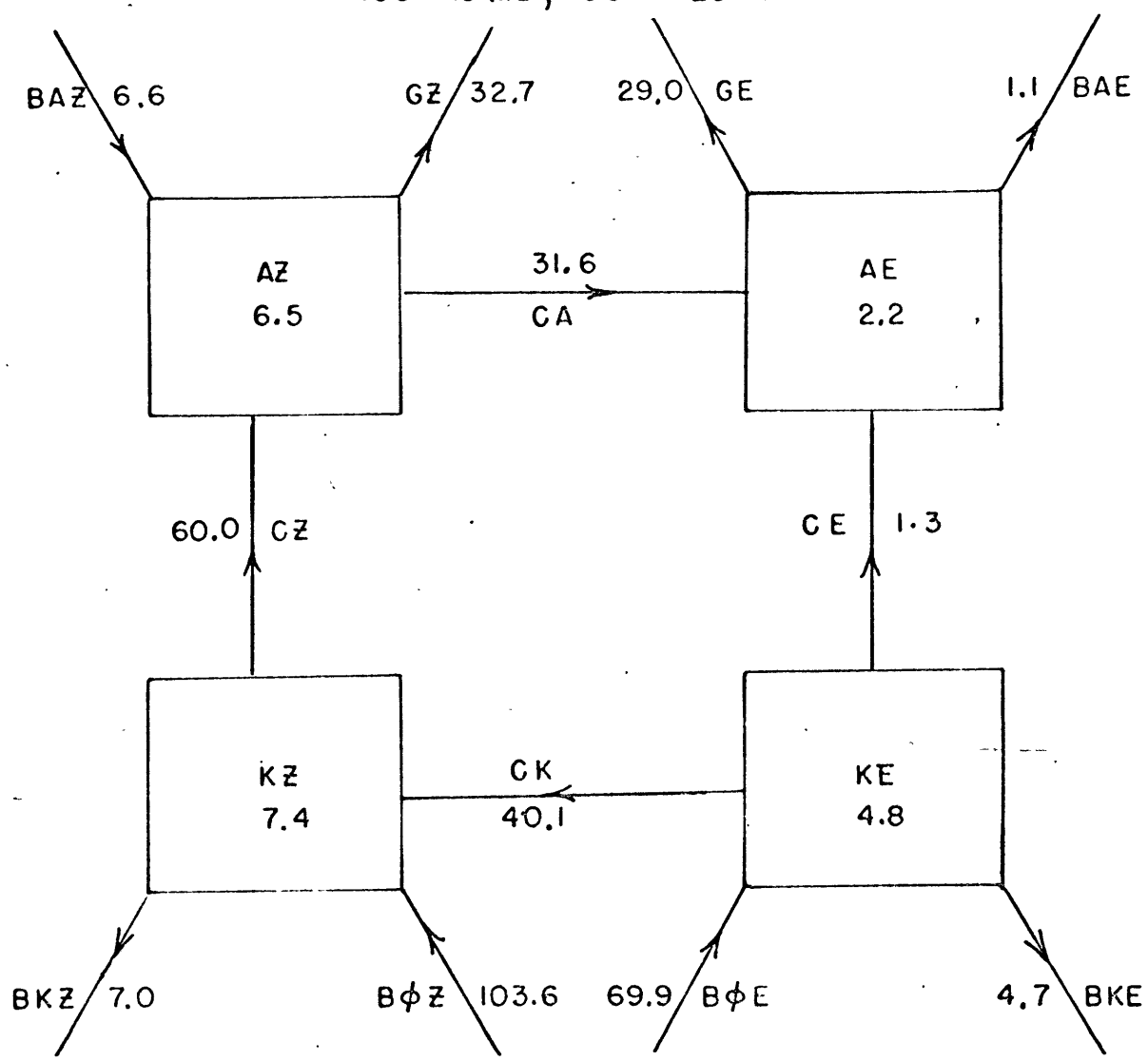
ENERGY CYCLE
1964
100 - 10 mb, 90° – 20° N
BAZ 6.6
GZ 32.7
29.0 GE
1.1 BAE
AZ
6.5
31.6
CA
AE
2.2
60.0 CZ
CE 1.3
KZ
7.4
CK
40.1
KE
4.8
BKZ 7.0
BφZ 103.6
69.9 BφE
4.7 BKE
CONVERSIONS (ERGS CM-2 SEC-1)
CONTENTS (x10^7 ERGS CM-2)

Figure 48.

VI. Conclusions

The first monthly mean global radiative heating rates have been obtained which show for all seasons that radiation cools the troposphere almost everywhere. This cooling is primarily due to water vapor and is maximum in the tropics. The tropical tropopause is a unique region because of the thermal heating by CO_2 and O_3 and minimum thermal cooling by H_2O. It is clear that radiation does not maintain the tropical tropopause as net thermal heating at the tropical tropopause is a result of the very cold temperatures. The tropical stratosphere is characterized by total radiative heating for all seasons due primarily to thermal and solar heating by ozone. This total radiative heating extends into the stratospheric mid-latitudes but higher latitudes exhibit cooling due principally to thermal cooling by CO_2 with the warmer hemisphere showing more cooling.

Comparison with previous theory in the N.H. shows qualitative agreement although the present study has more resolution because of the better specification of the radiative parameters, in particular, ozone and temperature. Comparison of the energy available to the earth-atmosphere system between theory and satellite measurements shows that the earth-atmosphere albedo is underestimated by theory which is probably due to the use of mean optical properties of clouds and the ground.

Approximate solutions of thermal cooling and solar heating are combined with the geopotential and temperature fields to examine the

energetics of the N.H. lower stratosphere on a daily basis for 1964 including radiative effects. Previous daily studies of the lower stratosphere have concentrated on sudden warming events and have generally excluded radiative effects.

From the present study it is found that in the winter months the eddies are maintained by the release of eddy available potential energy and absorption of tropospheric energy. For all other months the only energy source for the eddies is absorption of tropospheric energy. The zonal flow is maintained by the Reynolds' stresses and boundary forcing, principally lateral forcing in the winter and both lateral and vertical forcing in the warmer months.

It is now clear that absorption of tropospheric energy is important in all seasons and that the energetics of the lower stratosphere are closely coupled to the energy leakage from the lower atmosphere. The spring and fall seasons are particularly noteworthy since enhanced absorption of tropospheric energy altered the potential energy field in the spring, whereas in the fall the kinetic energy field was changed.

In the spring forced vertical motions were established by the absorption of tropospheric energy which subsequently required forced horizontal motions to redistribute the eddy temperature field. This eventually resulted in a reversal of the high latitude zonal temperature gradient. In the fall large absorption of tropospheric energy significantly increased the kinetic energy as the polar vortex began to intensify.

Radiation resulted in destruction of available potential energy for all months with the largest destruction in winter by the eddy radiative field and the largest destruction in summer by the zonal radiative field.

Significant periods of large upward energy flux into the upper stratosphere were found in winter and suggest a close coupling of the upper and lower atmospheres in winter.

VII. Recommendations

Solutions of thermal and solar heating depend critically on our knowledge of the radiative parameters. Temperature is probably the best known parameter but additional measurements are needed above 30 km especially in the S.H. Water vapor is well known below 300 mb from the North Pole to 15^{o}S but more observations are definitely needed in the N.H. above 300 mb. In the S.H. observations of water vapor are needed at all levels. Ozone is fairly well known in the N.H. but observations above 30 km are urgently needed in addition to observations at all levels in the S.H. More research is definitely required for solar heating in a cloudy atmosphere.

From the present study it is clear that the leakage of energy from the troposphere is of critical importance to the maintenance of the energy cycle of the lower stratosphere. Previous theoretical considerations have been primarily concerned with the interactions between the upper stratospheric and mesospheric wind fields and vertically propagating disturbances. In view of the significant

absorption of tropospheric energy in the lower stratosphere in the spring and fall, more attention must be given to the conditions that are favorable for enhanced absorption in the lower stratosphere. The large winter energy fluxes into the upper stratosphere also warrant further investigation.

A further area of investigation might be the use of statistics from the present study to approximately describe the eddy motions in the wintertime upper stratosphere as was suggested by Dickinson (1969).

Appendix

R	Gas constant for dry air.
C_p	Specific heat at constant pressure.
g	Acceleration of gravity.
Q	Diabatic heating per unit mass.
α	Specific volume.
p	Pressure in mb.
t	Time.
λ	Longitude, measured eastward.
φ	Latitude, measured northward.
a	Radius of the earth.
dM	$g^{-1} a^2 \cos\varphi \, d\varphi \, d\lambda \, dp$
dy	$a d\varphi$
dx	$a \cos\varphi \, d\lambda$
∇_p	Horizontal gradient on a constant pressure surface.
$\vec{V}_p$	Horizontal wind on a constant pressure surface.
Z	Height in geopotential units
ϕ	gZ
$[\,(\,)\,]$	Zonal average.
$(\,^*\,)$	Deviation from $[\quad]$.
$\langle(\quad)\rangle$	Area average on a constant pressure surface.
$(\,''\,)$	Deviation from $\langle(\quad)\rangle$.
$\overline{(\quad)}$	Time average.

u, v	Eastward and northward components of $\vec{V}_p$, respectively.
F_λ, F_φ	Eastward and northward components of the horizontal friction force vector on a constant pressure surface.
γ	$\left\langle \left(T - \frac{\rho C_p}{R} \frac{\partial T}{\partial \rho} \right) \right\rangle$
K	R/C_p
f	$2\Omega \sin\varphi$, Coriolis parameter.
v_g	$(fa\cos\varphi)^{-1} \frac{\partial \Phi}{\partial \lambda}$, Northward geostrophic wind.
q	Specific humidity.

BIBLIOGRAPHY

Barnes, A.A. Jr., 1962: Kinetic and potential energy between 100 mb and 10 mb during the first six months of the IGY. Final Report, Planetary Circulations Project, Dept. of Meteor., Mass. Inst. of Tech., pp. 8-131.

Charney, J.G. and P.G. Drazin, 1961: Propagation of planetary-scale disturbances from the lower into the upper atmosphere. J. Geophys. Res., 66, pp. 83-109.

Charney, J.G. and M.E. Stern, 1962: On the stability of internal baroclinic jets in a rotating atmosphere. J. Atmos. Sci., 19, pp. 159-172.

Cheltzov, N.I., 1952: Study of the reflection, transmission and absorption of radiation by clouds of certain forms. Trans. Centr. Aerol. Obs. No. 8.

Clark, J. and W. Hitschfeld, 1964: Heating rates due to ozone computed by the Curtis-Godson approximation. Quart. J. R. Met. Soc., 90, pp. 96-100.

Curtis, A.R., 1956: The computation of radiative heating rates in the atmosphere. Proc. Roy. Soc. A, 236, pp. 156-159.

Davis, P.A., 1963: An analysis of the atmospheric heat budget. J. Atmos. Sci., 20, pp. 5-22.

Dickinson, R.E., 1968a: On the exact and approximate linear theory of vertically propagating planetary Rossby waves forced at a spherical lower boundary. M.W.R., 96, pp. 405-415.

Dickinson, R.E., 1968b: Planetary Rossby waves propagating vertically through weak westerly wind wave guides. J. Atmos. Sci., 25, pp. 984-1002.

Dickinson, R.E., 1968c: Vertical propagation of planetary Rossby waves through an atmosphere with Newtonian cooling. J. Geophys. Res., 74, pp. 929-938.

Dickinson, R.E., 1969: Theory of planetary wave-zonal flow interaction. J. Atmos. Sci., 26, pp. 73-81.

Eliassen, A. and E. Palm, 1961: On the transfer of energy in stationary mountain waves. Geof. Pub., XXII, 23 pp.

Elsasser, W.M., 1942: Heat transfer by infrared radiation in the atmosphere. Harvard Meteor. Studies No. 6, Harvard Univ., 107 pp.

Fritz, S. and T.H. MacDonald, 1951: Measurements of absorption of solar radiation by clouds. Bull. A.M.S., 32, pp. 205-209.

Gabites, J.F., 1960: The heat balance of the Antarctic through the year. Antarctic Meteorology; proceedings of the symposium held in Melbourne, 1959. Pergamon Press, New York, pp. 370-377.

Goody, R.M., 1964a: Atmospheric Radiation. Oxford University Press.

Goody, R.M., 1964b: The transmission of radiation through an inhomogeneous atmosphere. J. Atmos. Sci., 21 pp. 575-581.

Handbook of Geophysics, 1961: Chapter 7 Clouds. U.S. Air Force, published by the Macmillan Company, New York.

Hering, W.S., C.N. Tovart and T.R. Borden Jr., 1967: Ozone heating and radiative equilibrium in the lower stratosphere. J. Atmos. Sci., 24, pp. 402-413.

Hilsenrath, E., L. Seiden and P. Goodman, 1969: An ozone measurement in the mesosphere and stratosphere by means of a rocket sonde. J. Geophys. Res., 74, pp. 6873-6880.

Houghton, J.T., 1963: The absorption of solar infrared radiation by the lower stratosphere. Quart. J. R. Met. Soc., 89, pp. 319-331.

Howard, J.N., D.L. Burch and D. Williams, 1955: Near infrared transmission through synthetic atmospheres. Geophys. Res. Papers No. 40, Geophys. Res. Dir., Air Force, Bedford, Mass.

Inn, E.C.Y. and Y. Tanaka, 1953: Absorption coefficients of ozone in the ultraviolet and visible regions. J. Opt. Soc. Am., 43, pp. 870-873.

Jensen, C.E., 1961: Energy transformation and vertical flux processes over the Northern Hemisphere. J. Geophys. Res., 66, pp. 1145-1156.

Julian, P.R. and K.B. Labitzke, 1965: A study of atmospheric energetics during the January-February 1963 stratospheric warming. J. Atmos. Sci., 22, pp. 597-610.

Katayama, A., 1966: On the radiation budget of the troposphere over the Northern Hemisphere. Part I, J. Met. Soc. Japan II, 44, pp. 381-401.

Katayama, A., 1967: On the radiation budget of the troposphere over the Northern Hemisphere. Part II, J. Met. Soc. Japan II, 45, pp. 1-25.

Katayama, A., 1967: On the radiation budget of the troposphere over the Northern Hemisphere. Part III, J. Met. Soc. Japan II, 45, pp. 26-38.

Kennedy, J.S., 1964: Energy generation through radiative processes in the lower stratosphere. Report No. 11, Planetary Circulations Project, Dept. of Meteor., Mass. Inst. of Tech., 116 pp.

Kondratiev, K. YA., 1969: Radiation in the atmosphere. International Geophysics Series, Vol. 12, Academic Press.

Kriester, B., 1968: Stratospheric warmings. Winds and Turbulence in Stratosphere, Mesosphere and Ionosphere, edited by K Rawer, John Wiley and Sons, New York, pp. 87-122.

Kriester, B., R. Scherlag and R. Stuhrmann, 1964: Daily and monthly Northern Hemisphere 10-millibar synoptic weather maps of the year 1964. Meteor. Abhand. Band IL - Heft 1, Inst. fur Meteor. und Geophys. der Freien Univ. Berlin.

Krueger, A.J., 1969: Rocket measurements of ozone over Hawaii. Annales de Geophys., 25, pp. 307-311.

Labitzke, K., 1965: On the mutual relation between stratosphere and troposphere during periods of stratospheric warmings in winter. J. Appl. Met., 4, pp. 91-99.

Lateef, M.S., 1964: The energy budget of the stratosphere over North America during the warming of 1957. J. Geophys. Res., 69, pp. 1481-1495.

London, J., 1957: A study of the atmospheric heat balance. College of Engineering, Res. Div., Dept. of Meteor. and Ocean., N.Y.U., Final Rep. AFC-TR-57-287, OTS PB 129551, 99 pp.

Lorenz, E.N., 1955: Available potential energy and the maintenance of the general circulation. Tellus, 7, pp. 157-167.

Malkmus, W., 1967: Random Lorentz band model with exponential-tailed S^{-1} line-intensity distribution function. J. Opt. Soc. Am., 57, pp. 323-329.

Mastenbrook, H.J., 1968: Water vapor distributions in the stratosphere and high troposphere. J. Atmos. Sci., 25, pp. 299-311.

Meteorological Rocket Network Committee: Data report of the Meteorological Rocket Network Firings. IRIG Document 109-62, Vols. 17-66, White Sands Missile Range, New Mexico, 1963-1967.

Meteorological Service of Canada: Ozone data for the World 1960-1968. Published by Meteor. Branch, Dept. of Transport, Meteor. Service of Canada, Toronto, Canada; in cooperation with World Meteor. Organization.

Miller, A.J., 1966: Vertical motion atlas for the lower stratosphere during the IGY. Report No. 16, Planetary Circulations Project, Dept. of Meteor., Mass. Inst. of Tech., 35 pp.

Molla, A.C. and C.J. Loisel, 1962: On the hemispheric correlations of vertical and meridional wind components. Geophys. Pura e Appl., 51, pp. 166-170.

Muench, H.S., 1965: On the dynamics of the wintertime stratospheric circulation. J. Atmos. Sci., 22, pp. 349-360.

Muller, P., 1964: Meteorological and atmospheric structure studies with grenades. Space Res. IV, pp. 155-170.

Murakami, T., 1967: Vertical transfer of energy due to stationary disturbances induced by topography and diabatic heat sources and sinks. J. Met. Soc. Japan, Ser. II, 45, No. 3, pp. 205-230.

Murray, F.W., 1960: Dynamic stability in the stratosphere. J. Geophys. Res. 65, 3273-3305.

Newell, R.E., 1961: The transport of trace substances in the atmosphere and their implications for the general circulation of the stratosphere. Geof. Pure e Appl., 49, pp. 137-158.

Newell, R.E., 1963: Transfer through the tropopause and within the stratosphere. Quart. J.R. Met. Soc., 89, pp. 167-204.

Newell, R.E., 1964: Further ozone transport calculations and the spring maximum in ozone amount. Pure and Applied Geophysics, 59, pp. 191-206.

Newell, R.E., 1966a: A review of studies of eddy fluxes in the stratosphere and mesosphere. Les problemes meteorologiques de la stratosphere et de la mesosphere, publ. by Presses Univ. de France, Paris, pp. 81-129.

Newell, R.E., 1966b: The energy and momentum budget of the atmosphere above the tropopause. Problems in Atmospheric Circulation, pp. 106-126, edited by R.V. Garcia and T.F. Malone, Spartan Books, Washington.

Newell, R.E., 1968: The general circulation of the atmosphere above 60 km. Meteorological Monographs, 9, publ. by the A.M.S., Boston, Mass.

Newell, R.E. and M.E. Richards, 1969: Energy flux and convergence patterns in the lower and middle stratosphere during the IQSY. Quart. J. R. Met. Soc., 95, pp. 310-328.

Newell, R.E., D.G. Vincent, T.G. Dopplick, D. Ferruzza and J.W. Kidson, 1970a: The energy balance of the global atmosphere. (To be published in the Proceedings of the Conference on the Global Circulation of the Atmosphere, London, August 1969).

Newell, R.E., J.W. Kidson and D.G. Vincent, 1970b: The general circulation of the tropical atmosphere and interactions with extratropical latitudes. (To be published by the M.I.T. Press).

Ohring, G., 1958: The radiation budget of the stratosphere. J. of Meteor., 15, pp. 440-451.

Oort, A.H., 1964: On the energetics of the mean and eddy circulations in the lower stratosphere. Tellus, 16, pp. 309-327.

Peng, L., 1965a: A simple numerical experiment concerning the general circulation in the lower stratosphere. Pure and Appl. Geophys., 61, pp. 197-218.

Peng, L., 1965b: Numerical experiments on planetary meridional temperature gradients contrary to radiational forcing. Pure and Appl. Geophys., 62, pp. 173-190.

Perry, J.S., 1967: Long-wave energy processes in the 1963 sudden straospheric warming. J. Atmos. Sci., 24, pp. 539-550.

Plass, G.N., 1956: The influence of the 9.6 O_3 band on the atmospheric infrared cooling rate. Quart. J. R. Met. Soc., 82, pp. 30-44.

Raschke, E., 1968: The radiation balance of the Earth-atmosphere system from radiation measurements of the Nimbus II meteorological satellite. NASA Tech. Note TND-4589, 81 pp.

Reed, R.J., J.L. Wolf and H. Nishimato, 1963: A spectral analysis of the energetics of the stratospheric sudden warming of 1957. J. Atmos. Sci., 20, pp. 250-275.

Richards, M.E., 1967: The energy budget of the stratosphere during 1965. Rep. No. 21, Planetary Circulations Project, Dept. of Met. M.I.T., 171 pp.

Rodgers, C.D., 1967a: The radiative heat budget of the troposphere and lower stratosphere. Report No. A2, Planetary Circulations Project, Dept. of Meteor., Mass. Inst. of Tech., 99 pp.

Rodgers, C.D., 1967b: The use of emissivity in atmospheric radiation calculations. Quart. J. R. Met. Soc., 93, pp. 43-53.

Rodgers, C.D., 1968: Some extensions and applications of the new random model for molecular band transmission. Quart. J. R. Met. Soc., 94, pp. 99-102.

Rodgers, C.D. and C.D. Walshaw, 1966: The computation of infrared cooling in planetary atmospheres. Quart. J. R. Met. Soc., 92, pp. 67-92.

Rofe, B., 1968: The stratosphere and mesosphere circulation of mid-latitudes of the Southern Hemisphere. Tech. Note PAD 115, Weapons Research Establishment, Australian Defense Scientific Service, Salisbury, South Australia.

Sellers, W.D., 1965: Physical climatology. Division of Chicago Press.

Smith, W., J. Theon, L. Katchen and P. Swartz: Temperature pressure, density and wind measurements in the upper stratosphere and mesosphere, 1960-63, 1964, 1965 and 1966. NASA Tech. Repts. TR R-211, TR R-245, TR R-263 and TR R-288.

Smithsonian Meteorological Tables, 1951, Vol. 114, Publ. by the Smithsonian Institution, Washington D.C.

Staff, Upper Air Branch, N.M.C. 1967: Weekly synoptic analyses, 5, 2 and 0.4 mb. surfaces for 1964. ESSA Tech. Report WB2, U.S. Dept. of Commerce, Silver Spring, Md.

Starr, V.P., 1960: Questions concerning the energy of stratospheric motions. Archiv. fur Met. Geophys. und Biokl., A., 12, pp. 1-7.

Starr, V.P., 1968: Physics of negative viscosity phenomena. McGraw-Hill Book Company, New York, 256 pp.

Starr, V.P., J.P. Peixoto and R.G. McKean, 1969: Pole-to-Pole Moisture Conditions for the IGY. Pure and Applied Geophysics, 75, pp. 300-331.

Telegadas, K. and J. London, 1954: A physical model for the northern hemisphere troposphere for winter and summer. Scientific Report No.1, Contract AF 19(122)-165, Research Division, College of Engineering, New York University.

U.S. Navy Marine Climate, 1965: Vol. VII, Antarctic, Navweps 50-1c-50. Atlas of the World.

Vigroux, E., 1953: Contributions à l'étude expérimentale de l'absorption de l'ozone. Annales de Physique, 8, pp. 709-762.

Vonder Haar, T.H., 1968: Variations of the earth's radiation budget. Meteorological Satellite Instrumentation and Data Processing. Final Scientific Rept. NAS-65, Dept. of Meteor., Univ. of Wisconsin, Madison, pp. 31-107.

Walshaw, C.D., 1957: Integrated absorption by the 9.6μ band of ozone. Quart. J. R. Met. Soc., 83, pp. 315-321.

Walshaw, C.D. and C.D. Rodgers, 1963: The effect of the Curtis-Godson approximation on the accuracy of radiative heating rate calculations. Quart. J. R. Met. Soc., 89, pp. 122-130.

White, R.M., 1954: The counter-gradient flux of sensible heat in the lower stratosphere. Tellus, 6, pp. 177-179.

White, R.M. and G.F. Nolan, 1960: A preliminary study of the potential to kinetic energy conversion process in the stratosphere. Tellus, 12, pp. 145-148.